

870651/

5032012

Sensitivity Verification of Radio  
Frequency Partial Discharge Detection in  
High Voltage Equipment

Sensitivity Verification of Radio  
Frequency Partial Discharge Detection in  
High Voltage Equipment

Abstract

The purpose of this paper is to present the results of a study on the sensitivity of radio frequency partial discharge detection in high voltage equipment. The study was carried out on a 100 kV oil-filled transformer. The results show that the sensitivity of the detection system is dependent on the frequency of the partial discharge signal and the distance between the detection system and the partial discharge source. The sensitivity is highest for signals with a frequency of 100 kHz and a distance of 10 cm.

Keywords

Radio frequency partial discharge detection  
Sensitivity  
High voltage equipment

Library

TR 155

602012

870651

Sensitivity Verification of Radio  
Frequency Partial Discharge Detection in  
High Voltage Equipment

# Sensitivity Verification of Radio Frequency Partial Discharge Detection in High Voltage Equipment

## Proefschrift

ter verkrijging van de graad van doctor  
aan de Technische Universiteit Delft  
op gezag van de Rector Magnificus prof.dr.ir. J.T. Fokkema  
voorzitter van het College voor Promoties,  
in het openbaar te verdedigen,  
op woensdag 4 november 2009 om 15:00 uur  
door

Panteleimon D. AGORIS

Master of Engineering  
in Electrical and Electronic engineering  
at Cardiff University of Wales  
geboren te Griekenland, Athene

TU Delft Library  
Prometheusplein 1  
2628 ZC Delft

Dit proefschrift is goedgekeurd door de promotor:  
Prof.dr. J.J. Smit

Samenstelling promotiecommissie:

Rector Magnificus	Voorzitter
Prof.dr. J.J. Smit	Technische Universiteit Delft, promotor
Prof. Ir. L. van der Sluis	Technische Universiteit Delft
Prof.Ir. W. Kling	Technische Universiteit Eindhoven
Prof.dr. M. Muhr	Technische Universiteit Graz
Prof.dr.ir. C. Karagiannopoulos	National Technical University of Athens
Prof.dr. M. Zeman	Technische Universiteit Delft
Dr.hab.ir. Edward Gulski (Prof. PUT)	Technische Universiteit Delft
Dr.Ir. S. Meijer	Technische Universiteit Delft

This research project has been supported by TenneT

ISBN: 978-90-8570-425-6

Copyright © 2009 by P.D.Agoris



## SUMMARY

*Electromagnetic Phenomena in Power Systems: A Challenge in*

The present work is a study of the electromagnetic phenomena in power systems. The main objective of this study is to analyze the electromagnetic phenomena in power systems and to develop a methodology for the measurement of the electromagnetic fields in power systems. The study is divided into two main parts: the first part is a study of the electromagnetic phenomena in power systems and the second part is a study of the measurement of the electromagnetic fields in power systems. The study is divided into two main parts: the first part is a study of the electromagnetic phenomena in power systems and the second part is a study of the measurement of the electromagnetic fields in power systems.

*In loving memory of my father,*

*and to my mother and sister*

The present work is a study of the electromagnetic phenomena in power systems. The main objective of this study is to analyze the electromagnetic phenomena in power systems and to develop a methodology for the measurement of the electromagnetic fields in power systems. The study is divided into two main parts: the first part is a study of the electromagnetic phenomena in power systems and the second part is a study of the measurement of the electromagnetic fields in power systems. The study is divided into two main parts: the first part is a study of the electromagnetic phenomena in power systems and the second part is a study of the measurement of the electromagnetic fields in power systems.

These uncertainties arise from the fact that the measurement of the electromagnetic fields in power systems is influenced by many parameters. In this thesis the type of effect and its location, the properties of the RF source and the measuring equipment, the measured output of the system. Therefore, a comparison is performed in conventional PD measuring systems and standards. For these reasons a study of verifying the measurement of PD measuring system is necessary. Such a procedure has been proposed for the case of GIS.

The final goal of this research is to develop a generalized methodology for the non-conventional RF PD measurement methodology that will be applicable for all HV equipment. To achieve this goal the following research questions have to be addressed in detail:

- The PD electromagnetic phenomena in terms of

On the 11th of August 1881  
I received from you

your letter of the 10th

concerning the matter of the  
the 11th of August 1881  
I have to inform you that  
the matter is being  
considered and I shall  
write you again as soon as  
I have more news.

Yours faithfully

Wm. E. Gladstone

11

## SUMMARY

### *Sensitivity Verification of Radio Frequency Partial Discharge Detection in High Voltage Equipment*

The condition of insulation plays a determining role in the life-time of high voltage (HV) equipment. Insulation defects or abnormalities will locally enhance the electric field strength and result in partial discharges. Therefore part of HV insulation diagnostics are the partial discharge (PD) measurements that provide an indication of the insulation condition. The requirements and standards for PD tests are prescribed in the IEC60270 standard. Nowadays, several techniques have been developed that can be used for PD detection in a different way than is prescribed in the IEC60270 standard, the so-called 'non-conventional' methods. These methods are ideal for on-site PD measurements while the HV component is in service (on-line), or when methods according to standards cannot be applied due to noise interference.

The 'non-conventional' method of interest to this research is the detection of the electromagnetic PD phenomena in the radio frequency (RF) range of 30 MHz to 3GHz. This method of PD detection has already been proved successful to detect PD in several HV equipment during after-laying tests or while the HV equipment is on-line. However, a means of verifying the sensitivity of the technique is not yet developed as is possible with the calibration procedure of conventional systems conforming to IEC60270 standards. Such a sensitivity check procedure is necessary primarily to reimburse for the uncertainties that exist due to lack of experience with this newly developed technique.

These uncertainties arise from the fact that the sensitivity of the RF PD measuring system is influenced by many parameters. As it will be studied initially in this thesis the type of defect and its location inside the HV equipment, the properties of the RF sensors and the measuring equipment have a great influence in the measured output of the system. Therefore, a calibration is not possible as is performed in conventional PD measuring systems that conform to the IEC60270 standards. For these reasons a means of verifying the detection sensitivity of the RF PD measuring system is necessary. Such a procedure has been proposed in the past for the case of GIS.

The final goal of this research is to develop a generalized sensitivity check procedure for the non-conventional RF PD measurement methodology that will be applicable for all HV equipment. To achieve this goal the following research questions have to be addressed in detail:

- The PD electromagnetic phenomena in terms of:

- Their frequency content
  - Propagation inside the HV equipment
  - Detection
- Identification of HV equipment related parameters, which are of importance for detection of the electromagnetic radiation emitted from PDs.
  - Evaluation of the RF PD detection technique with attention on its effect on measuring the PDs of various defects.
  - Proposal of a sensitivity check procedure based on the knowledge from GIS and the experiences of the author on the application of the RF PD measuring technique on HV equipment.
  - Verification of the sensitivity check procedure on actual cases of HV components.

For the purposes of this research the thesis will focus on the sensitivity capabilities of the RF PD measuring technique in its application in the following types of HV equipment:

1. Power transformers, and
2. Accessories of XLPE power cable systems.

The reason for choosing these two types of HV equipment is because of their different structure, which differentiates the application of the RF technique in each case. XLPE power cable accessories are simpler structures with electromagnetic waves transmitted via solid insulation. Electromagnetic radiation in transformers occurs in the oil (i.e. liquid insulation), and their complicated inner structure presents obstacles to electromagnetic radiation that result in complex propagation paths of the electromagnetic waves. This way the effect on the final sensitivity of the technique will be more considerable. Therefore, these two study cases offer two completely different cases of HV equipment where the sensitivity of the technique can be compared.

In the end the proposed sensitivity check procedure is easy to implement in other similar type of HV equipment. It can be used instead of a numerical technique because it takes into account the real construction of the HV equipment and the current noise conditions at the time of measurement. In addition it offers conclusions on the sensitivity of the RF PD measuring system that are comparable to conventional systems.



## SAMENVATTING

---

*Verificatie van de gevoeligheid van deelontlading diagnostieken welke gebaseerd zijn op het detecteren van de door de deelontlading uitgezonden elektromagnetische straling in radiofrequenties.*

De conditie van isolatie speelt beslissende rol voor de levensduur van hoogspanningscomponenten. Defecten of afwijkingen in het isolatiemateriaal zullen het elektrische veld lokaal versterken wat leidt tot deelontladingen. Daarom zijn ontladingsmetingen een diagnostiek om een indicatie te geven van de conditie van het isolatiemateriaal. De eisen en standaarden voor het uitvoeren van ontladingsmetingen zijn beschreven in de IEC60270 standaard. Verschillende technieken zijn ontwikkeld voor het uitvoeren van ontladingsmetingen op een manier die niet is beschreven in de IEC60270 standaard, de zogeheten niet-conventionele methoden. Deze methoden zijn vooral ideaal voor enerzijds on-site ontladingsmetingen waarbij de hoogspanningscomponenten niet uit bedrijf kunnen worden genomen en anderzijds in het geval dat conventionele meetopstellingen niet kunnen worden toegepast als gevolg van omgevingsruis.

In dit onderzoek ligt de nadruk op niet-conventionele technieken die gebruik maken van het detecteren van elektromagnetische straling, in het radiofrequentiegebied tussen 30 MHz en 3 GHz, veroorzaakt door ontladingsfenomenen. De ontladingsmeettechniek heeft zich al bewezen tijdens afnamekeuringen van hoogspanningcomponenten en aan in bedrijf zijnde installaties. Een manier om de gevoeligheid van de meettechniek te controleren is echter nog niet ontwikkeld, zoals wel het geval met de calibratieprocedure van conventionele meetssystemen gebaseerd op de IEC60270 standaard. Een procedure om de gevoeligheid te controleren is essentieel voornamelijk om de onzekerheden die optreden als gevolg van een gebrek aan ervaring met dit soort nieuw ontwikkelde technieken in te schatten.

Het doel van dit onderzoek is het beschrijven van een gevoeligheidsverificatie voor niet-conventionele RF ontladingsmeettechnieken welke algemeen toepasbaar is voor alle typen hoogspanningscomponenten. Om dit doel te bereiken zullen de volgende onderzoeksvragen beantwoord moeten worden en zijn onderzocht gedurende dit onderzoek:

- De elektromagnetische fenomenen behorende bij deelontladingen zoals:
  - o De frequentie inhoud
  - o Propagatieverschijnselen in hoogspanningscomponenten
  - o Detectie van elektromagnetische fenomenen

- Het bepalen van component gerelateerde parameters welke belangrijk zijn voor het detecteren van de elektromagnetische straling uitgestraald door deelontladingen
- Evaluatie van de RF ontladingsdetectie met nadruk op de invloed van verschillende isolatiedefecten
- Een voorstel voor een gevoeligheidsverificatie procedure gebaseerd op de enerzijds opgedane kennis bij GIS en anderzijds de ervaringen van de auteur bij diverse RF ontladingsmetingen aan andere hoogspanningscomponenten
- Toetsen van de voorgestelde gevoeligheidsverificatie procedure op diverse hoogspanningscomponenten.

Om de doelen van het onderzoek beschreven in dit proefschrift te bereiken ligt de focus op de eigenschappen die betrekking hebben op de gevoeligheid van de RF ontladingsmeettechniek toegepast op de volgende hoogspanningscomponenten:

- 1) Vermogenstransformatoren en
- 2) Accessoires van XLPE vermogenskabels

Deze twee type componenten zijn gekozen vanwege hun verschillende opbouw waardoor de toepassing van de RF techniek in beide gevallen verschilt. XLPE vermogenskabels zijn eenvoudiger waarin de elektromagnetische golven door het vaste isolatiemateriaal propageren. De elektromagnetische straling in transformatoren treedt op in de olie (vloeibaar isolatiemateriaal) en, als gevolg van hun complexe inwendige opbouw bestaande uit meerdere obstakels, zal een complex propagatie pad voor de elektromagnetische golven ontstaan. Dit heeft een significante invloed op de uiteindelijke gevoeligheid van de meettechniek. Daarmee bieden deze twee compleet verschillende hoogspanningscomponenten een goede mogelijkheid om de gevoeligheid van de techniek te vergelijken.

Uiteindelijk zal de voorgestelde procedure voor een gevoeligheidsverificatie eenvoudig implementeerbaar zijn in andere hoogspanningscomponenten van hetzelfde type. Het kan worden toegepast in plaats van een numerieke techniek omdat de procedure rekening houdt met de echte constructie van de hoogspanningscomponent en de tijdens de meting optredende achtergrondruis. Daarnaast geeft het een uitspraak over de gevoeligheid van het RF deelontlading meetsysteem welke vergelijkbaar is met een conventioneel meetsysteem.

# TABLE OF CONTENTS

---

<b>Summary</b> .....	<b>i</b>
<b>Sammenvating</b> .....	<b>iii</b>
<b>Table Of Contents</b> .....	<b>v</b>
<b>Chapter 1: Introduction</b> .....	<b>1</b>
1.1 Testing of High Voltage Equipment .....	1
1.2 State of the Art: Testing For Partial Discharges .....	3
1.3 The RF Measuring System .....	7
1.4 The Study Cases .....	11
1.4.1 Accessories of XLPE Cable Systems .....	12
1.4.2 Power Transformers .....	14
1.5 Aim of the Thesis .....	17
1.6 Thesis Layout .....	18
<b>Chapter 2: Partial Discharges In The Frequency Spectrum</b> .....	<b>19</b>
2.1 Introduction .....	19
2.2 The PD Mechanisms .....	20
2.3 PD Detection .....	22
2.3.1 The PD Current Pulse .....	22
2.3.2 Electromagnetic Radiation .....	25
2.3.3 Measured Spectra .....	28
2.4 Conclusions .....	32
<b>Chapter 3: Electromagnetic Radiation In Hv Equipment</b> .....	<b>35</b>
3.1 Introduction .....	35
3.1.1 Electromagnetic Waves .....	36

3.1.2	Modes of Propagation .....	37
3.1.3	Propagation in HV Equipment .....	38
3.2	Propagation in XLPE Power Cables .....	38
3.2.1	Mode of Propagation.....	39
3.2.2	Attenuation.....	40
3.3	Propagation in Power Transformers .....	48
3.3.1	Propagation in the Oil .....	48
3.3.2	A Cavity Resonator .....	49
3.3.3	Effect of Inner Structure.....	52
3.4	Conclusions.....	53
 <b>Chapter 4: Radio Frequency Partial Discharge Detection Circuit.....</b>		<b>55</b>
4.1	The RF PD Detection Circuit.....	55
4.2	The RF Sensors .....	57
4.2.1	Sensor Characteristics .....	58
4.2.2	Detection in Cables .....	61
4.2.3	Detection in Transformers.....	64
4.3	Miscellaneous Components .....	68
4.4	Conclusions.....	70
 <b>Chapter 5: Sensitivity Check In Power Cable Accessories.....</b>		<b>71</b>
5.1	Introduction.....	71
5.2	Sensitivity Check Procedure .....	72
5.3	Laboratory Test.....	76
5.3.1	Experiment I.....	76
5.3.2	Experiment II .....	81
5.4	On-Site Test.....	85
5.5	On-Site Performance Check .....	87
5.5.1	Experiment I.....	88
5.5.2	Experiment II .....	90

5.6	Conclusions .....	92
<b>Chapter 6: Sensitivity Check For Power Transformers..... 93</b>		
6.1	Introduction .....	93
6.2	Sensitivity Check Procedure.....	94
6.3	Laboratory Test .....	96
6.3.1	Experiment I .....	97
6.3.2	Experiment II.....	99
6.4	The On-Site Test .....	103
6.4.1	Experiment I .....	103
6.4.2	Experiment II.....	106
6.4.3	Experiment III.....	107
6.5	Performance Test.....	110
6.5.1	Experiment I .....	110
6.5.2	Experiment II.....	112
6.6	Conclusions .....	114
6.7	Generalization of Procedure .....	115
<b>Chapter 7: Conclusions And Future Work..... 119</b>		
7.1	Conclusions .....	119
7.2	Future Work .....	121
<b>References .....</b>		<b>125</b>
<b>Appendix A: Sensitivity Check Procedure In Gis.....</b>		<b>135</b>
<b>Appendix B: Frequency Response Measurements.....</b>		<b>139</b>
<b>Appendix C: Attenuation In Coaxial Cables.....</b>		<b>143</b>
<b>Appendix D: Insertion Depth In Oil-Valve Sensors .....</b>		<b>147</b>

<b>List Of Abbreviations</b> .....	<b>151</b>
<b>List Of Units</b> .....	<b>152</b>
<b>Acknowledgements</b> .....	<b>153</b>
<b>Biography</b> .....	<b>157</b>

# Introduction

---

*This chapter introduces the research presented in this thesis in the general framework of testing of high voltage equipment. The partial discharge detection in the radio frequencies of the spectrum is then discussed in order to present the motivation and background concerning the need for a sensitivity check of this technique. The objectives and the associated tasks for the current research are given. The chapter ends with an outline of the thesis's layout.*

## 1.1 Testing of high voltage equipment

The effective operation of the power transmission and distribution systems is mainly dependent on the efficient operation of their high-voltage (HV) components, which are vital parts of the total power system. Newly installed equipment has to conform to sufficient quality standards before they are put into service, in order to avoid unexpected failures. On the other hand utilities are faced with the approaching 'end of life' of the HV equipment with age.

Due to the increasing competitiveness of the market, most power companies need to develop appropriate strategies to manage their assets in a way that should minimize their costs. Therefore, they prefer to postpone replacement of aged HV equipment, if it is still functional, in order to minimize costs. Especially in the case of large and strategically important equipment, such as a large HV power transformer, of which replacement is an expensive operation.

However, due to the cross-boarder trade of energy, the increasing fraction of intermittent dispersed generation and the socially high reliance on uninterrupted electrical power supply certain HV equipment at key-nodes of the network need to be more dynamically loaded and reliable. This is a more demanding role for the equipment and weak ones in that position might not be able to fulfill the overloading requirements and thus should be replaced. For these reasons, the significance of diagnosing the condition of HV components is growing together with the changes in production, transmission, distribution, and consumption of electricity.

## 1.1 Testing of high voltage equipment

Several tests are performed in order to confirm the condition of HV equipment, during the three main stages of the HV equipment's lifetime:

- i) During its production: Type tests (TT), routine tests (RT) or other special tests (ST) are carried out to [61]:
  - ◆ "Prove the design meets requirements and to obtain HV equipment characteristics" (TT), (ST)
  - ◆ "Check that quality requirements have been met and that performance is within the tolerance guaranteed" (RT),
- ii) During its on-site installation, tests are carried out:
  - ◆ To detect any defects introduced by the transportation or installation process [12, 32, 36].
- iii) During the long term operation of the HV equipment:
  - ◆ Periodic or continuous on-site monitoring of its condition is also applied in order to detect any predisposition to unexpected failure [10, 71].

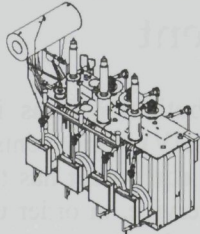
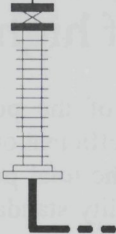
Power Transformers		EHV power cables (150-500 kV)	
	IEC 60076: Power Transformers		IEC62067: Power cables with extruded insulation and their accessories for rated voltages above 150 kV up to 500 kV – Test methods and requirements
<ul style="list-style-type: none"> <li>▪ No-load loss and magnetising current</li> <li>▪ Load losses and impedance</li> <li>▪ Winding resistance</li> <li>▪ Tap-changer operation [IEC60214]</li> <li>▪ Lightning and switching impulses</li> <li>▪ Partial discharge testing [2]</li> <li>▪ Induced Voltage test</li> <li>▪ Voltage test</li> </ul>		<ul style="list-style-type: none"> <li>▪ Dissipation factor</li> <li>▪ Withstand voltage during bending and cross-bonding leads</li> <li>▪ DC voltage test of the over-sheath</li> <li>▪ AC voltage test of the insulation</li> <li>▪ Partial discharge testing [2]</li> </ul>	

Table 1.1: Examples of tests performed on power transformers by IEC60076, and EHV power cables by IEC60076. These tests are recommended by the corresponding standards where also their procedure is prescribed. In case where the procedure of a test is prescribed in another standard it is noted next to the name of the test

For tests performed during production of the equipment, the technical requirements for the tests of all HV equipment are defined by National, European or International Standards. These standards prescribe performance levels that must be demonstrated for each type of HV equipment produced. Examples of international standards



concerning test techniques for power transformers and EHV power cables are demonstrated in Table 1.1. During the long term operation no standardisation exists yet, apart from certain guidelines proposed by CIGRE.

In this thesis the main focus will be partial discharge (PD) testing, which is a widely accepted test required for most HV equipment. PD tests and requirements for HV equipment are prescribed in IEC60270 [2]. Nowadays, however, several techniques have been developed that can be used for PD detection in a different way than is prescribed in the IEC60270 standard, the so-called 'non-conventional' methods [18]. These methods have already been applied in several HV equipment [38, 49, 76, 79] but since they do not conform to IEC60270 standards several technical aspects have to be considered before these methods can be applied.

## 1.2 State of the art: Testing for partial discharges

It is known that the condition of the insulation plays the main determining role in the life-time of the HV equipment, as is indicated by the failure experience of equipment in utilities, as it is shown in the example statistics presented in Figure 1.1 for power transformers and GIS.

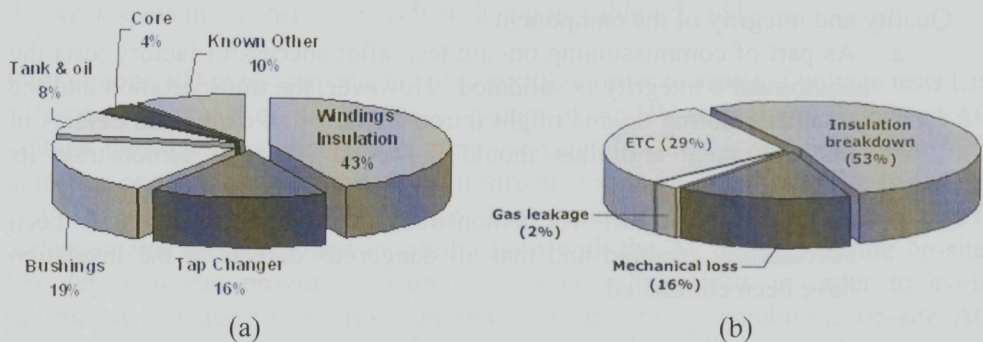


Figure 1.1: (a) Results from Doble's surveys for 1500 failures in transformers of all designs in the period from 1993 to 1998 [60]. (b) Fault trend of GIS in a 2002 domestic electric power company report [59, 14].

HV insulation failure can occur as a result of the normally applied operating voltage or during transient over-voltages, such as lightning or switching surges. In the first case, electrical failure of the insulation occurs if the localized electrical stresses are greater than the dielectric strength of the insulation materials in that area. In the case of over-voltages, electrical failure occurs when the bulk insulation material is degraded to the point where it cannot withstand the applied voltage. These cases may occur due to defects introduced in the insulation from [7, 15]:

- ◆ Bad design

- ◆ Improper manufacturing processes
- ◆ Improper handling during transportation and installation
- ◆ Ageing (thermal, mechanical, chemical or electrical).

The insulation defects that enhance the dielectric stresses inside the HV equipment will be accompanied by PD. Based on the absence or presence, and thus behavior, of PD activity from discharging insulation defects conclusions can be made about the actual dielectric insulation status. Additionally, although there is no direct relationship between PD and the long-term failure of the electrical insulation, it is a fact that PD processes accelerate the aging process of the insulation (liquid or solid). Their chemical by-products, the mechanical and thermal deterioration locally reduce the dielectric strength of the insulation [6, 71, 8, 3]. Furthermore, under the right conditions PDs might expand leading to the creation of electrical trees which provide conductive paths for breakdown and ultimate failure of the insulation [7, 8]. Therefore the presence and activity of a PD source in HV equipment is indicative of insulation problems and PD measurement is an indirect method for assessing the extent and the danger of HV insulation defects.

An important capability of PD testing is that it can be performed on-site, at the location of the HV equipment. By measuring on-site with PD measurements the following can be confirmed [32]:

1. Quality and integrity of the component
  - a. As part of commissioning on-site test: after successful factory tests the equipment's integrity is validated. However, the transportation and the final assembling on-site might introduce new and dangerous defects in the equipment and thus should be tested again to demonstrate its integrity.
  - b. After on-site repair: To demonstrate that the equipment has been successfully repaired and that all dangerous defects in the insulation have been eliminated.
2. Reliability of the HV equipment for diagnostic purposes
  - a. To estimate actual condition of the service aged component by checking the insulation degradation after a period of service operation e.g. 40 or 50 years.
  - b. By providing reference values to diagnostic tools for comparison purposes at later tests. This is a good practice to demonstrate whether the insulation is still free from dangerous defects or to monitor the condition of a previously detected defect to see if it is stable or worsening.

Insulation condition assessment	Type of diagnosis	Important parametrs	HV Equipment
<i>Weak spots</i>	PD measurements	<ul style="list-style-type: none"> <li>○ PD inception voltage (PDIV)</li> <li>○ PD magnitudes</li> <li>○ PD location/PD pattern</li> </ul>	<ul style="list-style-type: none"> <li>○ GIS</li> <li>○ Transformers</li> <li>○ Cables</li> </ul>
<i>Integral condition</i>	Dielectric losses	<ul style="list-style-type: none"> <li>○ <math>\tan\delta</math> behavior at voltages up to <math>1.7xU_0</math></li> </ul>	<ul style="list-style-type: none"> <li>○ Transformers</li> <li>○ Cables</li> </ul>
	Dielectric response	<ul style="list-style-type: none"> <li>○ Return voltage amplitude, shape, time behavior and linearity</li> </ul>	<ul style="list-style-type: none"> <li>○ Transformers</li> <li>○ Cables</li> </ul>

Table 1.2: Characterisation of on-site diagnostics parameters and HV equipment [15]

There are several other tests that can also be used to assess the condition of the insulation on-site, such as the dielectric loss tangent ( $\tan\delta$ ) or the dielectric response measurements [15]. These tests provide information for the integrity of the total insulation. PD testing can then be used complementarily in order to identify the weak spots in the insulation as it is shown in Table 1.2 [15].

Furthermore, PD measurements are also useful in order to assess if voltage tests had a destructive impact on the insulation system of the HV equipment. Enhanced AC voltage testing higher than the nominal voltage ( $U_0$ ) of the HV equipment with defective or aged insulation may have destructive influence on the service life of the component, even if no breakdown has occurred [29, 10, 12]. Since PD measurements are performed in combination with the AC voltage testing on-site, PD detection can provide a warning to stop voltage tests in order to avoid destructive damage of the HV equipment. Therefore by combining on-site AC voltage testing with PD detection the following is additionally achieved:

- i) it provides information about discharging insulation defects,
- ii) it can be assessed if the on-site test had a destructive impact on the insulation system.

The conventional detection systems for PD measurements are the electrical systems that obey to the recommendations defined by IEC 60270 (High Voltage Testing – Partial Discharge Measurements). These systems detect the pulses occurring in a specified electric circuit due to voltage drops appearing during a PD. Thus this type of PD detection requires special circuits and an external power source to energize it. The PD detection system measures the apparent charge (in [pC]), which is the integrated current pulse caused by a PD that flows through the test circuit. The

application allows for a precise calibration which is necessary for acceptance tests of HV equipment. Conventional PD measuring systems can be used in the factory/laboratory and on-site, but on-site their application is prone to noise interference.

During the last years several other techniques have been developed for the detection of PD in HV equipment. These techniques do not conform to IEC 60270 standards because the PD is detected based on different physical quantities than the apparent charge and thus are referred to as 'non-conventional'. The various 'non-conventional' methods that exist for PD detection are the following [18] (see also Figure 1.2):

- 1) Electric measuring systems which detect the electromagnetic (electromagnetic) radiation emitted from a PD. Narrowband or wideband filters are used in order to detect the signals which appear at the radio frequencies (RF) of the spectrum [49, 40].
- 2) Acoustic measurements which detect the sound waves emitted as a result of the pressure changes caused by the sparking in the insulation medium [46, 47, 48].
- 3) Other diagnostic methods which detect changes in gas pressure or chemical changes in the material subjected to the discharges e.t.c.

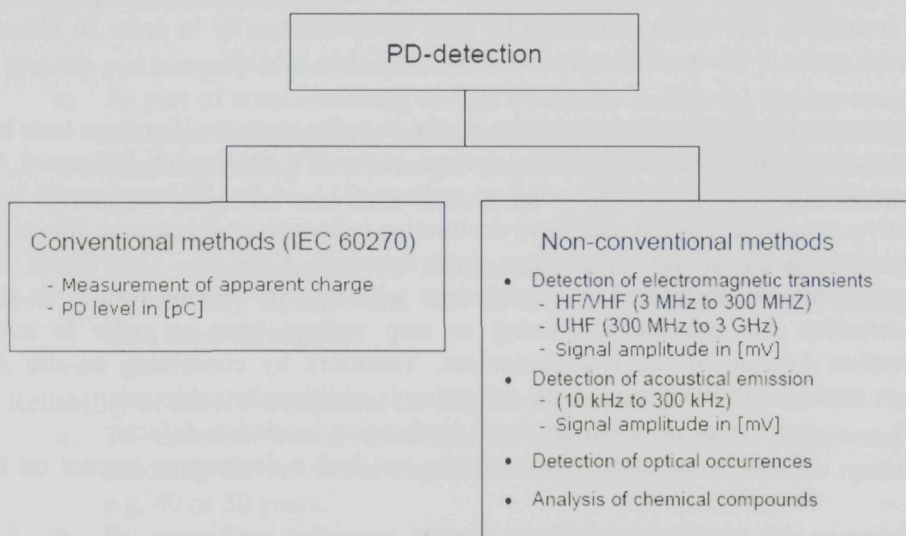


Figure 1.2: Methods for PD detection [18]

Since these newly developed PD measuring techniques do not measure the apparent charge of the PD their results cannot be used in accordance to IEC 60270 standards. Nevertheless, 'non-conventional' methods are preferred to conventional PD measuring systems in the following occasions:

- ◆ Conventional PD measurements cannot be performed because a suitable measuring circuit as defined by the IEC 60270 standards is not applicable.
- ◆ Presence of strong external disturbances prohibits the use of conventional PD measurements [12].
- ◆ It is required to localize the PD inside certain HV equipment (such as in transformers and GIS) [48, 39]

In this thesis, the investigation is confined to electric measuring systems which detect the electromagnetic radiation emitted from a PD. The *RF PD measuring systems* have been developed in the past decades and have been used up to now for PD detection on power cables, transformers, GIS and generators, but there are not yet generally accepted rules and guidelines for their application compared to conventional methods. Therefore, there are several issues to be solved concerning their application as a diagnostic tool for HV equipment.

### 1.3 The RF measuring system

The main concept of the RF PD measuring technique is that PD pulses, due to their short duration and rise times in the nanosecond regime, generate electromagnetic radiation at various frequencies within the range of the radio frequency (RF) spectrum [38], as it is displayed in Figure 1.3.

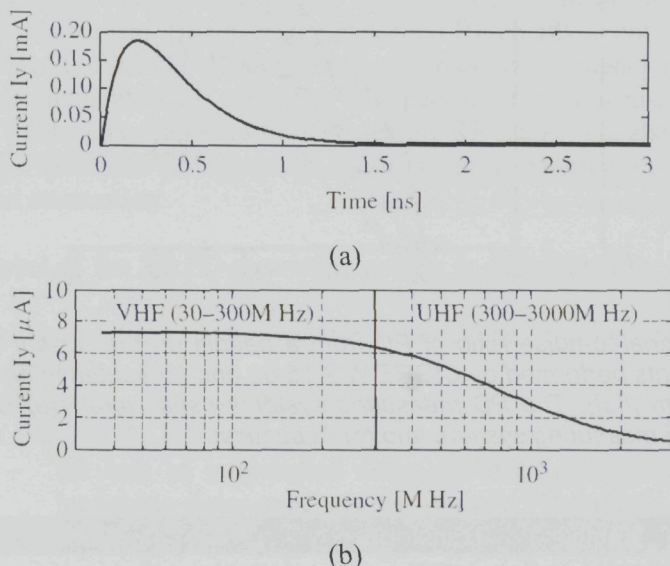


Figure 1.3: Simulation results taken from [44] for (a) the PD current and (b) the magnitude spectrum.

Even in liquid insulation, the discharge takes place in a gas-bubble under high pressure and results in a very steep current pulse. High frequency signals can thus be excited ranging up to 3 GHz. The RF range of the spectrum constitutes of the characteristic frequency ranges of HF (3 MHz -30 MHz), VHF (30 MHz - 300 MHz) and UHF (300 MHz - 3000 MHz). Appropriate RF sensors are used to pick-up the emitted electromagnetic waves and then narrowband or wideband filters are applied in order to measure the signals appearing in the desired frequencies within the RF range of the spectrum. These RF sensors can be incorporated in the HV equipment from its design or even placed while the equipment is in service.

Extensive research on the RF PD detection method as a diagnostic tool has already been carried out in gas insulated substations (GIS) [49, 19]. From the available electric PD detection techniques in GIS, the RF PD measuring system has been proven to be the most sensitive; as results from experiments performed by CIGRE WG 15-03 have shown [9, 63, 19]. The results from [9] for a needle defect attached to a busbar have been taken from [19] and are demonstrated in Figure 1.4. Recently, the technique has also been applied for power cable accessories [51, 52], power transformers [38, 54] and generators [81]. Table 1.3 below shows the applicability of certain frequency ranges for these components of the electricity network.

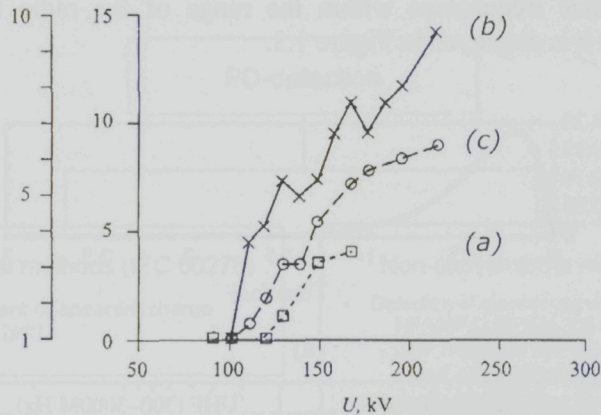


Figure 1.4: Signal-to-noise ratio of PD from a needle on the busbar as obtained from experiments performed by CIGRE WG 15-03 and presented in [9]. (The graph was taken from [63]). The PD measuring systems used were: (a) Conventional system, (b) RF measuring system, and (c) Acoustics.

	Cables	Transformers	GIS	Generators
HF	+	—	—	+
VHF	+	+	+	+
UHF	+ / —	+	+	—

Table 1.3: Most suitable frequency band for on-line PD detection in different components (reproduced from [18]).

In conventional measuring systems the characteristics of the measured pulse are dependent on the transfer characteristics of the measuring circuit and the propagation path within the HV equipment (e.g. transformer). For this reason a calibration procedure is performed before actual PD measurements in order to achieve the following:

- i) To verify that the measurement system is able to measure a specified PD magnitude correctly.
- ii) To determine a scale factor for the measurement of the apparent charge  $q$  for the specific measuring circuit and equipment.

The main advantage for the usage of conventional systems for PD detection by industries and utilities is that with conventional measuring systems, a fixed calibration procedure is used which later allows the measurement of the PD magnitude in Coulombs. Measuring in [pC] is important because it expresses the compatibility between component and defect that can be matched to certain acceptance standards, as is defined by IEC 60270 recommendations. The RF PD measuring systems, however, cannot be calibrated in such a way and hence the measured signals can only be measured in Volts.

Studies have been made to find a possible relationship between the two measuring principles and indeed results of [27] indicate that there might be a relationship between RF energy and apparent charge but it is dependent on the nature of the defect and its mechanism. However, the measured RF energy is not only dependent on factors related to the PD behavior itself but also on the frequency response of the RF detection equipment that is used. [74, 75] specifies that the measured RF energy is dependent on the characteristics of the detecting RF sensor, but also dependent on the resonances within the HV apparatus due to the propagation effects of reflection, dispersion and attenuation.

The output level of the RF PD measuring system is determined by several factors such as:

1. The type of PD (i.e. the electric stress caused by the defect's type and geometry)
2. The frequency response of the RF sensor
3. The effect of the HV equipment structure in terms of:
  - the loss of information about the discharge process itself with increasing distance between sensor and PD origin,
  - the increasing impact of pulse propagation path on PD waveform,
  - the superposition between different signals, e.g. multiple PD source, crosstalk, external interferences.

The effect of these factors on the measured output of the technique is demonstrated in Figure 1.5.

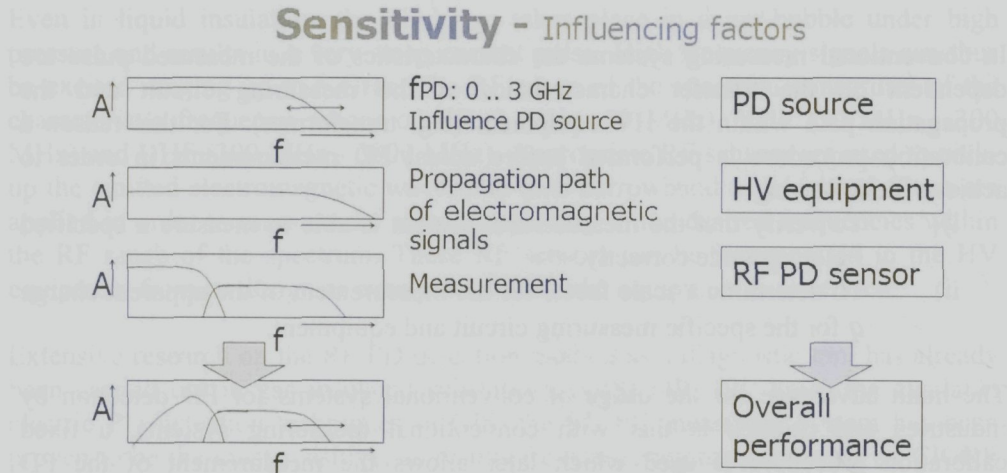


Figure 1.5: Different factors that affect the PD detection sensitivity of the RF measuring technique.

For the reasons discussed above, in the RF PD measuring technique, it is not possible to perform a calibration in the standardized way. Therefore, a sensitivity check is developed to verify the detection capabilities of the RF PD measuring system. CIGRE Task Force 15/33.03.05 of Working Group 15.03 in has proposed in [1] a sensitivity check procedure for the case of GIS. This sensitivity verification procedure “ensures that defects causing an apparent charge of 5 pC or more can be detected by such [i.e. RF] equipment” [1]. The procedure is a practical way of relating the RF signals to PD magnitude in [pC] by measuring a discharging defect simultaneously with the two techniques. An artificial pulse is determined that can simulate the discharges from the mentioned defect which is then used to test the sensitivity of the RF PD measuring technique at other compartments and combination of compartments of the GIS.

The challenge is to adopt the same sensitivity check procedure to other HV equipment. Potentially a generalized procedure emerges for testing the sensitivity of the RF PD measuring system applicable for all types of HV components. This will be the main drive of the research presented in this thesis. However, for that matter certain issues are raised that need to be clarified. These can be summarised in the following questions:

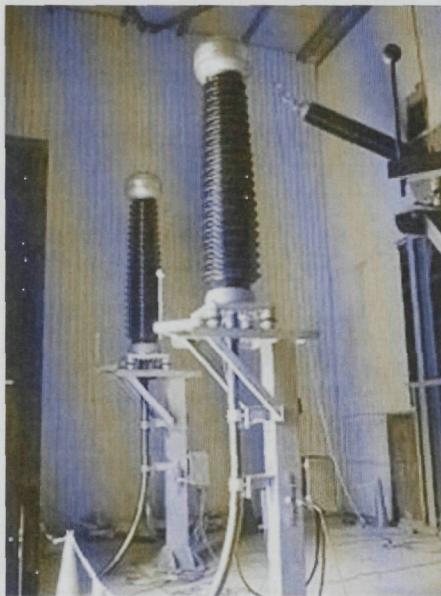
- Can systematic experience gained from the different HV equipment be combined to form generally accepted rules and guidelines?
- Does the sensitivity of the technique differ from its application at different types of HV components? And how can it be tested and defined?
- Is it possible to quickly expand the knowledge of the technique based on laboratory experience?



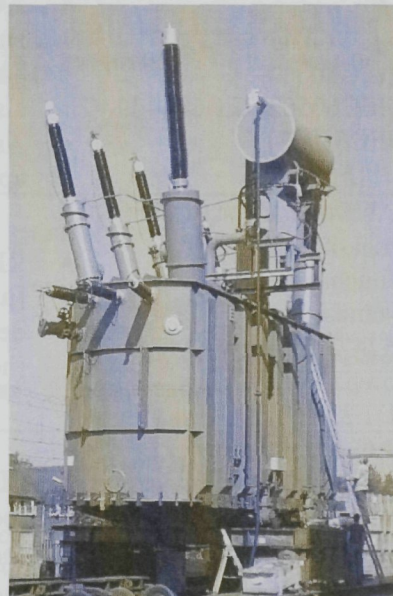
- Is it possible to perform some kind of sensitivity check to adjust the system readings hence performing a sort of calibration?

These questions constitute the starting point of this research that will explore the subject of sensitivity verification with the RF technique in HV equipment. For that purpose two study cases of HV equipment were considered for exploring the issues concerning the sensitivity of the RF PD measuring technique.

## 1.4 The study cases



(a)



(b)

Figure 1.6: (a) Power cable terminations. (b) A power transformer

For the purposes of this research, two types of HV equipment will be considered where the RF technique will be applied, in order to acquire more practical experience on the factors of influence. These cases are (see Figure 1.6):

- i) the accessories of an XLPE cable system, and
- ii) the power transformer

The reason for choosing these two types of HV equipment is because of their different structure, which differentiates the application of the RF technique in each case. XLPE power cable accessories are simpler structures with electromagnetic waves transmitted via solid insulation. Electromagnetic radiation in transformers occurs in the oil (i.e. liquid insulation), and their complicated inner structure

presents obstacles to electromagnetic radiation that result in complex propagation paths of the electromagnetic waves. This way the effect on the final sensitivity of the technique will be more considerable. Therefore, these two study cases offer two completely different cases of HV equipment where the sensitivity of the technique can be compared.

### 1.4.1 Accessories of XLPE cable systems

TEST TYPE	DESCRIPTION
1. AC voltage test, [IEC60060-3], [IEC60502, IEC60840, IEC62067]	<ul style="list-style-type: none"> <li>• AC test voltage 20-300 Hz substantially sinusoidal,</li> <li>• Test @ <math>1.7 U_0</math> / 1 h (but lower values are also allowed),</li> <li>• As alternative, a test @ <math>U_0</math> / 24 h may be applied</li> </ul>
2. AC voltage test & PD measurement (unconventional) not standardized (IEC 62478 under preparation, Cigre D1.33.03)	<ul style="list-style-type: none"> <li>• RF (up to 500 MHz) PD measurement in [<math>\mu</math>V]</li> <li>• detection of PD in cable accessories only (not applicable for direct buried cables)</li> </ul>
3. AC voltage test & PD measurement in accordance to IEC60270 and IEC885-3	<ul style="list-style-type: none"> <li>• PD level measurement in [pC]</li> <li>• localization of PD in cable insulation</li> <li>• localization of PD in cable accessories</li> </ul>

Table 1.4: Test types of PD measurements.

PD testing of XLPE insulated power cables is in use as an after-laying test to search for poor workmanship of installation or repair work or during the service life to search for insulation degradation processes [29, 32]. For the case of EHV XLPE cable systems (voltage class above 150 kV) several PD diagnostic methods are available for use in the field. In Table 1.4 an overview of these diagnostics and the corresponding PD energizing method are displayed.

The RF PD measuring system is mainly used instead of a conventional system when the noise from the energizing source appears within the measuring bandwidth of the conventional system. The noise originates from the power electronics of the source as is displayed in Figure 1.8 (b). The RF PD measuring technique uses several RF sensors in each of the accessories, as is demonstrated in Figure 1.7. PD detection with the RF system is usually performed during the standard voltage withstand tests. Sometimes they can be used to monitor for PD while raising the applied high-

voltage in small steps. If PD appears, the test is immediately abandoned and a complete breakdown is prevented. Experience shows that if PD occurs “the ‘time-to-breakdown’ ranges from only a few seconds to 16 minutes when testing at  $2xU_0$ , increasing to 23 minutes for  $1,7xU_0$ ” [12]. Therefore, in EHV XLPE cables no PD is accepted in the cable insulation [29].

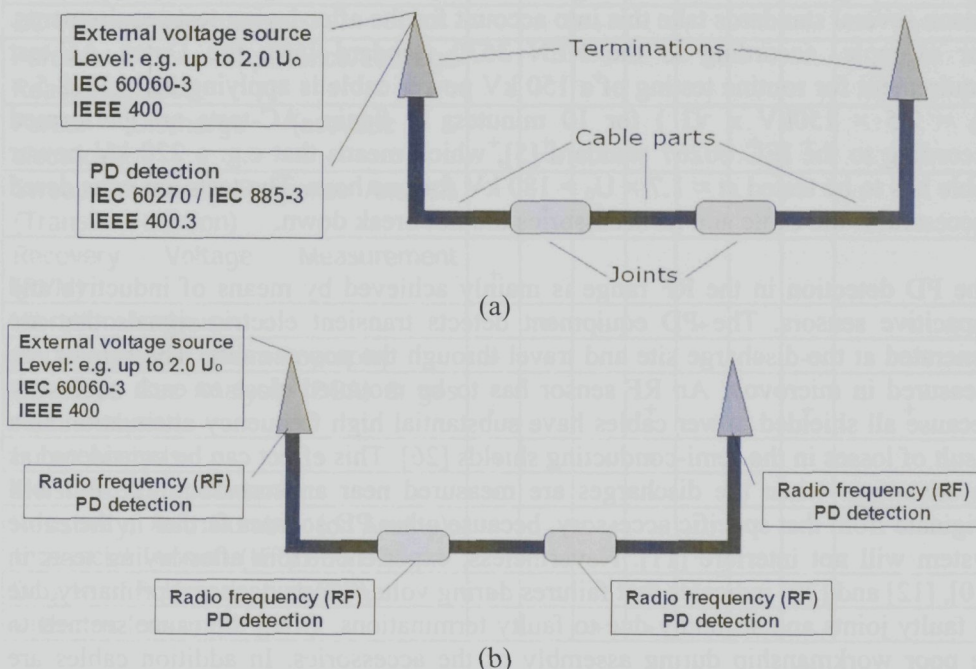


Figure 1.7 Principles of off-line PD detection methods for power cables: (a) Standardized and calibrated PD detection (conventional) applicable for both factory testing and on-site testing of cable insulation and cable accessories (b) Non-standardized and non-calibrated PD detection (unconventional) for on-site testing of cable accessories.

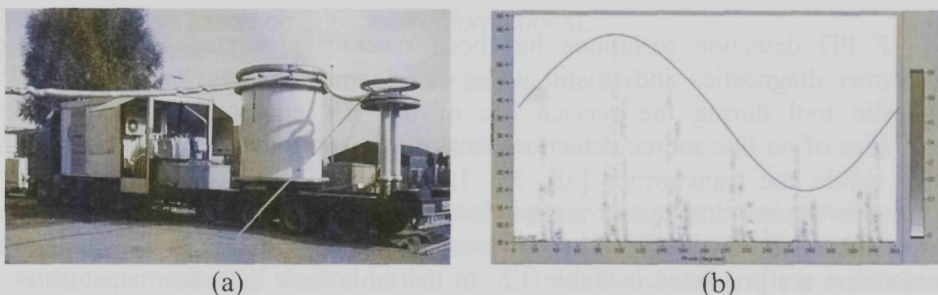


Figure 1.8: (a) Example of a mobile resonant test system for testing of installed power cables. (b) Pulses originating from the frequency converter may appear up to 6 MHz. This interferes with conventional systems whose operating range can be up to 400 kHz.

The voltages at which the tests are undertaken are above the nominal voltage rated for the cable, in accordance with IEC standards and CIGRE recommendations. This is because even if the PDIV (PD inception level) is higher than the operation voltage, the extinction voltage (PDEV) can be lower, and in case of over-voltages e.g. switching, the PD source will ignite and stay active during service [29]. For this reason several standards take this into account for the after-laying test requirements. For example, according to the NEN 3630 standard [58], the Dutch AC-test requirement for routine testing of a 150 kV power cable is applying 220 kV ( $2.5 \times U_0 = 2.5 \times 150\text{kV} \times \sqrt{3}$ ) for 10 minutes. In Spain, AC-tests are performed according to the IEC 60267 standard [5], which means that e.g. a 220 kV power cable has to be tested at  $\approx 1.7 \times U_0 = 180$  kV for one hour. The tests are considered successful if the cable and its accessories did not break down.

The PD detection in the RF range is mainly achieved by means of inductive and capacitive sensors. The PD equipment detects transient electric signals that are generated at the discharge site and travel through the power cable. The signals are measured in microvolt. An RF sensor has to be mounted close to each accessory because all shielded power cables have substantial high frequency attenuation as a result of losses in the semi-conducting shields [26]. This effect can be considered as an advantage when the discharges are measured near an accessory, the PD will originate from that specific accessory, because other PD sources farther in the cable system will not interfere [11]. Nevertheless, experience from after-laying tests in [10], [12] and [29] indicates that failures during voltage tests occurred primarily due to faulty joints and secondly due to faulty terminations. Often the cause seemed to be poor workmanship during assembly of the accessories. In addition cables are tested for PD in the factory using conventional techniques that conform to IEC standards and are thus delivered on-site PD-free.

### 1.4.2 Power transformers

The RF PD detection technique has been recently presented in the field of transformer diagnostics and is still under development. It can be used as a PD diagnostic tool during the service life of the HV equipment since it offers capabilities of on-line source detection, recognition and location of the discharging defect inside the transformer [38, 39, 15, 54]. To assess the condition of a transformer several diagnostics are needed in order to take into account all of its components and materials. The various diagnostics currently available for transformers are presented in Table 1.5. In the table their detection capabilities at defects in each transformer component are also indicated.

Method	1	2	3	4	5	6	7	On-Line
Infrared Scan		+			+	+	+	+
Dielectric Dissipation Factor (DDF) & Capacitance				+				
Winding Turns Ratio	+							
DC Winding Resistance			+				+	
Percent Impedance/Leakage Reactance Test			+					
Partial Discharge (acoustic & electrical)	+	+	+			+	+	+
Sweep Frequency Response Analysis (Transfer Function)		+	+					
Recovery Voltage Measurement (RVM)	+							
Vibration Analysis		+	+		+			+
Gel Permeation chromatography	+	+			+	+	+	
Dissolved Gas Analysis (DGA) & gas ratio analysis	+			+			+	+
Furan Analysis	+			+		+		
Moisture/Water content	+			+				
Resistivity, Acid Number (or Acidity), Interfacial Tension (IFT) and DDF				+				
Degree of Polymerisation (DP)	+							
Dielectric loss angle (DLA)			+	+		+		

Table 1.5: Various diagnostic tools used for the condition assessment of transformers [71]. Sign «+» indicates the capability of each diagnostic in detecting defects in that particular component:

- 1) Solid insulation (moistening, dirtying, destruction).
- 2) Magnetic system (core compressing, component to tank insulation damage, etc.).
- 3) Windings (buckling and other deformations).
- 4) Transformer oil condition.
- 5) Systems of oil cooling, treatment and protection.
- 6) Bushings.
- 7) Voltage regulators and contact system.

The advantage of the RF PD measuring technique over conventional systems is that it can be performed while the transformer is on-line using several sensors. The advantage of measuring on-line is that the PD evaluation may allow a statement about the actual condition of the insulation, because only in this case the electrical and thermal loads of the insulation are realistic [15]. On-line testing also allows the operator during the whole service life to monitor the condition of the insulation continuously, since the equipment can remain in service. [15] However, the RF

technique cannot be used during acceptance tests (in the factory or on-site after installation) because no indication of the discharge level in pC is possible. Power transformers are not discharge free [31] and since the minimum PD level in [pC], as is indicated by the existing standards, cannot be evaluated by the RF measuring equipment, it is not possible to assess in such a way the criticality of a defect.

The only way to assess the criticality of the PD with the RF technique is by identifying the PD based on its pattern and location and then by judging based on already existing experience [30, 31]. Experiences show that in practice, two types of patterns are measured [31]:

- 1) Regular PD patterns, which are patterns that are characteristic for a power transformer in good shape and
- 2) Irregular PD patterns, which are patterns that represent intolerable PD sources that can relate to insulation defects after manufacturing or aging effects during service life.

The distinction between the two categories can be made by comparing the newly measured pattern to the patterns of an extensive PD database with regular or irregular patterns. Important information for the database can be obtained during the one hour voltage-induced test of the transformer [31, 54]. Regular PD patterns can then be recorded of PDs that are within acceptance levels. Later, during in-service measurements, the general trends of the detected PD can be periodically monitored to detect other regular or irregular PD patterns [31, 45]. This is demonstrated in Figure 1.9. This way the RF PD measuring technique can provide an early warning system of the insulation condition.

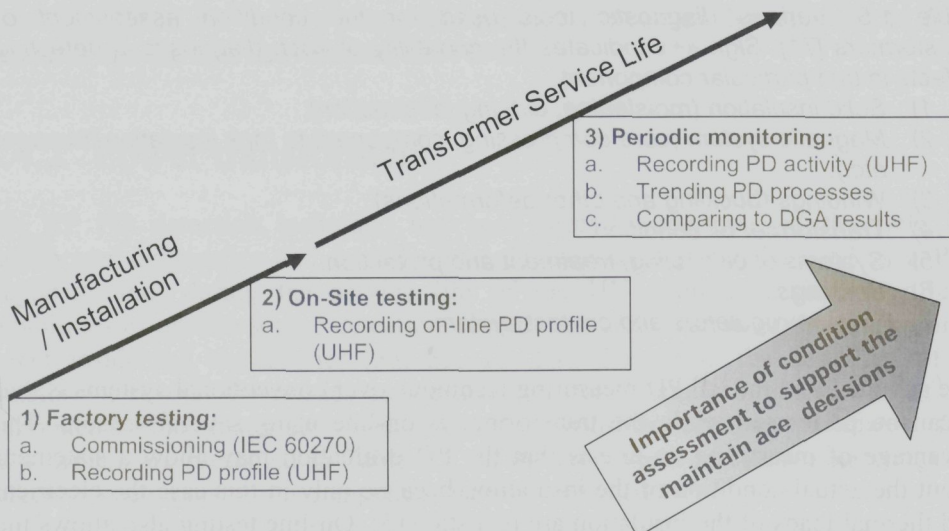


Figure 1.9: General usage of the RF PD measurements as a diagnostic tool in HV power transformers [15, 33].

RF PD detection in transformers is achieved by placing RF antennas, that can decouple the electromagnetic waves traveling in the oil, with view inside the transformer tank. This is required because the electromagnetic waves in the RF range are trapped within the steel tank since it acts as a Faraday cage [72, 13]. In order to achieve a view of the RF sensors inside the transformer dielectric windows are built on the tank where the RF couplers can be mounted, as in the application of the RF technique on a GIS [49, 19, 37, 40]. However, most of the currently operating transformers do not incorporate these windows by design and hence it is impossible to apply the technique in such a way. Therefore several internal sensors have been developed that can be inserted via the oil-valve of the transformer.

## 1.5 Aim of the thesis

The final goal of this research is to develop a generalized sensitivity check procedure for the non-conventional RF PD measurement methodology that will be applicable for all HV equipment. To achieve this goal the following research items have to be addressed in detail:

- The PD electromagnetic phenomena in terms of:
  - Their frequency content
  - Propagation inside the HV equipment
  - Detection
- Identification of HV equipment related parameters, which are of importance for detection of the electromagnetic radiation emitted from PDs.
- Evaluation of the RF PD detection technique with attention on its effect on measuring the PDs of various defects.
- Proposal of a sensitivity check procedure based on the knowledge from GIS and the experiences of the author on the application of the RF PD measuring technique on HV equipment.
- Verification of the sensitivity check procedure on actual cases of HV components.

For the purposes of this research the thesis will focus on the sensitivity capabilities of the RF PD measuring technique in its application in the following types of HV equipment:

- 1) Power transformers, and
- 2) Accessories of XLPE power cable systems.

The reason for choosing these two types of HV equipment is because of their different structure, which differentiates the application of the RF technique in each case. This way a generalized sensitivity check procedure can better be evaluated.

## 1.6 Thesis Layout

The thesis focuses on how each factor presented in Figure 1.5 can affect the PD detection capabilities of the RF measuring technique. Thus each chapter will focus on each influencing factor. Towards the end of the thesis the on-site sensitivity check of the technique will be tested for the two types of HV component based on the conclusions and suggestions made in the previous chapters.

In Chapter 2 a study of the PD phenomena takes place. The inherent factors to the PD that affect its energy in the RF spectrum are examined. In addition the factors that affect the energy of the electromagnetic radiation are also studied. Finally a few examples of PD detection in the RF spectrum are demonstrated.

In Chapter 3 the effect on the electromagnetic signal propagation of the power cable and transformer structures is studied in detail. Conclusions are made on how the sensitivity of PD detection in the RF range can be affected by each HV equipment's structure.

Chapter 4 studies the influence of the RF PD measuring system from the detection of the signals to their output to the measuring equipment. The miscellaneous individual components of the RF detection circuit will be studied separately. The main focus of the chapter are the various RF sensors that are currently used to decouple electromagnetic waves, since their influence on the detected waves is defining to the sensitivity of the system.

In Chapter 5 the sensitivity check procedure is applied for the purposes of PD measurements in cable accessories. Experimental work to evaluate the proposed procedure is then demonstrated.

In Chapter 6 the sensitivity check procedure is applied for the purposes of PD measurements in transformers. Experimental work to evaluate the proposed procedure is then demonstrated.

Chapter 7 presents the conclusions drawn in this research concerning the sensitivity check procedure of the RF PD measuring technique in high voltage equipment. Suggestions for further research are also given.



## CHAPTER 2:

# Partial Discharges in the Frequency Spectrum

*In this chapter a study of the partial discharge phenomena takes place. Initially the inherent factors to the partial discharge that affect its energy in the radio frequency spectrum are examined. In addition the factors that affect the energy of the electromagnetic radiation are also studied. Finally several experiments with artificial defects are presented in order to evaluate the conclusions from the study of the partial discharge phenomena.*

## 2.1 Introduction

The basis of all electrical partial discharge (PD) detection methods is the detection of the impulse current generated by the charge transfer caused by the discharge. It appears in a wide frequency range and thus there are different PD measuring techniques that each measure at different frequency ranges. The two categories of electrical PD detection systems are shown in Figure 2.1 and their frequency range of operation is displayed.

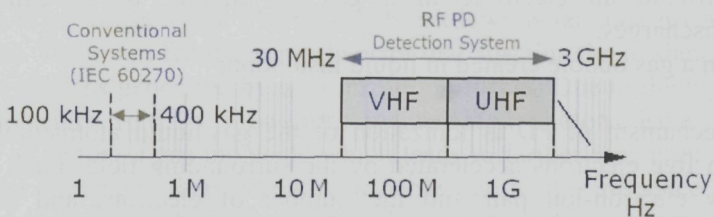


Figure 2.1: Frequency ranges of conventional and RF PD measuring systems.

The PD pulse currents have rise times in the nanosecond scale and exhibit a high energy spectrum in the frequency domain that may reach up to several gigahertz [72, 38]. PD measurements with conventional systems, based on the IEC 60270, operate in the frequency range below 1 MHz. These can be operated for wideband

or narrowband measurements, at pre-determined frequencies as defined by the measuring system. Narrow-band measurements are characterized by a centre frequency and its bandwidth between 9 and 30 kHz whereas wide-band measurements have a bandwidth between 100 and 400 kHz according to [2]. Conventional systems utilize a coupling capacitor connected in parallel to the test object in order to measure the charge transfer and voltage drop occurring at the circuit during the discharge. Because the measured charge displacement is not the exact charge transfer in the discharging area it is called the apparent charge.

The radio frequency (RF) PD measuring technique detects the transient electromagnetic phenomena generated by the charge displacement in the discharge area. A proper transducer is needed to de-couple the induced or radiated electromagnetic phenomena, as it will be presented in a later chapter of the thesis. The measuring frequency bandwidth for RF systems is in the VHF and UHF range. They can be operated for wideband or narrowband measurements, at frequencies where the signal-to-noise ratio of the signals is satisfactory for PD detection.

In this chapter the PD phenomena will be closely examined in order to study the relationship of the PD pulse current characteristics to the energy content of the pulse in the measuring frequencies of the RF PD measuring system.

## 2.2 The PD mechanisms

The definition for a partial discharge (PD) by [2] is: "*a PD is a localized electrical discharge that only partially bridges the insulation between conductors and which may or may not occur adjacent to a conductor*" (see Figure 2.2). Generally PD can be encountered in the following occasions in HV equipment:

- i) In a gas filled cavity inside a solid insulating material (Figure 2.2);
- ii) Along dielectric interfaces where a substantial tangential field strength is present;
- iii) Around an electrode in a gas (or liquid), the so-called corona discharges.
- iv) In a gas bubble created in liquid insulation;

The main mechanism of PD is ionization of the gas/liquid atoms/molecules by collision with free electrons accelerated by the surrounding field. Each ionization forms a new electron-ion pair and the number of electrons and ions grows exponentially forming avalanches. Electrons (-) move towards the anode while ions (+) move towards the cathode at much slower speed. An avalanche on its own cannot lead to breakdown unless a feedback mechanism supports its growth. Depending on the feedback mechanism two main types of discharges can be identified [68, 69]:

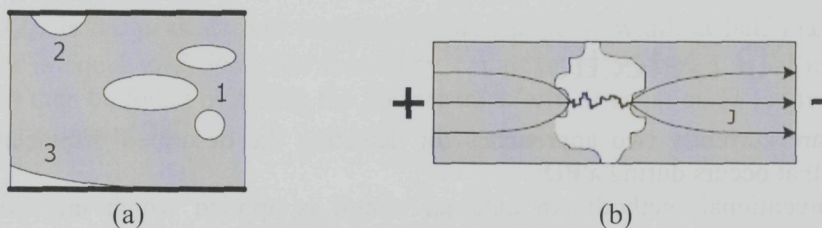


Figure 2.2: Examples of PD occurrence in the insulation of HV equipment in cavities:

(a) 1) surrounded by the dielectric, 2) with contact to an electrode, 3) detachment.  
 (b) Example of PD in a cavity where discharges only partially bridge the distance between the electrodes.

1) Townsend discharges

In Townsend discharges the main feedback mechanism is the “ $\gamma$  process”. When an ion collides with the cathode there is a probability  $\gamma$  that an electron is released from the cathode, which will eventually start new avalanches. There are also other secondary feedback mechanisms, such as by photons released from the excited atoms which either cause photo ionization when they hit another gas molecule or by reaching the cathode and releasing photo electrons.

In addition Townsend discharges occur mainly in gases at low pressure ( $p$ ) - a few mbar – between electrodes at large distances ( $d$ ), so that  $p \cdot d \ll 5$  bar.mm. For example, in solid insulation, at cavities of  $10\mu\text{m}$  to several millimeters length and containing gas at 1 Bar. The time to breakdown by this mechanism is in the order of  $\mu\text{s}$  and its breakdown voltage is defined by the Paschen’s curve.

2) Streamer mechanism

If the pressure or the distance are increased over 5 bar.mm the Townsend mechanism is no longer valid. The time to breakdown is far shorter (in the order of 1 to 100 ns). The main feedback mechanism that sustains the avalanche growth is then due to photons generated by the ionization process. Due to the high density of the gas molecules ( $p \cdot d > 5$  bar.mm) the released photons have an increased probability of hitting a gas molecule which leads to farther ionization. The growth of the initial avalanche then becomes unstable due to the influence of the space charge field at the head of the avalanche. The conditions for streamer formation are fulfilled if the number of ions in an avalanche reaches  $10^8$ .

## 2.3 PD Detection

There are currently two approaches for detecting the described displacement of charge that occurs during a PD:

1. Conventional method: An external circuit is applied which incorporates a coupling capacitor fitted in parallel to the HV equipment. When a PD occurs the HV equipment appears to the external circuit as a lumped capacitor with a depleted charge, then a replacement charge flows into the HV equipment and is measured using a quadruple and a detector.
2. RF detection method: The charge displacement at the PD site radiates electromagnetic (electromagnetic) radiation. Due to the very fast acceleration of electrons during the discharge (in the range of ns/mm) the energy spectra of the emitted waves extend to frequencies up to 2 GHz or more. This excites the HV equipment structure into various modes of electrical resonance that can be picked up by proper couplers.

It can thus be observed that the detection and measurement of PD is performed via the current generated by the charge displacement during the PD. Electrons initially at rest are accelerated and decelerated rapidly by the electric field which result in a short current pulse [67, 69]. In general the total duration of PD pulses is less than 1  $\mu$ s [63]. The high mobility of the electrons leads to a very fast rise time of the pulse in the sub-nanosecond range (it can be as short as 35 ps according to [83]), while the much slower ionic component shows rise times of some hundred nanoseconds [67]<sup>1</sup>. The spectral energy of pulses of such short durations reach up to the UHF frequencies of the spectrum. In fact the shorter the PD current pulses the more spectral energy appears at higher frequencies [38]. In the following paragraphs the effect of the PD pulse duration on the frequency-dependent emitted electromagnetic energy will be examined. In addition it will be studied how the PD pulse characteristics are defect dependent.

### 2.3.1 The PD current pulse

This can be demonstrated by using the Gaussian pulse as an example (shown in Figure 2.3(a)), which is similar to the shape of a PD current pulse. The Gaussian pulse is given by the following equation [83]:

$$i(t) = I_{\max} e^{-t^2/2\sigma^2} \quad (2.1)$$

---

<sup>1</sup> Typically, the ions have a speed in the order of 1 mm/ $\mu$ s, while the electrons move at about 100 mm/ $\mu$ s [68].

Where  $I_{max}$  is the peak current magnitude, and the pulse width at half maximum (*PWHM*) is equal to  $2.36\sigma$ . The frequency components contained in a Gaussian pulse can then be found by taking the Fourier transform of equation (2.1) giving the following equation [83]:

$$I(\omega) = I_{max} \sigma \sqrt{2\pi} e^{-\frac{\omega^2 \sigma^2}{2}} \quad (2.2)$$

Where  $\omega$  is the angular frequency ( $\omega=2\pi f$ ). For two different pulse durations (and hence rise-times) the frequency content is then calculated and displayed in Figure 2.3(b). The amplitude of each curve was normalized to demonstrate only the effect of the pulse rise and decay time in the frequency spectrum.

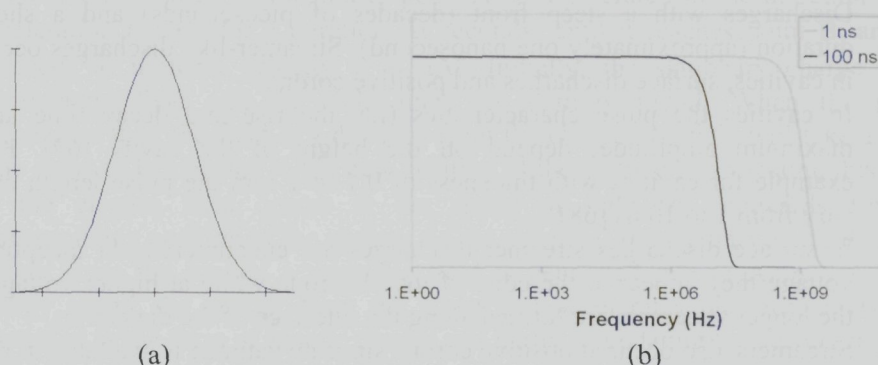


Figure 2.3: (a) A Gaussian pulse in time domain, and (b) the energy spectra of two Gaussian pulses of different rise-times in the frequency domain.

The duration and characteristics of the PD current pulses is determined by the physical conditions at the defect where the PD occurs. These conditions are defined by physical parameters such as the electric field, temperature, spatial distribution of charges and other products of prior discharges, physical properties of surfaces in the vicinity of the defect etc. [69]. Depending on the PD mechanism, however, two distinct shapes of PD pulses can be distinguished. Based on [69] and [68], depending on the PD mechanism, the following characteristics of the PD pulses can be identified:

1. Townsend-like discharges:

- *“The formation of the discharge is a “slow” process. The rise time of these pulses can be as long as several tens of nanoseconds and its duration can last several hundreds of nanoseconds.”* [69]
- Since for the occurrence of Townsend discharges a cathode is required to supply electrons, these discharges mainly appear within cavities and in negative corona (e.g. at a metallic needle at negative voltage in air). In unaged cavities within a dielectric, the initial mechanism are streamer

discharges, because no cathode is available. The overvoltage required to start a streamer is usually 5% higher than the voltage corresponding to the Paschen curve. After some time of successive discharging in the cavity (between 5 to 60 minutes depending on the dielectric material), due to the chemical changes at the walls of the cavity, organic acids are formed. Together with moisture in the air they form semi-conductive layers residing on the cavity walls that act as a cathode for the generation of Townsend discharges. During the transition time both types of discharges may occur.

- *“For cavity depths from 0.1 to 1 mm the pulse length can be from 80 ns to 0.8 $\mu$ s” [68].*

## 2. Streamer-like discharges:

- Discharges with a steep front (decades of picoseconds) and a short duration (approximately one nanosecond). Streamer-like discharges occur in cavities, surface discharges and positive corona.
- In cavities the pulse characteristics (i.e. the rise and decay time and maximum amplitude) depend on the height of the cavity [69]. For example for cavities with thickness of 0.1 to 1 mm the pulse length can vary from 1 to 10 ns [68].
- In surface discharges streamer discharges are encountered. At inception voltage they appear at the edge of the electrode while at higher voltages the longer streamers are formed along the interface of the dielectrics.
- Streamers also occur at positive corona since no cathode is available in the region of high field strength.
- Finally, in gas bubbles streamer discharges are also encountered due to the formation mechanisms of these bubbles which are initiated from streamer discharges [70].

Based on the above information and from the Gaussian pulse model it can be derived that the maximum frequency where discharges may appear will be between 0.6 MHz (0.8 $\mu$ s rise-time) and 2 GHz (1 ns rise-time). This indicates that there is a possibility that a Townsend-type PD might not be detectable for systems measuring above a few megahertz. Nevertheless discharges that occur at the following cases will be detected in frequencies in the VHF/UHF range:

- high electrical stresses (surface and positive corona discharges)
- in gases at high pressure (e.g. gas bubbles in the oil)
- in virgin cavities (e.g. cavities in power cable accessories during after-laying tests)

### 2.3.2 Electromagnetic radiation

During a PD discharge, electrons initially at rest are accelerated and decelerated rapidly by the electric field, which produces time-varying electric and magnetic fields that travel outward from the position of the charge. These radiated fields are called electromagnetic radiation. In this paragraph it will be theoretically shown how the electric component of the electromagnetic radiation is affected by the displacement current during a PD. Most of the theory described in this paragraph is taken from [82].

The excitation of the electromagnetic radiation from a single accelerated charge is demonstrated in Figure 2.4. The figure describes the situation where an initially static electric charge in vacuum at point A, is accelerated in the direction X. The acceleration  $a$  lasts for a duration  $\Delta t$  seconds, until it reaches point B, and then proceeds at uniform velocity  $v = a\Delta t$ . Initially, the stationary charge has an electrostatic field and the field lines are entirely radial. When the particle accelerates then the field at a distance from the charged particle will take a certain time delay to be updated to the new position of the particle<sup>2</sup>. In vacuum, this update of the electric field occurs at the speed of light ( $c$ ), outwards from the corresponding position of the charge. As the electrical field is thus updated/changed farther from the source, a magnetic field is generated due to Ampere's law. In energy terms, the energy from the force that accelerates the electron is partly expended in the form of kinetic energy and partly in updating the surrounding field in the form of electromagnetic radiation.

During the acceleration of the charge the update of the electric field lines occurs by way of a "kink", which propagates outwards along the field lines as a wave pulse. These kinks constitute the electric components of an electromagnetic radiation field which are accompanied by magnetic-field components as well, which are not shown here. Outside of the leading edge of the kink, the electric field is that of the original static charge at A. Inside of the trailing edge of the kink, the electric field is that of a charge in uniform translational motion.

---

<sup>2</sup> From Einstein's theory on relativity: No particle, energy, or information can travel faster than the speed of light.

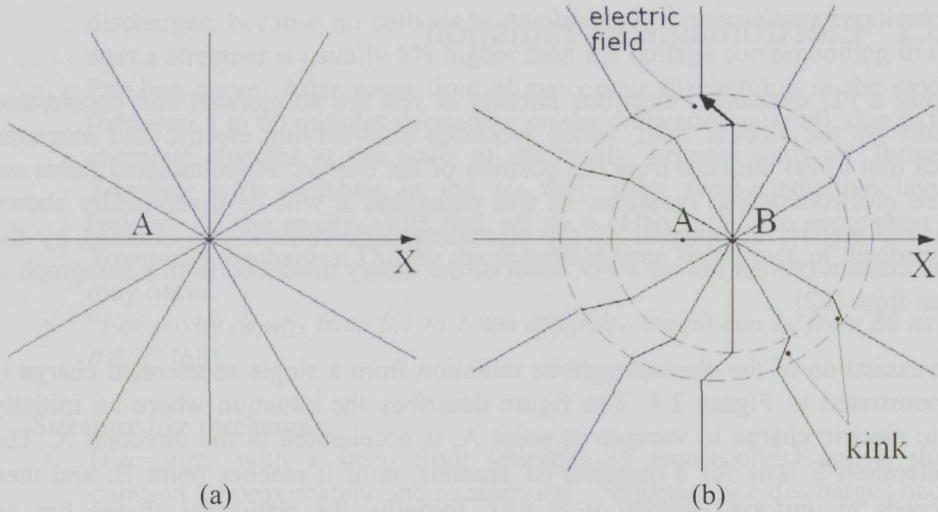


Figure 2.4: (a) An initially static electric charge in vacuum at point A. (b) The charge is accelerated in the X direction and produces electromagnetic radiation.

In the region of the kink the electric field can be divided in two components as it is shown in Figure 2.5.  $E_t$  is the transverse component of the electric field and  $E_r$  is the radial Coulomb field. The transverse component of the field is the one responsible for radiation because the Poynting vector  $\mathbf{S} = \mathbf{E} \times \mathbf{H}$  (where  $\mathbf{S}$ ,  $\mathbf{E}$  and  $\mathbf{H}$  are vector quantities) has a radial direction transferring energy away from the charge, as is demonstrated in Figure 2.5 (a). The radial component results in a Poynting vector completely confined within the spherical surface and thus does not radiate away from the charge.

Figure 2.5 (b) shows one of the field lines at time  $t$  after the initial acceleration, where the charge moving with a constant velocity  $v = a\Delta t$  reaches a point C farther in the direction of X. If it is assumed that the motion of charge is non-relativistic ( $v \ll c$ ) and that  $t \gg \Delta t$  so that the distance  $r = AB + BC \approx BC = vt$  and also  $r \gg c\Delta t$ . Then from Figure 2.5 we have:

$$\begin{aligned} \frac{E_t}{E_r} &= \frac{vt \sin \theta}{c\Delta t} = \frac{at \sin \theta}{c} = \frac{\alpha r \sin \theta}{c^2} \\ \Rightarrow E_t &= E_r \frac{\alpha r \sin \theta}{c^2} = \frac{q}{4\pi\epsilon_0} \frac{\alpha \sin \theta}{c^2 r} \end{aligned} \quad (2.3)$$

This is the usual expression for the radiation field of an accelerated charge, where it can be seen that the radiated electric field is proportional to the charge's acceleration. And for  $N$  moving charges:



$$E_t = \frac{Nq}{4\pi\epsilon_0} \frac{\sin\theta}{c^2 r} \left[ \frac{dv}{dt} \right] = \frac{1}{4\pi\epsilon_0} \frac{\sin\theta}{c^2 r} \left[ \frac{dJ}{dt} \right] \quad (2.4)$$

Where the electric current density  $J=Nqv$  is introduced. From equation (2.4) it can be concluded that the emitted radiation from a PD is proportional to:

- The changes of the pulse PD current: the faster the acceleration of the electrons (i.e. steeper current pulse), or the larger number of charges that take place in the discharge (i.e. the larger pulse amplitude), the higher the amplitude of the radiated field.
- The inverse of distance
- The angle of observation: The maximum radiated electric field occurs along the line that is perpendicular to the charge's acceleration.

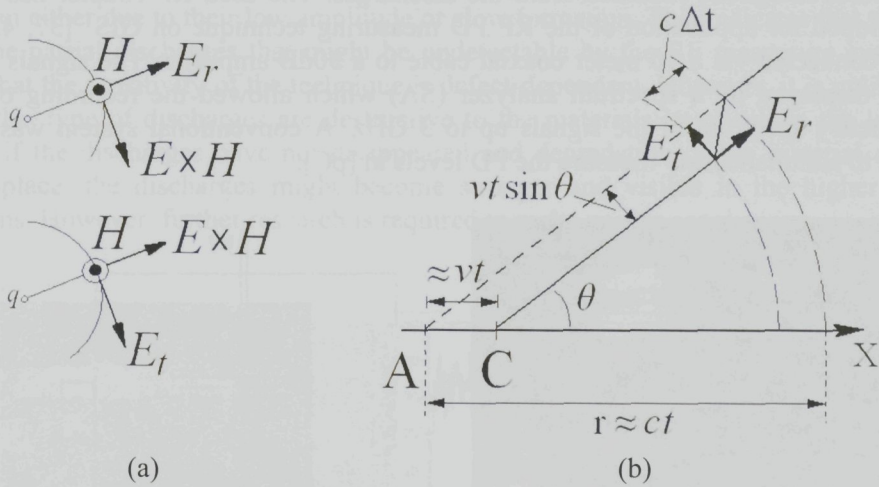


Figure 2.5: (a) The Poynting vector associated with each component of the electric field. (b) The components of the electric field at an arbitrary angle  $\theta$  caused by a charge  $q$  accelerated at a distance AB (see Figure 2.4) and then continuing to point C at constant velocity. Distance AB is considered very small compared to distance AC and hence is not displayed in the figure.

### 2.3.3 Measured spectra

Different defects were built in the laboratory to test their frequency response in the RF range. These will be presented in the following paragraphs for the case of transformers and cable accessories.

#### Transformer Defects

The artificial models that have been used are the following:

1. Positive (HV) corona in oil (see Figure 2.7)
2. Cavity discharges (see Figures 2.9 and 2.11)
3. Surface discharges (see Figure 2.8)

The models were inserted inside a glass box filled with oil as is demonstrated in Figure 2.6. An RF coupler was mounted on the glass box and was used to pick-up the electromagnetic radiation from the discharges. The used RF coupler has been developed for application of the RF PD measuring technique on GIS [37, 42]. It was connected via a 10 meter coaxial cable to a 30dB amplifier. The signals were then displayed by a spectrum analyzer (SA) which allowed the recording of the frequency spectrum of the signals up to 3 GHz. A conventional system was also used to simultaneously measure the PD levels in [pC].

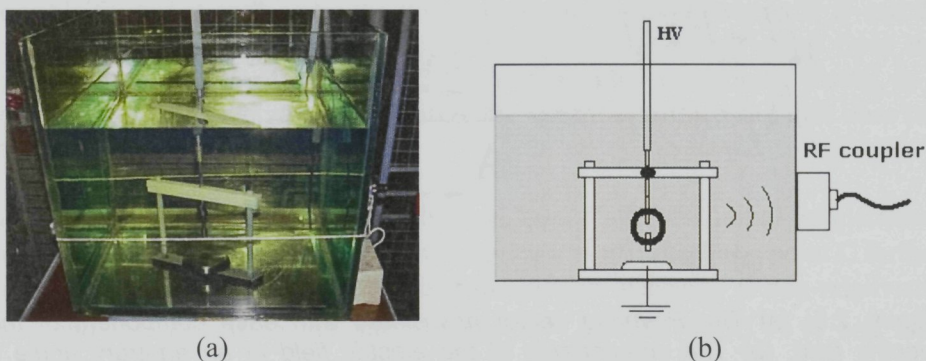
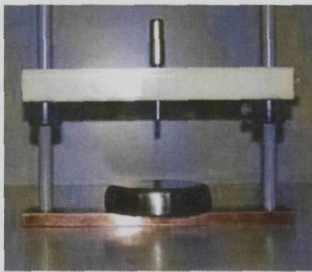


Figure 2.6: (a) Glass box filled with oil for insertion of artificial discharge models. (b) Schematic diagram of (a).

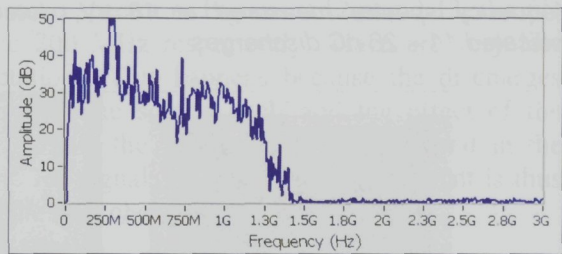
The frequency spectra of the discharges were obtained by taking the maximum of a total of 20 sweeps of 1 second using the SA in the displayed frequency range. The S/N was then calculated by subtracting from the PD spectra the noise spectra similarly recorded when no PD is present. Figures 2.7 to 2.11 display the calculated S/N from the PD generated by each model. Although within each sweep (1 sec) of the SA several successive discharge pulses occur, the successive pulses are expected to have similar shape (with small variations) in the short time of measurement [68, 67].

From the measured spectra in Figures 2.7 to 2.9, it can be seen that the maximum frequency where the PD can be detected is between 1.5 and 2 GHz. This confirms our expectations based on the Gaussian pulse model. In the case of the cavity defect of Figure 2.10 the measured spectra (see Figure 2.11) are very low in the RF range. The existence of discharges is indicated by the conventional measuring system. The exact discharge mechanisms that take place in this model are difficult to determine. This is because of the constant variation of the conditions within the cavity. Oil might have flowed within the cavity due to the oil pressure in the tank with gas slowly being released from the pressboard. For this reason it is possible that no discharges occur across the gap of the cavity but rather there are surface discharges occurring at the cavity walls. Another reason could be that the measured discharges do not originate from the artificial cavity but from several gas bubbles formed between the layers of the pressboards.

In any case, the resulting discharges are barely detectable by the RF measuring system either due to their low amplitude or slow formation. This indicates that there can be partial discharges that might be undetectable by the RF measuring system and that the sensitivity of the technique is defect-dependent. However, it is unlikely that this type of discharges are destructive to the materials involved. In the long-term if the discharges have not disappeared and degradation of the material does take place, the discharges might become stronger and visible in the higher RF regions. However, further research is required to make proper conclusions.

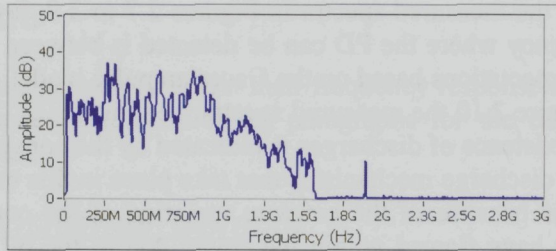


(a)



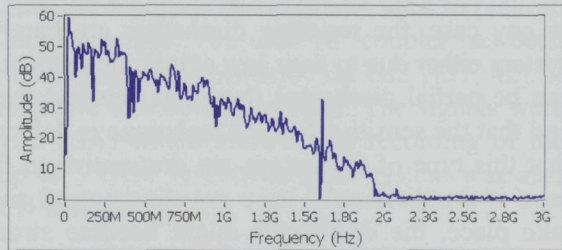
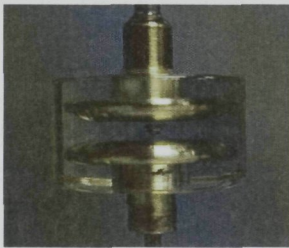
(b)

Figure 2.7: (a) The model for HV corona. Distance between electrodes is 4 cm. (b) S/N of the frequency spectra measured at 35 kV where the pulses were sufficiently frequent; the PD level was of 8-11 nC.



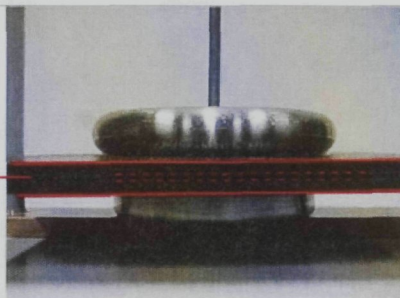
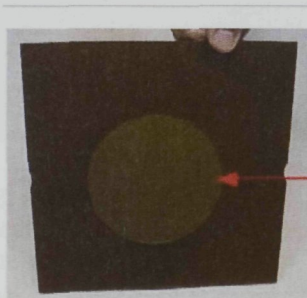
(a)

Figure 2.8: (a) Surface discharges will be generated due to the strong tangential electric stresses generated by the HV electrode placed on a piece of pressboard. (b) S/N of the frequency spectra measured at the inception voltage of 16 kV. The PD level was 2.2nC.



(a)

Figure 2.9: (a) Model for discharges in cavities. It incorporates an air-filled cavity (2 mm) in the middle of two brass electrodes, cast in polyester mass. (b) S/N of frequency spectra measured at 18 kV; detection with an IEC 60270 system indicated 11 – 20 nC discharges.



(a)

(b)

Figure 2.10: (a) A 1mm thickness pressboard sheet is drilled in the middle to create a cavity of 1mm radius. (b) The pressboard is then sandwiched between two thicker pressboard sheets (3mm thick).

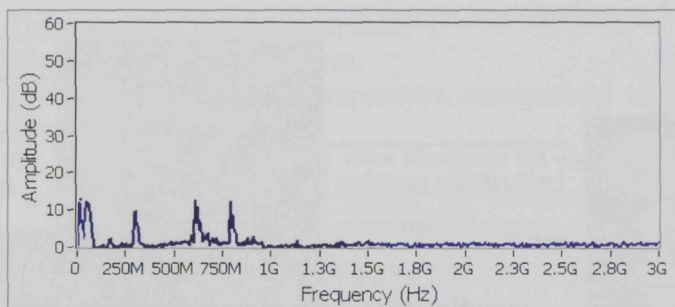


Figure 2.11: S/N of frequency spectra recorded by discharges generated in cavity of model in figure 2.10. The PD level was 300-500 pC at 18kV.

### Cable Accessory Defects

In addition, PD detection with the RF measuring system was tested in the case of cables in an actual cable set-up. The set-up consisted of a 150kV HV XLPE cable of 100m of length, two terminations and a click-fit type joint. Internal inductive RF sensors had been constructed close to each termination and joint. Two artificial defects were introduced in one of the terminations and at the joint of the setup:

1. Setup that generates surface discharges which is connected to the termination of the cable setup. (Figure 2.13)
2. Missing insulation screen at the cable/joint transition which generates incorrect distribution of the electrical field inside joint (Figure 2.12)

As it can be observed from the measured spectra in Figures 2.12 and 2.13, the PD can be detected up to 400 MHz and 200 MHz respectively, which are very low frequencies compared to our expectations. This happens because the discharges from the defects are measured far from the source itself and the effect of the termination or joint on the propagation of the signals is also considered in the measurements. The attenuation of the PD signals within the HV equipment is thus also important and will be studied in the next chapter of the thesis.

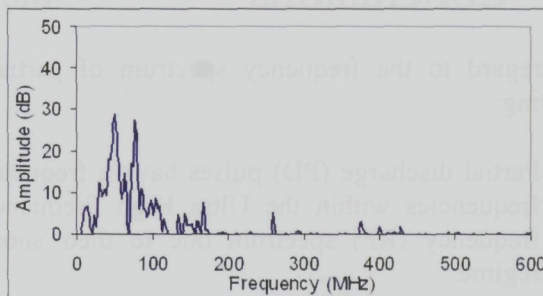
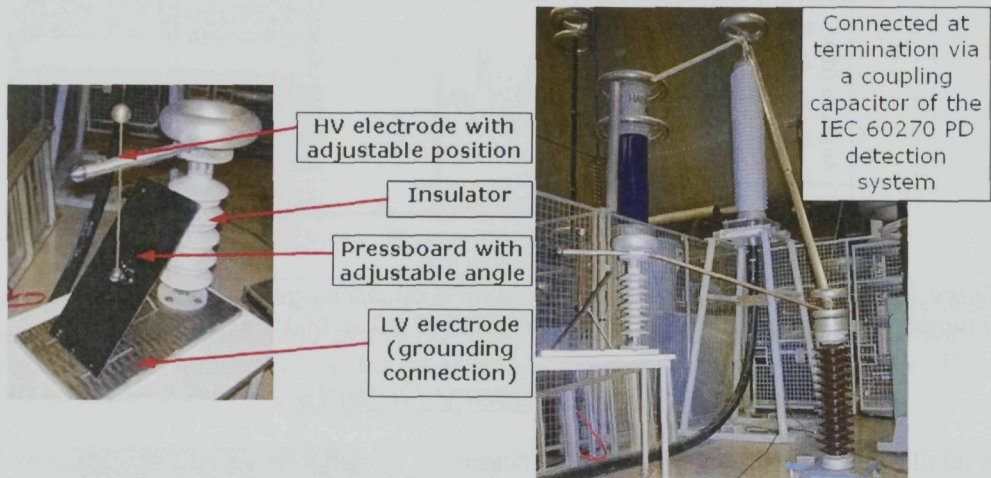
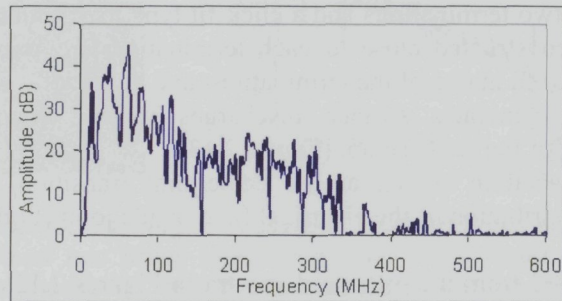


Figure 2.12: (left) Defect: Missing insulation screen at the cable/joint transition. (right) S/N of spectra measured at internal inductive sensor mounted close to the joint 33kV. Detection with an IEC 60270 system indicated 100pC.



(a)



(b)

Figure 2.13: (a) Defect: Surface discharges defect setup connected to the top of the termination. (b) S/N of spectra measured at internal inductive sensor in the same termination at 30kV, 50Hz AC excitation voltage. Detection with an IEC 60270 system indicated 100-300pC.

## 2.4 Conclusions

With regard to the frequency spectrum of partial discharges we conclude the following:

- Partial discharge (PD) pulses have a frequency spectrum that reaches up to frequencies within the Ultra High Frequency (UHF) range of the radio frequency (RF) spectrum due to their short duration in the nanosecond regime.
- The duration and amplitude of the PD pulse current is defined by the current conditions in the area of the discharge, such as:

- The strength of the electrical field.
  - The size of the discharge area.
  - The local gas pressure, temperature, conductivity of surfaces in the discharge area.
- Based on the Gaussian pulse model the maximum frequency where discharges may appear will be between 0.6 MHz (0.8 $\mu$ s minimum rise-time measured for Townsend discharges) and 2 GHz (1 ns maximum rise-time measured in Streamer discharges).

The following was concluded in terms of electromagnetic radiation emitted from PD:

- Due to the varying speed of the electrons forming the single or successive avalanches of a partial discharge energy is emitted away from the PD source in the form of electromagnetic radiation.
- The amplitude of the emitted electromagnetic radiation is proportional to:
  - The rate of change of electron speed and hence the duration of the PD pulse current
  - The amplitude of the PD pulse current.
  - The inverse of distance from the PD source
  - The angle of observation: The maximum radiated electric field occurs perpendicular to the charge's acceleration. No radiation occurs in the same axis of the charge displacement.
- In practice, detection of the electromagnetic radiation in the RF range was confirmed in the following cases:
  - Discharges occurring in the oil could be detected up to 2 GHz.
  - Discharges transmitted via the XLPE cable accessories could be detected up to 400 MHz.

### 3. The Effect of the Short Circuit

The effect of the short circuit on the discharge characteristics of the capacitor is shown in Figure 2. The discharge current is plotted against the discharge time. The discharge current is seen to increase with the discharge time. The discharge current is also seen to increase with the discharge time. The discharge current is also seen to increase with the discharge time.

The discharge current is plotted against the discharge time. The discharge current is seen to increase with the discharge time. The discharge current is also seen to increase with the discharge time.

The discharge current is plotted against the discharge time. The discharge current is seen to increase with the discharge time. The discharge current is also seen to increase with the discharge time.

The discharge current is plotted against the discharge time. The discharge current is seen to increase with the discharge time. The discharge current is also seen to increase with the discharge time.

The discharge current is plotted against the discharge time. The discharge current is seen to increase with the discharge time. The discharge current is also seen to increase with the discharge time.

## 2.4 CONCLUSIONS

With regard to the frequency spectrum of a pulse discharge, we consider the following:

1. Pulse discharge (PD) with a high frequency spectrum is obtained with a frequency with the PD with frequency (BPF) with a high frequency (HF) spectrum and a short duration in the discharge region.

The discharge current spectrum of the PD pulse current is defined by the current spectrum during the time of the discharge, such as:



# Electromagnetic Radiation in HV Equipment

---

*In this chapter the propagation of the electromagnetic waves within power cables and transformers is examined. The effect from the high voltage equipment structure on the propagation and attenuation of the emitted electromagnetic radiation is the main focus of the chapter. The end goal is to determine how the sensitivity of the RF PD measuring system differentiates between the two structures. This chapter is thus divided into two major parts: one for the case of power cables and one for the case of power transformers. Initially some theory on electromagnetic radiation is also presented, which outlines the basic themes and concepts of electromagnetism that are used in the later paragraphs.*

## 3.1 Introduction

The main concept of the RF PD measuring technique is that PD pulses, due to their short duration and rise times in the nanosecond regime, generate electromagnetic radiation at various frequencies within the range of the radio frequency (RF) spectrum. The generated electromagnetic radiation then propagates from the defect site along the HV equipment and is picked up by proper RF coupling electrodes. Along the propagation path inside the HV equipment discontinuities and resonance effects are encountered that strongly affect the characteristics of the traveling signals. Power cables and power transformers are two very different structures that transmit the emitted radiation in subsequently different ways. Power cables are long coaxial structures while transformers are enclosed metal cages with a very complex interior. Before entering into more details concerning the propagation of electromagnetic waves in each case it is necessary to present certain concepts of electromagnetism that will be used for our discussions in this chapter.

A more detailed theory of electromagnetism can be found in [64, 65, 84]. In the next paragraphs a few concepts of electromagnetism, as presented in these references, will be outlined.

### 3.1.1 Electromagnetic waves

Electromagnetic radiation is a continuous field change in space and time and can be visualized as a *wave*, as it is shown in Figure 3.1, which propagates away from the accelerating charge. It has both electric and magnetic components with the time-varying electric field generating a magnetic field (Ampere's law) and vice versa (Faraday's law).

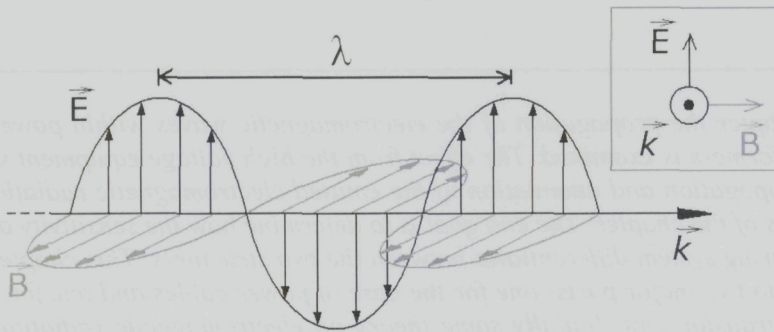


FIGURE 3.1: *Electromagnetic waves*

An important aspect of waves is *frequency*: The frequency ( $f$ ) of a wave is its rate of oscillation and is measured in hertz (Hz), where one hertz is equal to one oscillation per second. The distance traveled at one oscillation is called a *wavelength* ( $\lambda$ ) and is the distance between two adjacent crests or troughs of the wave. The wavelength of an electromagnetic wave that is traveling in free space<sup>3</sup> is *characteristic* of the wave's frequency and is called its characteristic wavelength. It is defined by the equation [65]:

$$\lambda = \frac{c}{f} \quad (3.1)$$

Where  $c$  is the speed of light. The characteristic wavelengths of signals in the UHF range and the VHF range are:

$$100 \text{ mm} \leq \lambda_{\text{UHF}} \leq 1 \text{ m}$$

<sup>3</sup> This is a property only of electromagnetic waves. Most other wave types cannot propagate through vacuum and need a transmission medium to exist.

$$1 \text{ m} \leq \lambda_{VHF} \leq 10 \text{ m}$$

In a medium other than vacuum, however, electromagnetic radiation travels slower at a ratio  $\eta$ , called the refractive index of the material. The refractive index is dependent on the material's permittivity and permeability and is defined as:

$$\eta = \sqrt{\epsilon\mu} \quad (3.2)$$

Where  $\mu = \mu_r\mu_0$  is the permeability and  $\epsilon = \epsilon_r\epsilon_0$  the permittivity of the medium. In this case, the wavelength of radiation is also dependent on the material properties.

### 3.1.2 Modes of propagation

Electromagnetic waves may be contained in a waveguide or a cavity resonator. Example of a waveguide is the coaxial line, which confines the electromagnetic wave to the area inside the cable, between the center conductor and the shield. A cavity resonator is a waveguide whose openings are closed by conductive surfaces hence trapping electromagnetic radiation within. Due to the boundary conditions imposed on the waves by these structures different modes of electromagnetic wave propagation occur from the interference of the electromagnetic fields. Hence the basic field patterns that can exist inside a waveguide are described by:

- The transverse electromagnetic modes (*TEM*), which have no electric and magnetic field in the direction of propagation.
- The transverse electric modes (*TE*), which have no electric field in the direction of propagation.
- The transverse magnetic modes (*TM*), which have no magnetic field in the direction of propagation.

*TE* and *TM* are referred to as the higher order propagation modes and can only propagate in the waveguide when the frequency of the waves exceeds a certain value. This value is known as the cut-off frequency of the mode and is denoted by  $f_c$ . At frequencies below  $f_c$ , the signal decays exponentially with distance as it attempts to propagate along the line and the higher order mode is said to be evanescent. There can be also hybrid modes of propagation which have both electric and magnetic field components in the direction of propagation. But these modes are not encountered in hollow metallic waveguides filled with a homogeneous, isotropic material or in cases of special symmetry such as the coaxial cable.

### 3.1.3 Propagation in HV equipment

The transient electromagnetic signals that are emitted by a partial discharge propagate inside the HV equipment in the basic mode ( $TEM$ ) but also in many higher order modes ( $TE$  and  $TM$ ), depending on the size and structure of the HV equipment.

Power cables have a coaxial structure and thus can be treated as waveguides for the electromagnetic waves. The transmission of energy in the line occurs totally through the dielectric inside the cable between the conductors. In the RF range, the wave propagates in the transverse electromagnetic mode ( $TEM$ ) and above a certain cut-off frequency, for which the wavelength (in the dielectric) is significantly shorter than the circumference of the cable, transverse electric ( $TE$ ) and transverse magnetic ( $TM$ ) waveguide modes can also propagate.

Transformers act as cavity resonators since the electromagnetic waves are trapped within its closed metallic tank and the oil serves as the transmission medium of the electromagnetic waves. Due to the complex inner structure of the transformer, complex propagation paths for the electromagnetic signals occur, which involve reflections at the conductive core and windings' structure. For that reason hybrid propagation modes may occur which makes a numerical calculation of the eventual field patterns impossible.

Hence, in the next paragraphs the propagation of electromagnetic radiation in power cables and transformers will be studied in order to determine a theoretical maximum sensitivity of the RF PD measuring technique.

## 3.2 Propagation in XLPE Power Cables

In the case of cables the electromagnetic waves are trapped between the cable's conductor and shield and are transmitted along its length. Until a certain cutoff frequency the electromagnetic waves propagate only in the transverse electric magnetic ( $TEM$ ) mode. Beyond that frequency, transverse electric ( $TE$ ) and/or transverse magnetic ( $TM$ ) modes can also propagate, as they do in a waveguide. In Chapter 2, while measuring the spectra of PD from artificial defects in cable accessories, it was observed that no signal was detected beyond 400 MHz. However, it could not be concluded that this observation was due to the PD source itself or the attenuation of the signals within the accessory and the cable itself until the measuring RF coupler. In the next paragraphs the excitation and propagation of the signals within a power cable will be studied.

### 3.2.1 Mode of propagation

The PD charge displacement induces currents at the surrounding conductive materials that constitute the cable. The emitted currents generate electric fields within the cable that can be found in *TEM* and in higher modes. The cut-off frequency of the (*TE<sub>11</sub>*) mode is the lowest of all the higher order modes and can be used to calculate the highest frequency below which signals propagate only in *TEM* mode. The following expressions for cut-off wavelength ( $\lambda_c$ ) and frequency can be used [15]:

$$\lambda_c \approx \pi(r + R) \quad (3.3)$$

and

$$f_c = \frac{v}{\lambda_c} \approx \frac{c}{\pi(r + R)\sqrt{\mu_r \epsilon_r}} \quad (3.4)$$

Where  $r$  is the radius of the inner cable conductor, and  $R$  the radius of the cable's outer sheath.  $\mu_r$  and  $\epsilon_r$  are the relative permeability and the relative permittivity of the XLPE insulation respectively. Equations (3.3) and (3.4) are accurate to within 5 % in case of  $R/r < 7$ .

The desired parameters for the evaluation of the equations can be found in literature [62]. High-voltage XLPE cables constitute of several layers of materials each with certain functionality. These layers are demonstrated in Figure 3.2 where the typical layout of a cross-linked polyethylene (XLPE) insulated high-voltage cable is shown. With reference to the figure the equation (3.4) parameters can be determined from the following [62]:

- The relative permeability of the XLPE insulation:  $\mu_r = 1$ .
- The relative permittivity of the XLPE insulation:  $2.3 \leq \epsilon_r \leq 2.5$
- Radius of the inner conductor according to the cross-section:  $15 \leq r \leq 30$  mm
- Thickness of the semi-conducting conductor screen:  $1 \leq d_1 \leq 1.5$  mm
- Thickness of the XLPE insulation according to the applied voltage and the cable cross-section:  $15 \leq d_2 \leq 30$  mm
- Thickness of the semi-conducting insulation screen plus semi-conducting swelling tape:  $1 \leq d_3 \leq 1.5$  mm

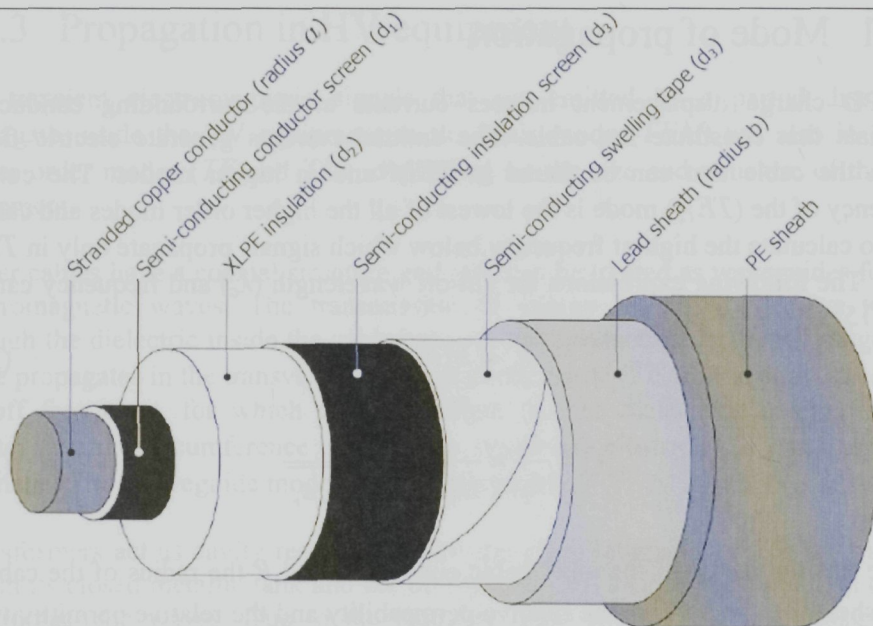


Figure 3.2: XLPE insulated cable

The minimum cut-off frequency can be calculated by taking the maximum values for all the parameters:  $\epsilon_r = 2.5$ ,  $r = 30 \text{ mm}$ ,  $d_1 = 1.5 \text{ mm}$ ,  $d_2 = 30 \text{ mm}$  and  $d_3 = 1.5 \text{ mm}$ . This leads to  $r = 30 \text{ mm}$  and  $R = 63 \text{ mm}$  and a minimum cut-off frequency that amounts to  $649 \text{ MHz}$ . The maximum cutoff frequency can be calculated by taking the minimum values for all the parameters:  $\epsilon_r = 2.3$ ,  $r = 15 \text{ mm}$ ,  $d_1 = 1 \text{ mm}$ ,  $d_2 = 15 \text{ mm}$  and  $d_3 = 1 \text{ mm}$ . This leads to  $r = 15 \text{ mm}$  and  $R = 32 \text{ mm}$  and a maximum cut-off frequency of  $1340 \text{ MHz}$ .

Since the lowest cut-off frequencies are larger than the detectable frequencies of the PD signals (see Chapter 2) it can be assumed that the principal mode of propagation along the cable is in the *TEM* mode. Thus the cable can be treated as a transmission line, which facilitates the estimation of electromagnetic signal attenuation along XLPE cables, as it will be studied in the following paragraphs.

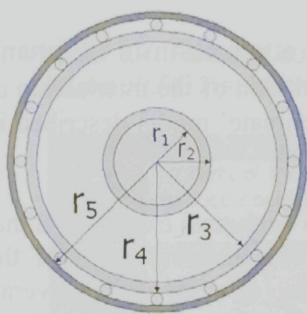
### 3.2.2 Attenuation

The high frequency (HF) attenuation in polymeric cables has already been investigated by Stone and Boggs in [21]. By using an equivalent circuit approach, Stone and Boggs showed that the semi-conducting screens of power cables have a significant influence on the attenuation of HF signals. In this chapter the same models used by Stone and Boggs will be used to calculate the VHF and UHF attenuation per meter in a 345 kV XLPE power cable. The theoretical results will

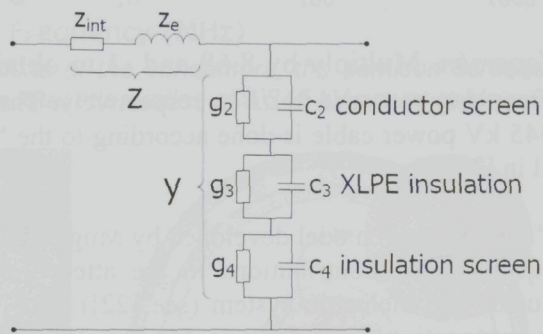
then be compared with measurements performed in an actual 345 kV XLPE cable. The equivalent circuit models that will be used for this purpose were developed by Mugala and can be found in [22].

Figure 3.3 (a) shows a cross-section of a typical XLPE insulated power cable. In the cross-section, the following layers can be distinguished:

- Inner conductor with radius  $r_1$
- Semi-conducting conductor screen with outer radius  $r_2$
- XLPE insulation with outer radius  $r_3$
- Semi-conducting insulation screen with outer radius  $r_4$
- Outer conductors with outer radius  $r_5$



(a)



(b)

Figure 3.3: (a) Cross-section of a typical XLPE insulated power cable. (b) Equivalent high-frequency model.

Figure 3.3(b) contains the equivalent circuit representation of the cable in figure 3.3(a).  $g_k$  and  $c_k$  correspond to the conductance and capacitance of the layer with outer radius  $r_k$ , with  $k \in \{2, 3, 4\}$ .  $z_{int}$  corresponds to the internal impedances of the core and the metallic screen conductors and  $z_e$  corresponds to the external impedance.

With reference to Figure 3.3(b), according to [22], the core conductor and lead/conductor screen contribute to the series impedance of the cable. The shunt path is made up of the admittances of the semi-conducting conductor screen, XLPE insulation, semi-conducting insulation screen and semi-conducting screen bed.

The purpose of modeling the power cable is to obtain the propagation factor of HF signals propagating through the cable. The propagation factor of electromagnetic waves in the TEM mode is given in the following formula:

$$\gamma = \alpha + j\beta = \sqrt{zy} \tag{3.5}$$

where  $\alpha$  is the attenuation constant in  $Np/length$  ( $1.00 Np = 8.686 dB$ ) and  $\beta$  is the phase constant (rad/length).  $y$  and  $z$  are the total shunt admittance and the total series impedance of the power cable respectively (see Figure 3.3(b)).  $y$  and  $Z$  can both be calculated on the basis of the geometric and material properties of the different layers of the power cable, as is described in [22].

When the propagation factor is known, the high frequency attenuation in the 345 kV power cable can be calculated by extracting the real part from the calculated propagation factor  $\gamma(\omega)$ :  $\alpha(\omega)$  (equation (3.5)), and filling in  $\alpha(\omega)$  into the following equation:

$$Attenuation = 20 \log e^{\alpha(\omega)} \quad (3.6)$$

in *Nepers/m*. Multiply by 8.68 and -1 to obtain the attenuation in *dB/m* and the frequency response in *dB/m* respectively. The calculation of the attenuation of the 345 kV power cable is done according to the 'approximate' model described in detail in [22].

The 'approximate' model developed by Mugala provides analytical expressions that can quantify the contributions to the attenuation by the different parts of the conductor and dielectric system (see [22]). It is suitable for studying the overall cable propagation characteristics, but is not well adopted for separating the effects from the diverse constituents of the cable. The approximate model can discriminate between the contributions from the dielectric system and the conductors and makes a further breakdown into their respective constituents:

$$\alpha_{approx} = \alpha_{conductors} + \alpha_{dielectric} \quad (3.7)$$

with

$$\alpha_{conductors} = \alpha_{inner-conductor} + \alpha_{outer-conductor} \quad (3.8)$$

and

$$\alpha_{dielectric} = \alpha_{semicon1} + \alpha_{semicon2} + \alpha_{XLPE} \quad (3.9)$$

In Figure 3.4 the percentage contributions of the conductors, the semiconducting screens and the XLPE insulation to the total attenuation of the 345 kV power cable are shown. The percentage contributions are calculated as the ratio of the attenuation of a particular layer and the total attenuation. Figure 3.4 clearly shows the dominance of the conductors in the low frequency region and the dominance of the semiconducting screens in the high frequency region.



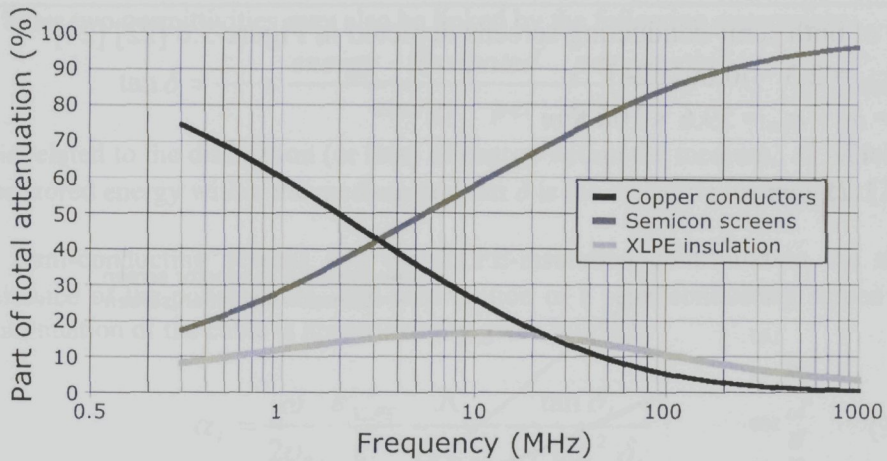


Figure 3.4: Relative contributions of the conductors, the semicon screens and the XLPE insulation to the total attenuation of a 345 kV power cable.

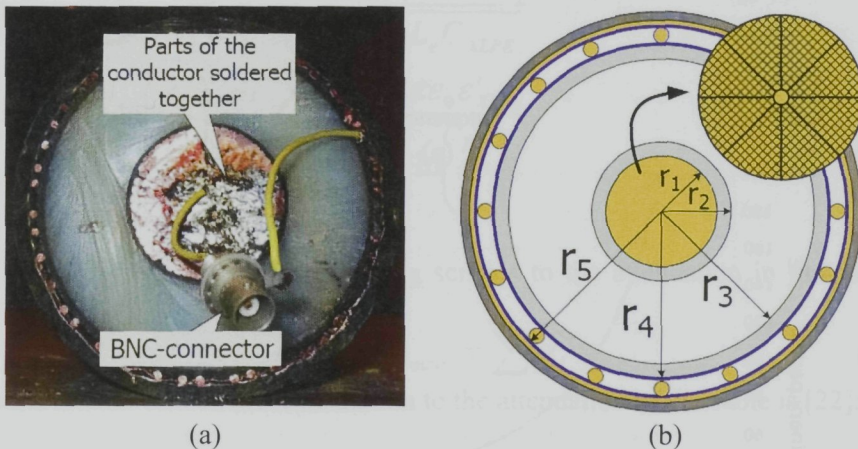


Figure 3.5: (a) 345 kV cable with BNC-connector. (b) Cross-section of the 345 kV power cable

According to the model presented in the previous paragraphs, a 345 kV power cable<sup>4</sup> is modeled, displayed in Figure 3.5. The following parameters were used:

- $r_1 = 24.5 \text{ mm}$
- $r_2 = 26.5 \text{ mm}$
- $r_3 = 53.5 \text{ mm}$
- $r_4 = 55.5 \text{ mm}$
- $r_5 = 58.5 \text{ mm}$

<sup>4</sup> Type: MX CC MK - Cu surface  $1 \times 1600 \text{ mm}^2 / 345 \text{ kV}$  made by Prysmian Cables & Systems

- $\epsilon^*$  of both semi-conducting screens depicted in Figure 3.6 [22] [24]
- $\epsilon_{XLPE}^* = 2.3 - j0.001$  [24]
- $\sigma_1 = \sigma_5 = \sigma_{cu} = 59.6 \times 10^6 \text{ S/m}$
- $n = 47$
- $\rho = 1.25 \text{ mm}$

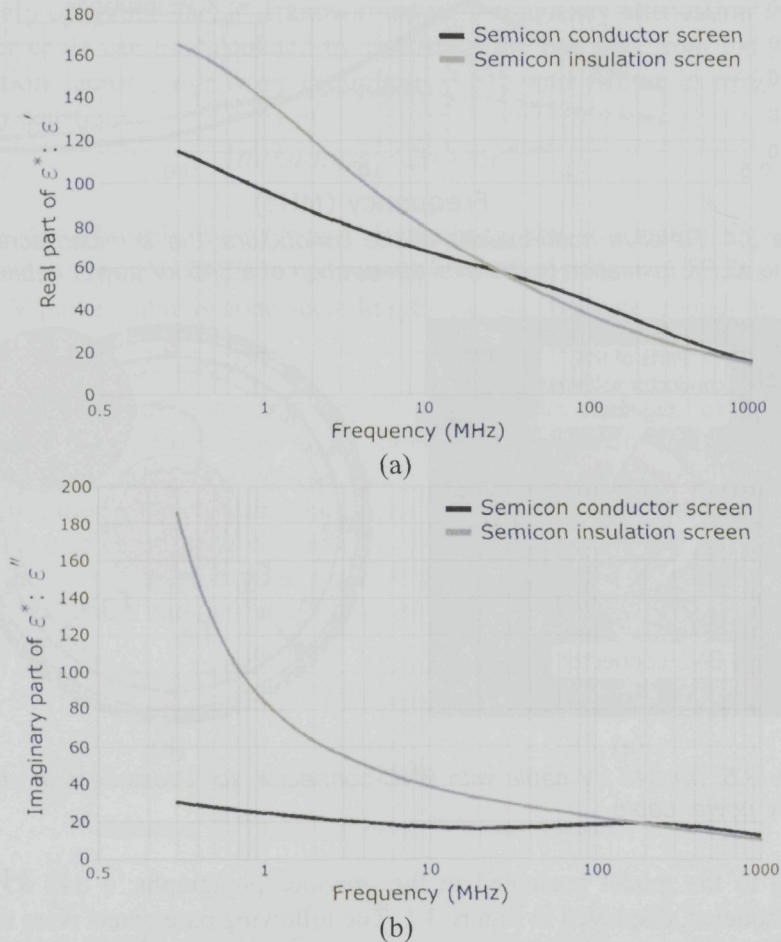


Figure 3.6: Relative complex permittivities  $\epsilon^*$  of both semi-conducting screens: (a) Real parts of  $\epsilon^*$ :  $\epsilon'$ . (b) Imaginary parts of  $\epsilon^*$ :  $\epsilon''$ .

Where  $\epsilon^*$  is the relative complex permittivity and is given by  $\epsilon_k^*(\omega) = \epsilon_k'(\omega) - j\epsilon_k''(\omega)$ , with  $\epsilon_k'(\omega)$  and  $\epsilon_k''(\omega)$  being the real and imaginary parts of the relative complex permittivity respectively, and  $k \in \{2, 3, 4, 5\}$  as indicated in Figure 3.5(b).

The latter two permittivities may also be linked by the following expression:

$$\tan \delta = \frac{\varepsilon''}{\varepsilon'} \propto \frac{\text{energy dissipated per cycle}}{\text{energy per cycle}} \quad (3.10)$$

$\varepsilon''$  is related to the dissipation (or loss) of energy within the medium,  $\varepsilon'$  is related to the stored energy within the medium and  $\tan \delta$  is the dielectric loss tangent [23].

The semi-conducting screens and the XLPE-insulation contribute to the shunt admittance of the power cable. The contribution of a semi-conducting screen  $l$  to the attenuation of the cable is approximately given by [22]:

$$\alpha_l = \frac{\omega}{2\nu_0} \frac{\varepsilon'_{XLPE}}{\varepsilon'_l} \frac{\Lambda_l}{\Lambda_{XLPE}} \frac{\tan \delta_l}{1 + \tan^2 \delta_l} \quad (3.11)$$

where  $\Lambda = \ln(r_{outer} / r_{inner})$  and  $\nu_0 = \frac{1}{\sqrt{L_e C_{XLPE}}}$

with  $L_e = \frac{\mu_0}{2\pi} \ln\left(\frac{r_5}{r_1}\right)$  and  $C_{XLPE} = \frac{2\pi\varepsilon_0\varepsilon'_{XLPE}}{\ln\left(\frac{r_3}{r_2}\right)}$

The contribution of all semi-conducting screens to the attenuation in the cable is [22]:

$$\alpha_{semicon-screens} = \sum \alpha_l \quad (3.12)$$

The contribution of the XLPE-insulation to the attenuation of the cable is [22]:

$$\alpha_{XLPE} = \frac{\omega}{2\nu_0} \tan \delta_{XLPE} \quad (3.13)$$

The semi-conducting screens and the XLPE-insulation make up the insulation system of the cable. The sum of the attenuation due to the semiconducting screens and the XLPE-insulation represents the total losses in the insulation system, which is the dielectric losses in the cable given by equation (3.9).

The core conductor and metallic screen contribute to the series impedance of the cable. The losses due to the core conductor are given by [22]:

$$\alpha_{inner-conductor} = \frac{\sqrt{\omega}}{2\nu_0 r_1 \sqrt{2} \sqrt{\mu_0 \sigma_1} \ln\left(\frac{r_5}{r_1}\right)} \quad (3.14)$$

where  $\sigma$  is the conductivity of the conductor. The losses due to the metallic screen conductors are given by [22]:

$$\alpha_{outer-conductor} = \frac{\sqrt{\omega}}{2\nu_0 n \rho \sqrt{2} \sqrt{\mu_0 \sigma_5} \ln\left(\frac{r_5}{r_1}\right)} \quad (3.15)$$

where  $n$  is the total number of conductors in the metallic screen and  $\rho$  the radius of one conductor in the metallic screen. The total losses due to the conductor system are given by equation (3.8).

The sum of the equations (3.9) and (3.8) gives an approximation of the total attenuation of the power cable, see equation (3.7). Finally using equation (3.6) the attenuation in the cable was calculated for the various frequencies as shown in Figure 3.7.

To verify the HF model of the power cable, the attenuation has also been measured using a vector network analyzer. A piece of power cable with a length of 12.56 m is connected to the network analyzer by soldering female BNC connectors to both sides of the cable as can be seen in Figure 3.5(a). Because the inner copper conductor of the cable is divided into smaller stranded conductors separated by semi-conducting material, the conductors are soldered together to use them all during the measurement.

The result of the measurement is shown also in Figure 3.7. Up to 200 MHz, there is a very reasonable agreement between theory and experiment. At frequencies greater than 400 MHz, the two graphs start to deviate. This deviation might be because the actual 345 kV power cable contains more layers than are used in the model i.e. the two moisture barriers and the copper foil directly under the polyethylene oversheath. Also, the inner conductor is considered solid in the model, while in reality the conductor is stranded and consists of more parts with semi-conducting material in between to suppress the skin-effect. These differences to the actual cable structure might result in the deviation between simulated and actual attenuation of the cable.

Nevertheless, from Figure 3.7 it can be concluded that electromagnetic PD signals propagating through a power cable are differently attenuated depending on their frequency. For signals in the UHF range the attenuation is such a way that it should be difficult to see any discharges beyond several meters. Therefore, when measuring PD in cable accessories it is required that the sensor is close to the accessory under test in order to have proper detection sensitivity.

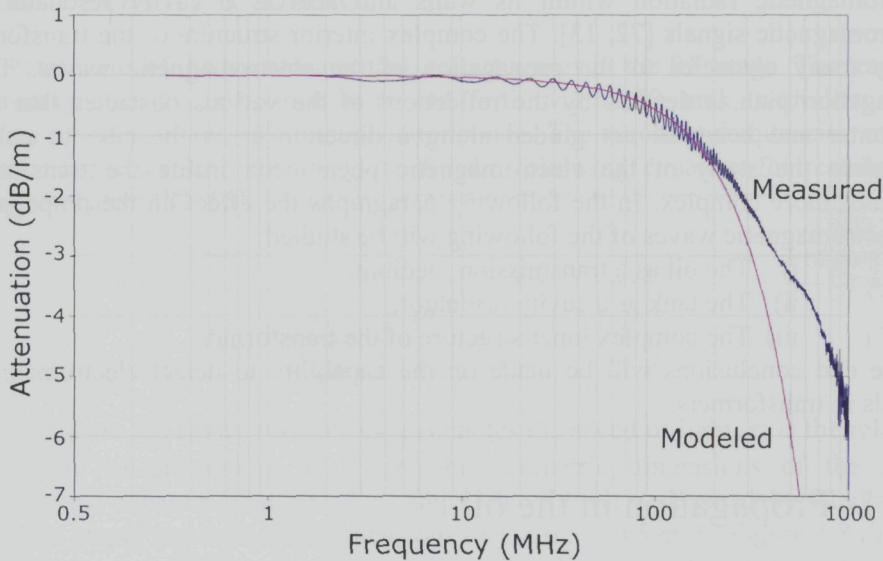


Figure 3.7: Calculated and measured HF attenuation of the 345 kV power cable

### 3.3 Propagation in power transformers

PD inside a transformer generates electromagnetic waves that propagate inside the oil at various directions. Being a closed metal cage, the transformer tank traps electromagnetic radiation within its walls and acts as a cavity resonator for electromagnetic signals [72, 13]. The complex interior structure of the transformer offers many obstacles to the propagation of the electromagnetic waves. Their propagation path is defined by the reflections at the various obstacles that they encounter and hence is not guided along a direction as in the case of cables. Therefore the study of the electromagnetic phenomena inside the transformer becomes more complex. In the following paragraphs the effect on the propagation of electromagnetic waves of the following will be studied:

- i) The oil as a transmission medium.
- ii) The tank as a cavity resonator.
- iii) The complex inner structure of the transformer.

In the end conclusions will be made on the capability to detect electromagnetic signals in transformers.

#### 3.3.1 Propagation in the oil

Initially the propagation of electromagnetic waves in the oil is examined. A *TEM* plane wave is assumed that propagates in oil with no other fields encountered in its propagation so no interference occurs. At high frequencies for insulators the conductivity  $\sigma \ll \omega\epsilon_0\epsilon_r$  and the phase velocity of the *TEM* waves is almost equal to the group velocity of the signal [84]:

$$v_g \approx v_\phi \approx \frac{1}{\sqrt{\mu\epsilon}} \quad (3.17)$$

This means that all frequencies travel at the same speed and no dispersion of the electromagnetic waves occurs. With a relative permittivity of  $\epsilon_r = 2.2$  and  $\mu_r = 1$ , the propagation velocity of the waves at high frequencies is calculated from equation (3.17) to be  $2 \times 10^8$  m/s.

Furthermore, with conductivity  $\sigma \ll \omega\epsilon_0\epsilon_r$ , the attenuation constant  $\alpha$  is given by [84]:

$$\alpha \approx \frac{\sigma}{2} \sqrt{\frac{\mu}{\epsilon}} \quad (3.18)$$

For the case of un-aged oil ( $\sigma = 10^{-14}$ ) this results in an attenuation of  $1.27 \times 10^{-11}$  Nepers/m or  $-1.1 \times 10^{10}$  dB/m using equation (3.22). Hence, oil is a lossless transmitter for the electromagnetic waves generated by the PD. Even in the case of aged oil where  $\sigma = 10^{-11}$  [71] the attenuation is  $-1.1 \times 10^{-8}$  dB/m.

### 3.3.2 A cavity resonator

The metal walls of the transformer tank reflect waves in the RF range. The trapped electromagnetic waves bounce back and forth within the tank, with low loss, creating standing waves by mutual interference. The resonant frequencies of the signals trapped in the tank are given by the following equation for rectangular cavity resonators [72, 65]:

$$f_{nmp} = \frac{c_0}{2\sqrt{\epsilon_r}} \sqrt{\left(\frac{m}{a}\right)^2 + \left(\frac{n}{b}\right)^2 + \left(\frac{p}{c}\right)^2} \quad (3.19)$$

Where  $f_{nmp}$  are the cavity resonances,  $c_0$  denotes the speed of light,  $\epsilon_r$  is the relative permittivity of oil and  $a, b, c$  are the geometric dimensions of the tank. Experimental measurements on this subject have been performed by Markalous [13] in an empty test tank with dimensions of  $1 \times 0.5 \times 0.5$  m. In Figure 3.8 (b) the spectrum corresponding to the UHF time signal of Figure 3.8 (a) is shown together with some cavity resonances (values of  $m, n, p$  are given in the boxes) as it was measured by Markalous. The calculated cavity resonances can be used to perform advantageous narrow-band measurements [13].

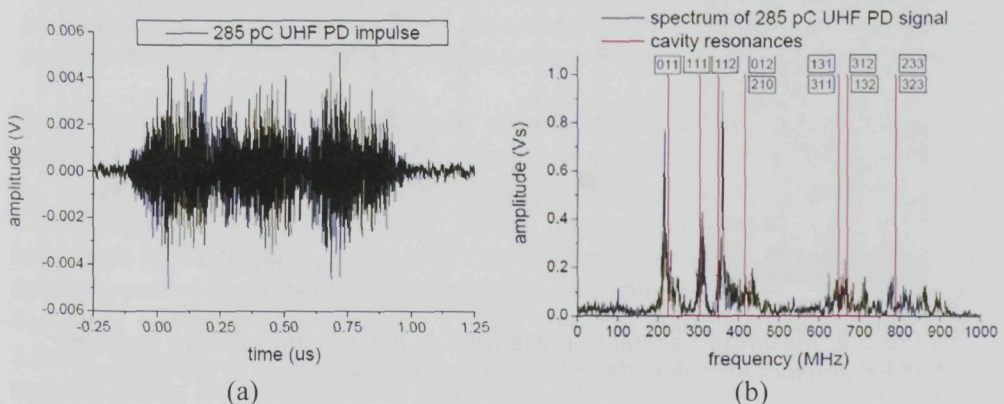
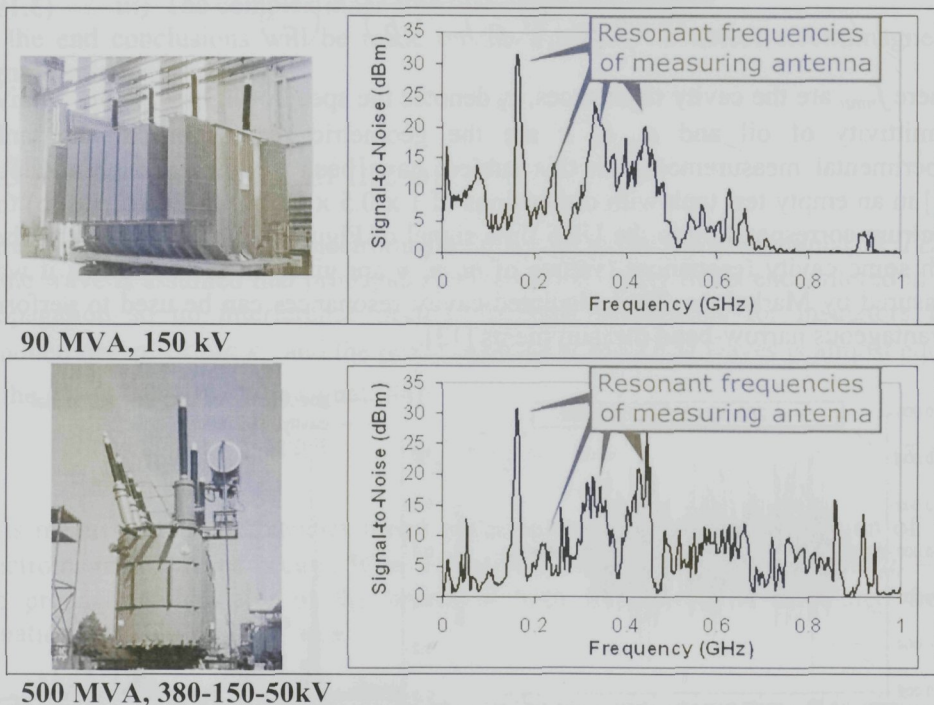


Figure 3.8: (a) UHF PD impulse (apparent charge 285 pC); (b) corresponding UHF PD spectrum with some dominant cavity resonances. Both pictures were extracted from [13]

In actual transformers the effect of the winding structure on the standing waves created within the tank should also be considered. Thus the cavity resonances that are determined by equation (3.19) will be detuned or absorbed by the windings [72, 13]. In order to determine the resonant frequencies in a transformer experimentally a pulse generator (of 45 V output, rise time of 400 ps and pulse width of 10 ns) was used to transmit pulses via one of the RF sensors mounted on the transformer. The transmitted pulses were then detected and measured by the other RF sensors mounted at the other sides of the transformer tank. A spectrum analyzer was used to record the frequency spectra of the received signals at each sensor. The signal-to-noise of the recorded spectra was then determined and the final results at all sensors were maximized to enhance the signal amplitude at the resonant frequencies. The experiment was performed on two transformers of different design and size, shown in Figure 3.9. Both transformers incorporated the same type of RF sensors and dielectric windows. The signal-to-noise ratios of the resulted maximized spectra are also displayed in Figure 3.9.



**500 MVA, 380-150-50kV**

*Figure 3.9: Maximized signal-to-noise ratio of the spectra as were detected at all RF sensors from injection of pulses in the tank via one of the sensors.*

The frequencies at which the resonant modes occur are at the various peaks of the spectra. However these resonances are not entirely due to the transformer tank. Several peaks occur also due to the resonances of the RF sensors used for the



measurement. These can be identified as the common peaks between the two cases of spectra of the two transformers, which will also be identified in Chapter 4 when measuring the frequency response of these RF sensors. It can be observed from the graphs that the 500 MVA transformer (larger tank) has higher resonant frequencies than the 90 MVA transformer (smaller tank). It is not possible to say why this occurs since it may be affected by different parameters such as the relative location of the sensors and the construction of the transformer.

The RF antennas pick-up the standing waves that are generated in their vicinity. These standing waves are the result of transmitted electromagnetic signals that travel different propagation paths until they reach each receiving sensor. In time domain an example of detected signals is displayed in Figure 3.10 along with the original injected pulse. The dispersed shape of the received pulse is mainly due to the multiple internal reflections of the signal at the tank walls and the obstacles introduced by the transformer winding circuit [13, 38]. A closer examination of the detected pulse in time domain follows in order to support the above statement.

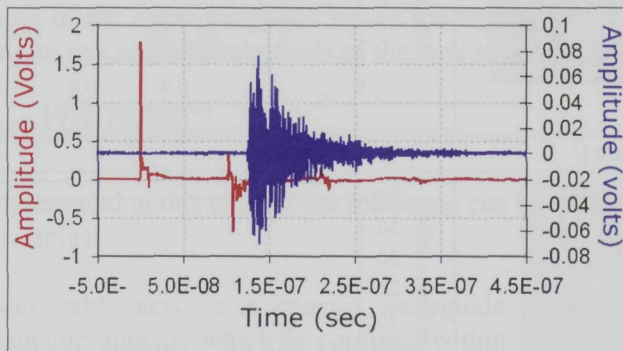
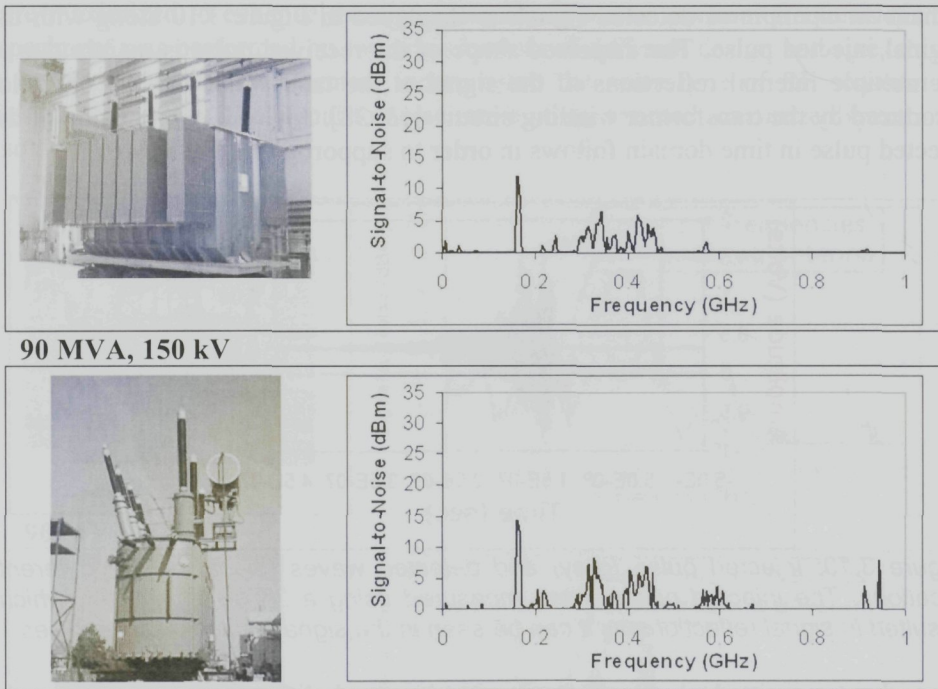


Figure 3.10: Injected pulse (grey) and detected waves (black) at two different locations. The injected pulses were measured using a 25 dB attenuator, which resulted in signal reflections as it can be seen in the signal as successive pulses.

Since the transmitted electromagnetic signals travel different propagation paths until they reach each receiving sensor, the electromagnetic waves that have traveled the shortest propagation path appear first at the beginning of the recorded signal. Electromagnetic waves following longer propagation paths, due to farther reflections inside the tank, arrive with certain time delay and correspond to the long decaying part of the signal as it can be seen from Figure 3.10 [38]. The beginning of the signal in Figure 3.10 is around  $1.3 \times 10^{-7}$  seconds and the signal resonates until  $3.2 \times 10^{-7}$  seconds. This indicates that, for a propagation speed of  $2 \times 10^8$  m/s, signals arriving within the indicated time range have traveled up to 38 m longer paths than the shortest propagation path of the first signals. This value is a rough estimation since the end of the pulse is not clear from the noise level and also the dispersive effect of the windings on the signals was not considered.

### 3.3.3 Effect of inner structure

Due to the complex interior structure of the transformer, the emitted radiation will encounter many boundaries at obstacles inside the tank. Such obstacles are the windings, the core structure, the tap changer setup (if it is located inside the tank) and the tank walls. At the different conductive surfaces the radiation will totally reflect. In addition at the complex structure of the windings, the multiple boundary conditions at the different materials that make the windings will result in diffraction of the incident signals. The resulting waves will additionally interfere with each other resulting in standing waves and different modes of propagation.



**90 MVA, 150 kV**

**500 MVA, 380-150-50kV**

*Figure 3.11: Signal-to-noise ratio of the spectra detected at the RF sensor placed to the opposite side of the tank than the injecting sensor.*

The effect on the signals is evaluated experimentally from the injection measurements that were presented in the case of the two transformers in the previous paragraph. In Figure 3.11 is displayed the signal-to-noise ratio of the spectra of the detected signal at the RF sensor mounted on the opposite side of the transformer than the side of the injecting sensor. This way the transmitting and receiving sensors are at opposite sides of the tank (as is displayed in Figure 3.12) and the windings obstruct the transmission from one sensor to the other. It can be

seen that the transmission of the injected signals across the windings is very weak and hinders the sensitivity of the RF sensor to the injected signals.

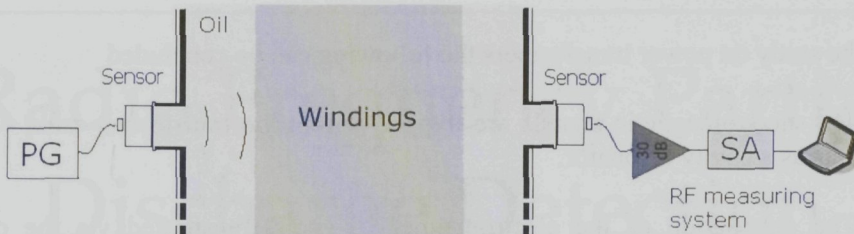


Figure 3.12: The windings obstruct the transmission of the injected pulses.

The main factor that affects the sensitivity of the technique is the position of the RF sensor relative to the PD source. Optimum sensitivity of the RF PD measuring technique is achieved when the sensor is in direct sight to the PD source. The sensitivity deteriorates when the view of the RF sensor is blocked by the windings of the transformer. The complex inner structure of the transformer distracts the direct propagation of the electromagnetic waves towards the sensor. Therefore for optimum sensitivity one sensor at each side of the tank should be placed.

### 3.4 Conclusions

From the study presented in this chapter the following can be concluded for the case of XLPE power cables:

- The power cable acts as a coaxial waveguide for the propagation of electromagnetic signals, which is confined within the space between inner and outer cable conductors.
- Below 600 MHz electromagnetic signals travel in TEM mode only and the power cable can be treated as a transmission line.
- Beyond 10 MHz, the attenuation of electromagnetic signals propagating along the power cable, increases linearly with the frequency of the signals:
  - At 100 MHz, the attenuation is - 0.6 dB/m
  - At 300 MHz, the attenuation is - 3 dB/m
  - At 500 MHz, the attenuation is - 6 dB/m
- The detection area of the electromagnetic signals has to be a couple of meters away from the PD source in order to detect in the VHF/UHF range. At farther distances detection of the electromagnetic signals from the PD can be done only at the HF/VHF range.

- The RF sensors used for PD detection in power cables should have their operating bandwidth in the VHF range.

From the study on power transformers the following can be concluded

- The electromagnetic signals are trapped within the transformer tank, which acts as a cavity resonator.
- The attenuation of the electromagnetic signals transmitted via the oil is negligible.
- The complex inner structure of the transformer presents obstacles to the direct propagation of the electromagnetic waves. Signals reaching the other side of the transformer will be highly attenuated.
- Detection of electromagnetic signals in the UHF range is possible when the RF sensor is located at the same side of the tank as the PD source.
- The sensitivity deteriorates when the view of the RF sensor is blocked by the windings of the transformer.
- One RF sensor placed at each side of the transformer is required for optimum sensitivity to all areas around the tank.

# Radio Frequency Partial Discharge Detection Circuit

---

*In this chapter it will be described how the sensitivity of the PD measurements is defined by the RF PD detection circuit itself. The PD detection circuit consists of individual components with different transfer characteristics that influence the detected signals. Each component will be initially identified and then its frequency response will be measured in order to observe its influence on the detected signals. Extra focus will be given on the available types of RF sensors because of their key role in converting the electromagnetic signals to circuit currents.*

## 4.1 The RF PD detection circuit

A complete detection circuit as employed for the RF PD measurements is shown in Figure 4.1. The part of the detection circuit that permits the coupling with the electromagnetic signals is a sensor device designed for optimum operation at specific frequencies. The detected signals are transmitted via coaxial cabling, a pre-amplifier and a filter, to a measuring device, which can be a spectrum analyzer or an oscilloscope.

The characteristics of the measured signals are defined by the individual transfer functions of each component of the detection circuit. A measure of the transfer function of a system is the frequency response, which can be determined by measuring the output of the system while the frequency of the input signal is varied. Then the ratio of the output voltage to the input voltage is taken and converted in decibels (dB)<sup>5</sup>. A sinusoidal function generator that can cover the range 0 > 500

---

<sup>5</sup> The frequency response is typically characterized by the magnitude of the system's response, measured in decibels (dB), and the phase, measured in radians, versus

MHz was used to generate the input signal at various frequencies, while the spectrum analyzer was used to measure the output voltage of the component under test. A detailed description of the frequency response measurements of each component is given in Appendix B. In this chapter the results of these measurements will be presented and the effect of each component on the sensitivity of the complete detection circuit is discussed.

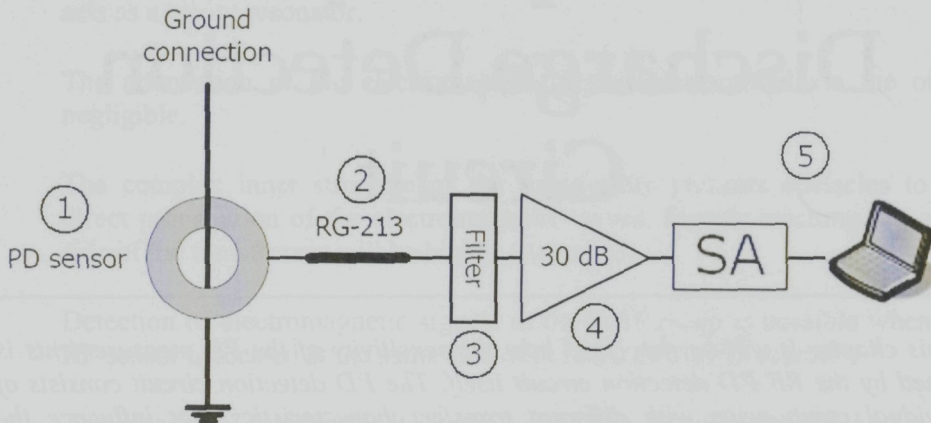


Figure 4.1: Schematic of the RF PD detection circuit, which consists of the following components:

1. An RF sensor
2. A coaxial cable (RG-213)
3. A protective filter mainly used to protect the RF amplifier against high-energetic low frequency disturbances picked up by the PD sensors.
4. An RF 30 dB pre-amplifier used to enhance the detected signals.
5. A measuring device, such as a spectrum analyser (SA) controlled by appropriate computer software.

The rest of the chapter is divided into two parts. The first part discusses the effect of the RF sensors on the sensitivity of the system. The second part discusses the effect of the other miscellaneous components of the RF PD detection circuit, as they were presented in Figure 4.1. A separate look is given to the RF sensors because of the various types of RF sensors that can be used for the de-coupling of the electromagnetic signals. In the end, the frequency response of the complete detection circuit will be determined, where it will be seen the choice of RF sensor plays a significant role on the system's sensitivity.

frequency. Since we are not interested in the phase difference between the input and output signals but rather on the time-averaged energy transfer we will consider only the magnitude of the system's response in dB.

## 4.2 The RF Sensors

Extraction of the transmitted electromagnetic fields generated by a PD is achieved by different means of electromagnetic coupling. Electromagnetic fields will interact with an appropriate detecting circuit and induce in them corresponding charges or currents. Three ways of electromagnetic coupling are employed for the detection of PD signals:

- i. Capacitive coupling: Via the capacitance created between the detecting circuit and the PD source. The voltage across this capacitance can be measured with high impedance equipment.
- ii. Inductive coupling: Via the mutual inductance between the source and the detection circuit. Current is induced in the detection circuit by the magnetic field produced by the source.
- iii. Radiated coupling: The type of coupling in which an electric current is induced in the detection circuit by electromagnetic radiation produced by the electromagnetic source.

Based on these coupling methods the extraction of the emitted PD signals in power transformers and cables is achieved as is demonstrated in Figure 4.2.

In the case of transformers an opening at the tank is required to allow extraction of the enclosed signals. This can be achieved either via the use of dielectric windows (similarly to GIS) or by using available openings on the tank, such as the oil-valves. A current probe can also be used at the grounding of the transformer tank to measure the induced currents. Finally, capacitive sensors can be used at the bushings in order to detect any induced currents.

In the case of cables extraction of the electromagnetic signals can be performed either with a current probe at the grounding of the cable sheath or via sensors internally built in the cable during the manufacturing process. The method of coupling for the internal sensors can be either capacitive or inductive, as it will be demonstrated in the later paragraphs.

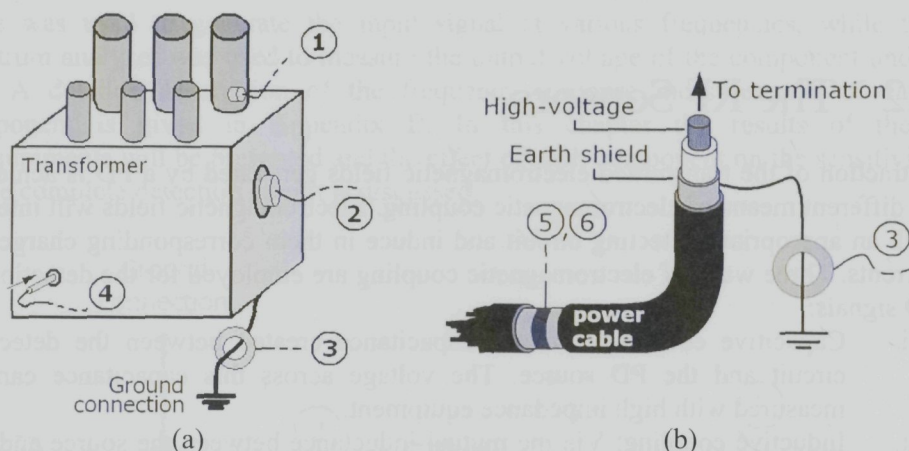


Figure 4.2: Possible PD detection methods in (a) transformers, and (b) power cable accessories.

1. Capacitive sensor at bushing (capacitive coupling)
2. Antenna on dielectric window (radiated coupling)
3. Current probe at grounding cable (inductive coupling)
4. Antenna inserted through an oil-valve (radiated coupling)
5. Internal capacitive sensors (capacitive coupling)
6. Internal inductive sensors (inductive coupling)

### 4.2.1 Sensor characteristics

Generally, a receiving sensor extracts power from the field in its vicinity and delivers it to a load or terminating impedance  $Z_L$ . In the circuit of Figure 4.3, the equivalent circuit of a sensor connected to the RF measuring circuit is shown. The sensor is represented by a generator having a current  $I$  (induced by the changes in the field) or voltage  $V$  (due to the charge displacement), and internal impedance  $Z_A$ .  $Z_A$  depends on the sensor material and construction and includes the RF equivalent circuit of the sensor but also the power losses due to heating at the sensor. Commercially available sensors already contain a matching circuit to match the sensor output impedance to 50 ohm load, which is the standard impedance for measuring equipment.

The sensor electrical characteristics are constant within a certain frequency range depending on its design and materials. Because the permittivity of the materials is complex and depends on frequency, the response of the sensor is also frequency dependent. The frequency range over which the impedance of the sensor remains



constant, within a given tolerance, is called the bandwidth of the sensor<sup>6</sup>. Hence, there can be narrow-band or broad-band sensors depending on the width of the frequency range of their bandwidth. Correspondingly, for PD detection with the RF measuring system, both narrow-band and wide-band measurements can be performed using the proper sensor.

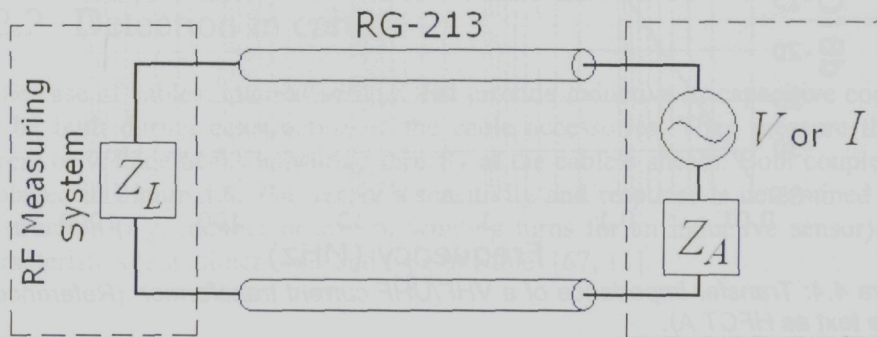


Figure 4.3: Equivalent circuit of a sensor connected to the measuring circuit

The bandwidth of a sensor is described by its *transfer impedance*. The transfer impedance can be measured by using an input signal of varying frequency but constant amplitude and then measuring the response of the sensor at the corresponding frequencies. Examples of transfer impedances of two inductive sensors (current transformers) are displayed in Figure 4.4 and 4.5. They were measured with the aid of a network analyzer by passing a known RF current ( $I_p$ ) through a conductor wire, which serves as the primary conductor for the transformer, and then noting the voltage ( $E_s$ ) developed across a 50-ohm load<sup>7</sup>. Then using the following equation the transfer impedance ( $Z_A$ ) could be estimated:

$$Z_A = \frac{E_s}{I_p} \quad (4.1)$$

Or, in dB:

$$Z_A (dB\Omega) = E_s (dB\mu V) - I_p (dB\mu A) \quad (4.2)$$

The transfer in Figure 4.4 displays a flat response in the RF frequency range of interest (VHF and UHF) with approximately 0 dB amplitude which neither attenuates nor amplifies the signals. It can thus be used for narrowband and wideband PD measurements.

<sup>6</sup> There can be other parameters that define the bandwidth of a sensor depending on the application. For example, in telecommunications, in the case of a log-planar antenna the bandwidth is defined as the frequency range where its polarization remains constant [Dys0].

<sup>7</sup> See Appendix B for a description of these measurements.

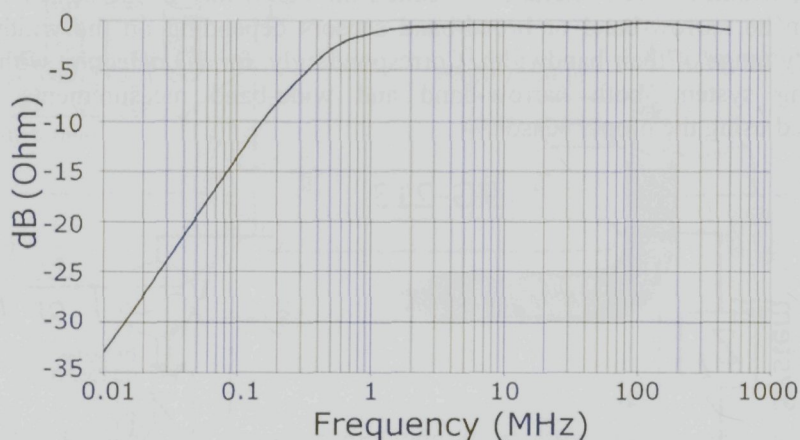


Figure 4.4: Transfer impedance of a VHF/UHF current transformer. (Referenced in the text as HFCT A).

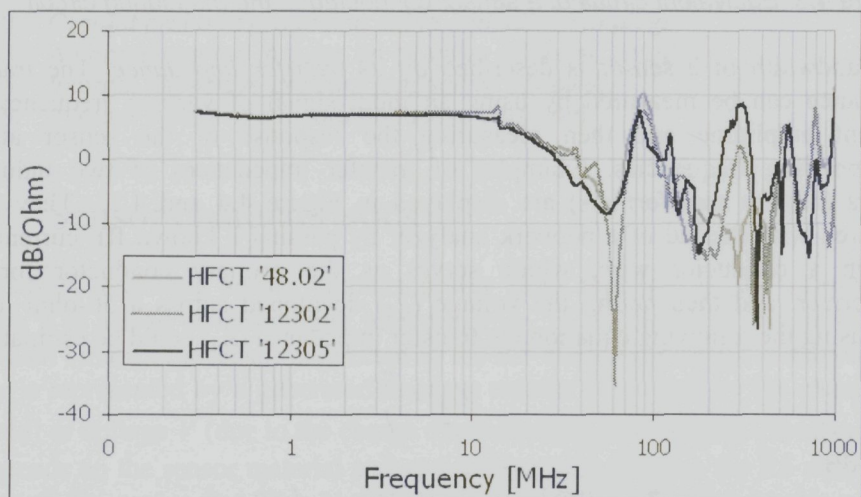


Figure 4.5: Transfer impedance of an LF/HF current transformer (Referenced in the text as HFCT B).

The frequency response in Figure 4.5 is flat up to 10 MHz and beyond that it is varying. This occurs because this current probe was designed to operate at lower frequencies in the HF range. In addition, for several current probes of the same model a varying response beyond its operating frequency band can be observed. Nevertheless, it can be used for narrow band measurements at the VHF/UHF frequencies where its response is 0dB or higher.

It should be noted that for the case of antennas the transfer impedance as defined here is not sufficient to describe their response to detected signals. Antennas are

anisotropic devices and their reception (or radiation) characteristics are different in each direction from the antenna [65]. Thus antennas have a “preferred” direction or directions of reception. This is partly due to the effect of the dependence of the radiated field on the observation angle, as it was mentioned in chapter 2.

## 4.2.2 Detection in cables

In the case of cables, internal sensors that provide inductive or capacitive coupling can be built during construction of the cable accessories. They measure the PD current or voltage peaks appearing directly at the cable’s sheath. Both couplers are displayed in Figure 4.6. The sensor’s sensitivity and response is determined by its construction (e.g. number or size of winding turns for an inductive sensor) cable characteristics (e.g. dimensions and type of cable) [67, 11].

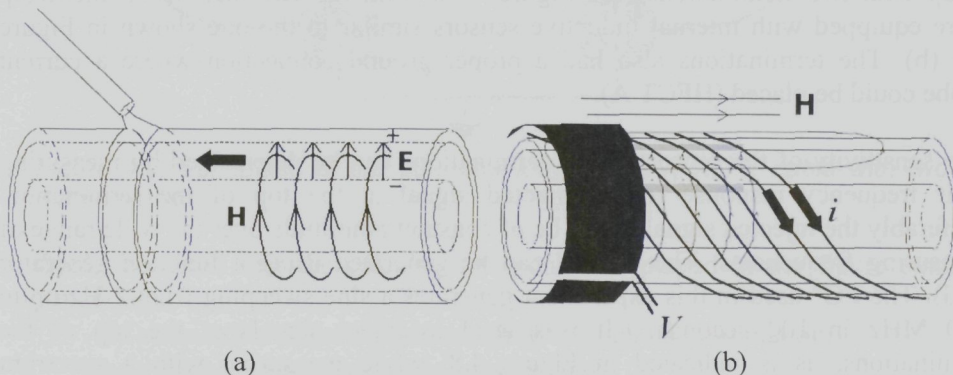


Figure 4.6: Examples of (a) capacitive, and (b) inductive internal sensors as employed in cables [11]. (a) The charge displacement is picked up via an interruption at the cable’s metallic sheath. (b) Earth screen of helically wound wires induces current to a single-turn coil connected to the measuring equipment.

A current probe can also be used at the grounding of the cable sheath to detect the induced currents (see Figure 4.7). Current probes are essentially current transformer devices whose primary winding is the grounding conductor where they are clamped on. In general, the sensitivity of internal sensors is expected to be higher than current probes because the detection occurs directly at the cable’s sheath. When a current probe is used the current that is measured at the grounding conductor is generated by the voltage difference that appears across the wire once the PD current transient is terminated at the corresponding cable end. Therefore, the current that passes through the primary conductor of the probe is affected by the reflection coefficient at the interface of the grounding conductor and cable sheath.

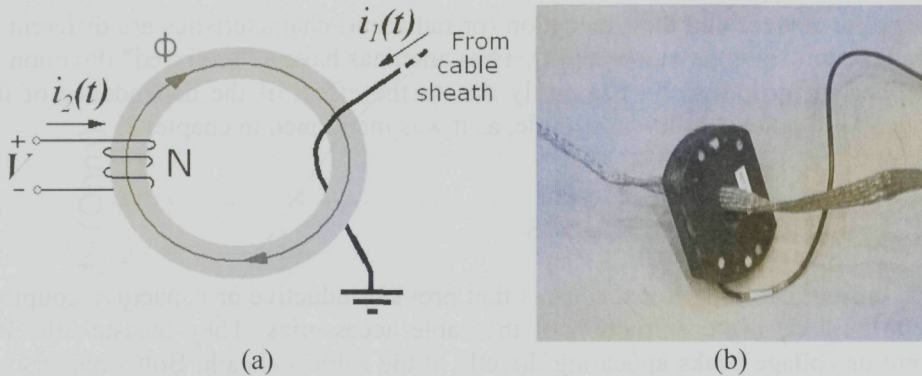


Figure 4.7: (a) Schematic diagram and (b) photograph of a current probe.

In order to compare the sensitivity of current probes and internal sensors the following setup was used in the laboratory: a 30-meter long, 345 kV, XLPE cable setup with two terminations (see Figure 4.8). Both the terminations in the setup were equipped with internal inductive sensors similar to the one shown in Figure 4.6 (b). The terminations also had a proper ground connection where a current probe could be placed (HFCT A).

The sensitivity of the sensors at the terminations can be determined by measuring their frequency response to an injected signal at the top of the termination. Preferably the injected signal has to be of constant amplitude over the wide range of measuring frequencies. The desired can be generated using a function generator (FG). The FG<sup>8</sup> used in this experiment generates a sine sweeping from 1 Hz up to 400 MHz in 100 seconds. It was used to inject signals at the top of the terminations, as is indicated in Figure 4.8, while measuring with a spectrum analyzer at the internal sensors and the current probes using the complete RF detection circuit but without the coaxial cable RG-213. The function generator was adjusted to sweep continuously over the desired range of frequencies and the spectrum analyzer was adjusted to hold the maximum value at every frequency. The response of the system was then calculated for each frequency using the following equation:

$$Gain_{dB} = 20 \log \left( \frac{V_{MEASURED}}{V_{INJECTED}} \right) \quad (4.3)$$

Where  $V_{INJECTED}$  is the injected signal amplitude of the function generator and  $V_{MEASURED}$  is the measured signal amplitude at the same corresponding frequency. The responses of all the sensors are displayed in Figure 4.9.

<sup>8</sup> Tabor Electronics 1281A

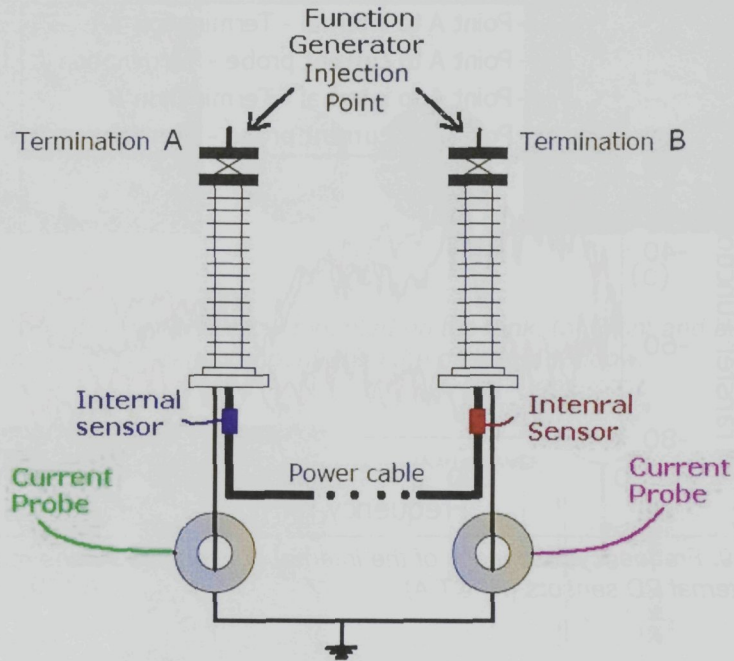


Figure 4.8: Schematic of the 30-meter long, 345 kV, XLPE cable with two terminations.

It should be noted that the calculated responses displayed in the figure contain information on:

- the attenuation of the signals traveling through the termination,
- the transfer impedances of the sensors, and
- the frequency response of the RF measuring circuit.

In each termination the attenuation of the signals is the same since the terminations are identical models. Similarly, since the same RF measuring system was used to measure at all sensors the frequency response of the complete detection circuit is the same. Therefore, the significant differences in their responses are due to the coupling capabilities of the sensors themselves. It can be seen that the internal inductive sensors have a much higher sensitivity than the externally applied current probes.

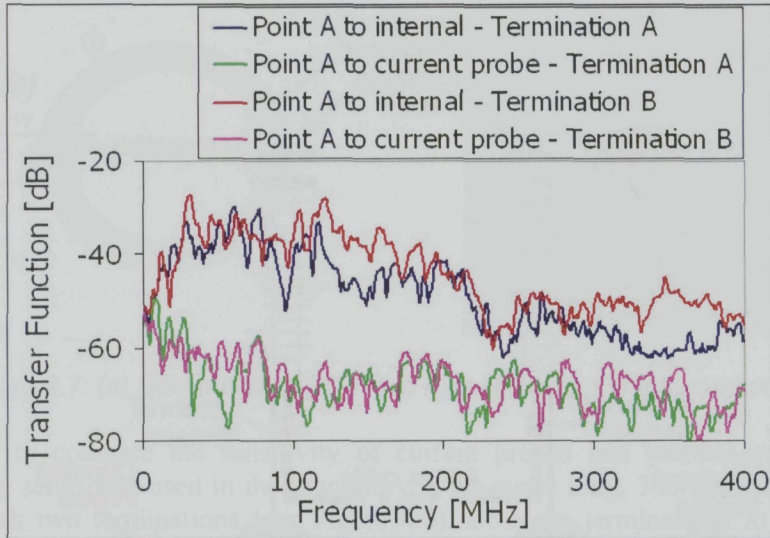


Figure 4.9: Frequency responses of the internal PD sensors vs. the responses of the external PD sensors (HFCT A).

### 4.2.3 Detection in transformers

For power transformers detection of electromagnetic detection can be performed as follows:

- i) Antennas can detect Electromagnetic waves radiated in the oil. A window to the interior of the tank is required for electromagnetic detection. Thus the antennas can be used as follows [13, 18]:
  - a. Mounted on dielectric windows built on the tank as shown in Figure 4.10.
  - b. Inserted via an oil-valve on the tank as it is shown in Figure 4.11
- ii) Capacitive sensors mounted on the bushings of the transformer, that detect the PD current induced at the HV or LV conductors.
- iii) Inductive sensors mounted at the grounding of the transformer that detect the PD current induced at the ground circuit as it was described in the case of cables.

In the two latter methods external electric signals are induced in the current-carrying conductors, which might interfere with the PD measurements. Instead the use of antennas is usually preferred due to less noise interference.

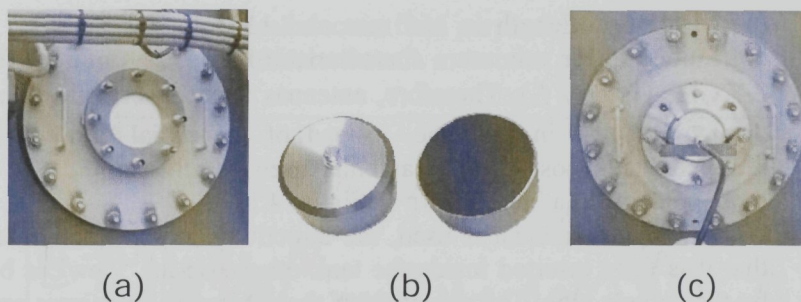


Figure 4.10: (a) Dielectric window mounted on the tank. (b) Front and back sides of a RF sensor. (c) RF sensor mounted on the dielectric window.

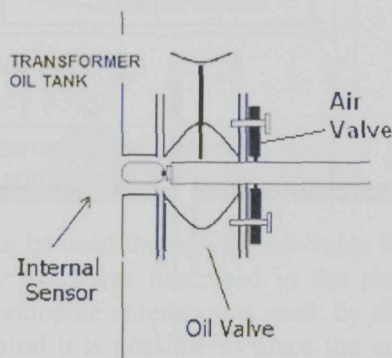
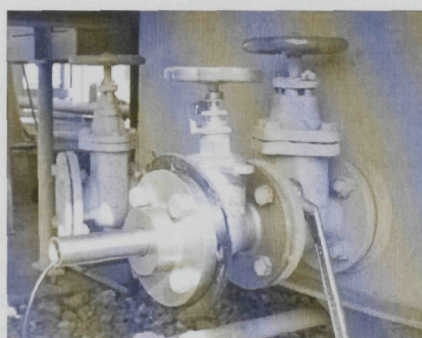


Figure 4.11: (a) Sensor inserted in the oil-valve of a transformer as is demonstrated in the schematic diagram in (b).

In the case of RF antennas, certain practical limitations are encountered in their application via the oil-valve of the transformer:

- i) The antenna should be inside the tank for optimum sensitivity. A very small percentage of the emitted signals can be detected within the valve. The oil valve itself acts as a hollow single-conductor waveguide, which allows the transmission of high frequency waves in higher modes only and no *TEM* propagation. The sensitivity of an antenna through the oil-valve is experimentally determined in Appendix D for various insertion depths.
- ii) In order to measure in the UHF range larger radial antenna dimensions are required. For example, if a loop antenna is used for detection then the length of the loop should be taken equal to the wavelength of the desired signals [64], hence:

$$D = \lambda / \pi \quad (4.4)$$

Where  $D$  is the diameter of the loop and is limited by the oil-valve diameter. Hence, for a diameter  $D = 53$  mm or  $35$  mm, the maximum

measuring wavelength is 166 mm and 110 mm respectively, which correspond to the minimum characteristic frequencies of 1.8 GHz and 2.7 GHz ( $\lambda = c/f$ ). Therefore, antennas that can effectively use the available length in the tube, instead of the radial dimensions, are required. The most popular antenna used for this application is the monopole antenna [13], shown in Figure 4.12.

- iii) If a monopole antenna is used, the directivity of the antenna requires that it is fully inserted inside the tank otherwise its “view” is blocked by the valve’s tube. The reception of the monopole antenna is optimum in the plane perpendicular to the monopole axis and zero in the direction of its axis, as it can be seen from its reception pattern displayed in Figure 4.12.

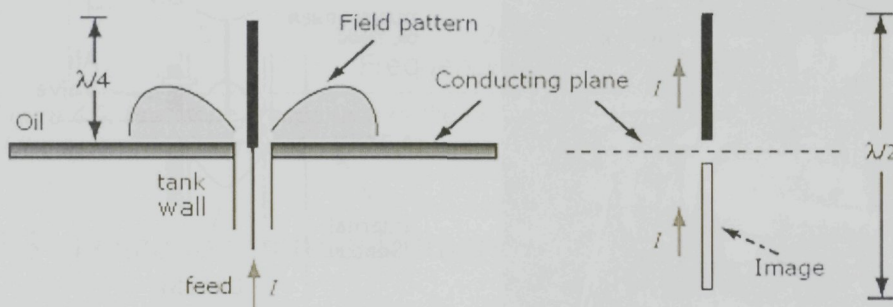


Figure 4.12: The monopole antenna: It consists of a conductor of  $\lambda/4$  length near a conductive surface (where  $\lambda$  is the wavelength of the desired signals). The conductive surface works as a reflector to the current generated in the real antenna [65].

- iv) Even in the case of the monopole antenna, however, certain size limitations also apply. It is a narrowband antenna resonant at a wavelength one quarter of its size. Its size should be chosen between 25 mm and 25 cm in order to detect signals of a specific wavelength within the UHF range. The allowed depth inside the tank limits its length. For example for an insertion depth of 4 cm (and thus a maximum antenna length of 4 cm) a minimum operating frequency of 1.87 GHz is achieved. Since as it was already discussed in the previous chapters PD signals barely appear beyond 1.5 GHz the antenna will have to operate below its resonant frequencies, which will hinder its sensitivity. The larger the measured wavelengths the less efficient the antenna will be to measure the induce currents.
- v) Finally, it is a linearly polarized antenna and thus can detect only the electric field components of the incoming signal that are parallel to its polarization. Otherwise there is polarization mismatch and only the field component parallel to the antenna axis is detected. If the incoming



signal has the total electric field perpendicular to the antenna axis then the signal is not detected at all.

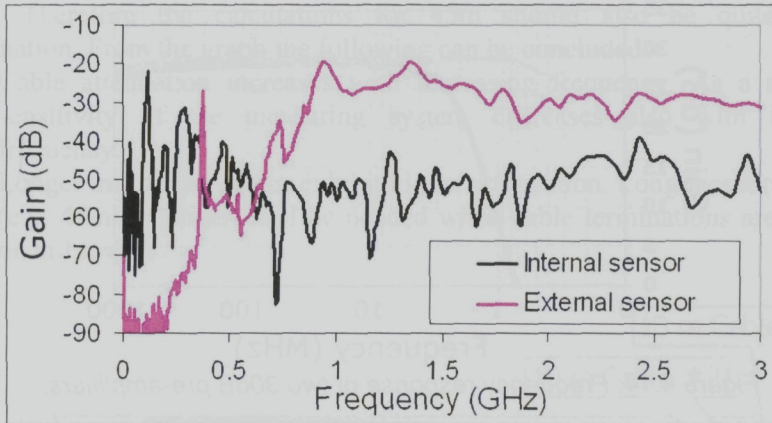


Figure 4.13: Frequency response of external sensor shown in Figure 4.4 (measured without the dielectric window) and a spiral monopole antenna.

It is possible that other designs of sensors can be used through the oil-valve but the size limitations will hinder their sensitivity as it was described in the previous paragraphs. In this thesis a variation of the monopole antenna was used: by shaping the conductive wire of the antenna into a spiral it is possible to place the antenna inside the oil-valve and have a longer conductive element than a simple monopole. Hence induced currents of long wavelengths can better be detected. This is demonstrated in the following experiment. The frequency response of a UHF sensor (shown in Figure 4.10) and the spiral internal antenna was measured using a network analyzer<sup>9</sup>, as is described in Appendix B. From Figure 4.13 it can be seen that the internal sensor has a higher frequency response up to 500 MHz, while the external sensor has a considerably better response above 600 MHz where its operating bandwidth is located [37, 42]. The optimum sensitivity of the internal sensor below 500 MHz is because its longer conductive element can support the induced currents of the long wavelengths appearing in that frequency range.

<sup>9</sup> Rohde & Schwarz ZVB 4 Vector Network Analyzer

## 4.3 Miscellaneous components

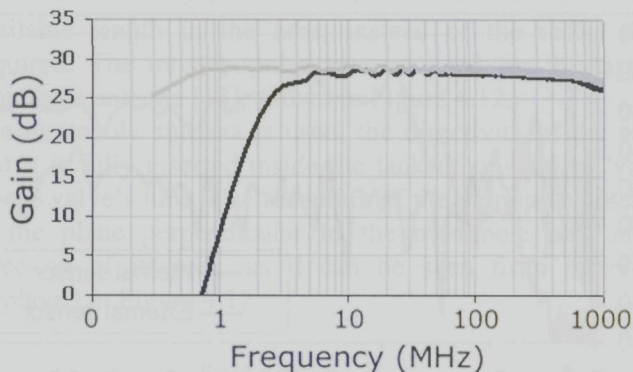


Figure 4.14: Frequency response of two 30dB pre-amplifiers.

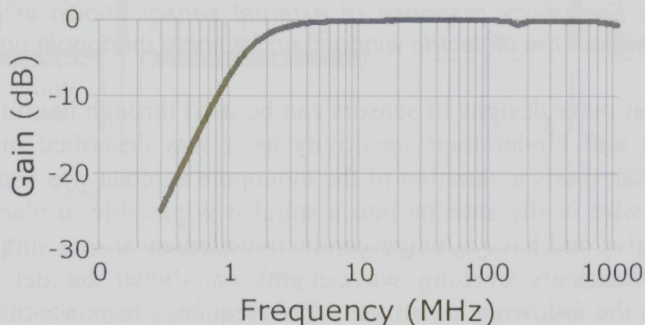


Figure 4.15: Frequency response of a high-pass filter.

The individual responses of the other components of the detection circuit will be examined in this paragraph to determine the frequency responses of the different components of the system, a network analyzer was used. Figure 4.14 shows an example of the frequency response of two of the pre-amplifiers. The difference below 10 MHz is because one of the amplifiers has a filter built-in. Above 10 MHz it can be seen that they have a similar flat response of 28 dB up to 1000 MHz. As a result, it can be said that the amplifier has no significant influence in the signal response other than increasing the signal in a similar way at all frequencies. A similar statement can be made for the high-pass filter whose frequency response is shown in Figure 4.15.

The frequency response of the RG-213 measuring cables is shown in Figure 4.16. It shows measured and theoretically<sup>10</sup> calculated values for 10m, 15m and 45m long

<sup>10</sup> See Appendix C for the derivation.

measuring cables. The frequency response of the cable was calculated using the method as described in [85], and is demonstrated in Appendix C. It can be seen that, for the 10m and 15m cables, the measurements and calculations agree well within 0.2 dB. Therefore the calculations for 45m should also be quite a good approximation. From the graph the following can be concluded:

- Cable attenuation increases with increasing frequency. As a result, the sensitivity of the measuring system decreases also with increasing frequency.
- Longer measuring cables exhibit higher attenuation. Long measuring cables (e.g. 45m or longer) will be needed when cable terminations are mounted on tall towers.

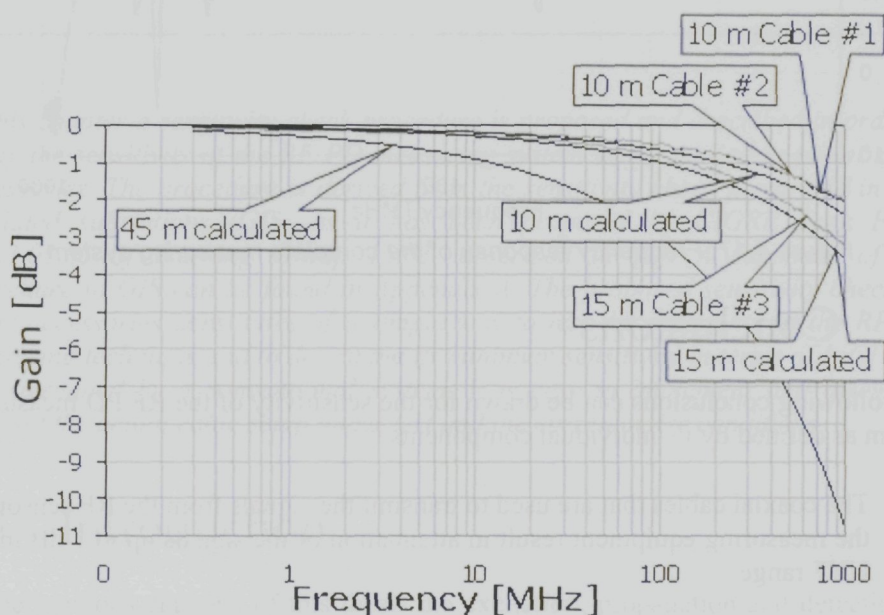


Figure 4.16: Calculated and measured frequency response of different lengths of measuring cables.

Finally the frequency response of the whole RF measuring circuit (as shown in Figure 4.1) can be determined by the superposition of the responses of all the components, as is demonstrated in Figure 4.17. In the figure the frequency response of the complete detection system consisting of: an RF sensor, a 20m RG-213 cable, a filter and an amplifier is demonstrated for the HFCT A and B current probes. It can be seen that the response of the system equipped with each sensor is proportional to their transfer impedances in Figures 4.4 and 4.5. The steepness of the lines is caused by the attenuation of the RG-213 cable, which increases with the frequency. In the end the most influential role to the response of the whole RF PD measuring system is attributed to the RF sensors that are used.

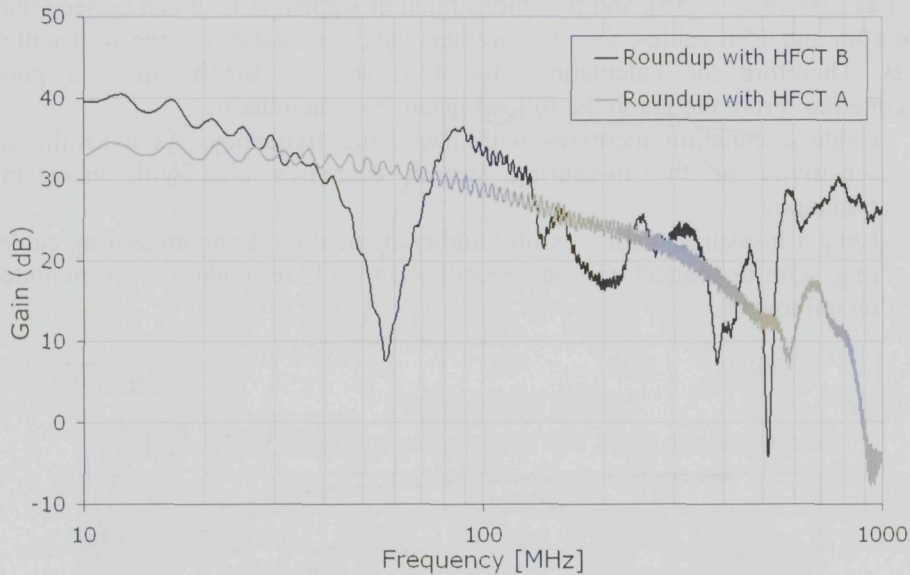


Figure 4.17: Frequency response of the complete measuring system

## 4.4 Conclusions

The following conclusions can be drawn for the sensitivity of the RF PD measuring system as defined by its individual components:

- The coaxial cables that are used to transmit the signals from the RF sensors to the measuring equipment result in attenuation of the signals up to 3 dB in the UHF range.
- The transfer impedance of the RF sensors used defines the range of frequencies where the sensitivity of the system is optimum. In the following cases of RF sensors the transfer impedance at the RF measuring frequencies is unknown:
  - Internal inductive and capacitive sensors applied in power cables.
  - Internal monopole sensor through the oil-valve
- In the case of internal sensors through the oil-valve of a transformer the following complications occur:
  - The antenna's size is too small to measure efficiently in the VHF/UHF range.
  - The antenna has to be inside the transformer tank for optimum sensitivity.

# Sensitivity Check in Power Cable Accessories

---

*In this chapter a sensitivity check procedure is proposed and described in order to verify the sensitivity of the RF PD measuring system when applied in power cable accessories. The procedure is derived from the sensitivity check performed in gas-insulated substations (GIS) as it has been proposed by CIGRE Task Force 15/33.03.05 of Working Group 15.03, described in [1]. A summary of this procedure in GIS can be found in Appendix A. The proposed sensitivity check for cable accessories constitutes of a simple way to test the sensitivity of the RF PD measuring technique and to determine its minimum sensitivity in terms of [pC] level as determined by a conventional system. It is easy to implement and takes into account the actual cable setup under test and the current noise conditions.*

## 5.1 Introduction

In the previous chapters of this thesis the excitation, propagation and detection of the electromagnetic phenomena in power cables, as generated by partial discharges in the RF range of the spectrum, has been studied. It was concluded that in practice there are cases where the sensitivity of the RF measuring system is hindered. The following should be taken into account when measuring in cable accessories:

- It was seen that the attenuation of the RF signals reaches up to 4 dB/m in the VHF range and above 7 dB/m in the UHF range. If the sensor is placed several meters away from the accessory then the sensitivity of the RF measuring system is heavily decreased. Such situations occur in the case of terminations residing on pylons, or at underground joints, where the grounding link boxes are quite far from the accessory.
- The frequency response of internal inductive or capacitive sensors cannot be determined. In this case the frequencies where the sensitivity of the RF PD measuring system is low, due to the low transfer of the sensors, should be avoided during PD measurements.

Therefore, a means of verifying the sensitivity of the RF PD measuring system is needed. Such a procedure will be described in this chapter.

Therefore, a means of verifying the sensitivity of the RF PD measuring system is needed. Such a procedure will be described in this chapter. During the years of this research this procedure has been adopted and applied in the laboratory and field by other researchers in the TUDelft. In a recent CIGRE publication [86] the procedure is also presented for the purposes of the sensitivity check of the PD measuring techniques in the VHF range.

## 5.2 Sensitivity check procedure

Although in GIS several sensors are used in order to establish sufficient sensitivity in the complete structure, in the case of cable accessories only a couple of sensors are needed. More specifically in the case of a termination an RF sensor (internal or external) can be placed below the termination. In the case of joints rarely there will be found more than one sensor (internal or external) available. Therefore, the sensitivity check will be used to confirm the detection capability of one sensor.

However, the application of only one sensor prohibits the simultaneous injection and detection of an artificial pulse in the HV equipment as it was performed in the sensitivity check for GIS and transformers. In the case of joints, if an internal sensor close to the joint and an external sensor at its shield grounding are not available, injection and detection of artificial pulses are not possible. In the case of terminations the pulse generator can be connected across the termination in order to inject pulses in its conductor, as is displayed in Figure 5.1.

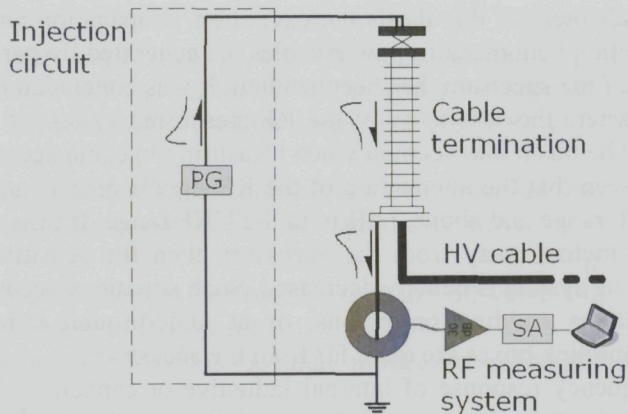


Figure 5.1: Injecting pulses in cable terminations requires the application of an extra circuit as is demonstrated in the figure.

The sensitivity check procedure for GIS consists of two main parts, as is presented by [1]:

- A. Laboratory Test: An artificial pulse is determined which emits a signal similar to that of an actual defect and is equivalent to an apparent charge of 5 pC.
- B. On-site Test: This artificial pulse is then injected in the GIS and the RF sensors are used to detect the pulse at different positions on the GIS.

Each part is performed in several steps that are described in Tables A.1 and A.2, of Appendix A. The proposed procedures for the laboratory and on-site tests of the sensitivity check in power cable accessories are outlined in Tables 5.1 and 5.2. The field test in power cable accessories has the following requirements in order to be performed correctly:

- a) It should be performed on the same type of accessory and power cable as in the laboratory test.
- b) The same sensor should be used to detect the signals as in the case of the laboratory test.
- c) The same cable should be used to inject the artificial pulses as in the laboratory test.

These requirements ensure that the transfer characteristics from injection point to detection point are the same as in the laboratory test and the response of the injected artificial pulse remains equivalent to the determined defect discharges. If any of these requirements is not met then the sensitivity check cannot be performed. However, a means of testing the detection capabilities of the RF PD measuring system is still required. For this reason another procedure is proposed that is similar to a sensitivity check but it does not offer any comparable results to actual defects. It is mainly used to test the performance of the RF measuring system to the artificial pulses of an appropriate pulse generator. This procedure will be referred to as the performance check and is outlined in Table 5.3 below.

In the following paragraphs experiments of the laboratory tests and performance checks will be presented. During this research there was no option to perform an on-site test on the same type of cable accessory as the accessories used for laboratory tests and therefore no such experiment will be presented. Nevertheless, a detailed explanation of the procedural steps of an on-site test will be given. The steps described in Tables 5.1 to 5.3 will provide the main guidelines for each procedure.

<b>Laboratory Test</b>	
<b>1</b>	Installation of an artificial PD defect on the accessory
<b>2</b>	<ul style="list-style-type: none"> <li>▪ Installation of measuring RF sensor(s)</li> <li>▪ Connection of a PD detection circuit (IEC 60270) to the whole cable setup.</li> </ul>
<b>3</b>	<ul style="list-style-type: none"> <li>▪ Energizing of the cable setup (and thus defect) and PD detection at inception voltage using both systems:</li> <li>▪ IEC 60270 conventional system in order to determine the discharge level in pC.</li> <li>▪ RF PD detection system:               <ul style="list-style-type: none"> <li>▪ Full Span:                   <ul style="list-style-type: none"> <li>- Record the RF spectra (magnitude <i>A</i>)</li> <li>- Determine signal-to-noise ratio</li> </ul> </li> <li>▪ Zero Span:                   <ul style="list-style-type: none"> <li>- Record PD in phase domain at frequencies of high signal-to-noise.</li> </ul> </li> </ul> </li> </ul>
<b>4</b>	Installation of injection circuit Inject artificial pulses in injection circuit with the following characteristics: <ul style="list-style-type: none"> <li>▪ Rise time <math>\leq 1</math> ns</li> <li>▪ Pulse width <math>&gt; 500</math> ns (rectangular pulses)</li> <li>▪ PWHM <math>&gt; 20</math> ns (double exponential pulses)</li> <li>▪ Time between consecutive pulses <math>&gt;</math> duration of RF signal. (Usually less than 100 kHz).</li> </ul>
<b>5a</b>	Full Span: <ul style="list-style-type: none"> <li>- Acquire signal RF spectra (magnitude <i>B</i>) at RF sensor.</li> <li>- Compare magnitudes <i>B</i> and <i>A</i> obtained in step 3.</li> <li>- Vary amplitude of artificial pulse until <math>B = A</math> within an appropriate frequency range.</li> </ul>
<b>5b</b>	Zero Span: <ul style="list-style-type: none"> <li>- In each frequency chosen for phase domain measurements in step 3 vary amplitude of artificial pulses to match amplitude of PD recordings.</li> <li>- Determine a [pC]/ [V] ratio for all frequencies where a PD recording has been done. Where [V] is the amplitude of the injected artificial pulse in Volts.</li> <li>- Decrease voltage of injected pulses to determine the minimum signal that can be detected in each frequency.</li> <li>- Using the [pC]/ [V] determine the minimum [pC] level of discharges that can be detected by the RF PD measuring system.</li> </ul>

Table 5.1: Steps for the laboratory test for the sensitivity check of the RF PD measuring system in power cable accessories.



<b>On-site Test</b>	
<b>1</b>	<ul style="list-style-type: none"> <li>▪ Installation of injection circuit in the case of a termination</li> <li>▪ Injection of the artificial voltage pulses as were obtained in step 5 of the laboratory step. The same type of measuring equipment (pulse generator, cable and RF sensor), injecting circuit, power cable type and accessory has to be used as for the laboratory test.</li> </ul>
<b>2</b>	Full Span: <ul style="list-style-type: none"> <li>▪ Measure RF signal at RF sensor in frequency range determined in step 5 of the laboratory test. If signal is detected the sensitivity verification is successful.</li> </ul>

*Table 5.2: Steps for the on-site test for the sensitivity check of the RF PD measuring system in power cable accessories.*

These requirements ensure that the transfer characteristics from injection point to detection point are the same as in the laboratory test and the response of the injected artificial pulse remains equivalent to the determined defect discharges. If any of these requirements is not met then the sensitivity check cannot be performed. In addition, it is possible that at the frequency range where the laboratory test was valid there is high noise interference present in the field conditions. In these cases verifying the sensitivity of the RF PD measuring system to specific defects and in comparison to conventional systems is not possible. However, a means of testing the detection capabilities of the RF PD measuring system is still necessary. For this reason a variation of the on-site test procedure is proposed that can test the detection performance of the measuring system. It is called a performance check and is mainly used to test the performance of the RF measuring system to artificial pulses injected from an appropriate pulse generator. The procedure is outlined in Table 5.3.

<b>On-site performance check</b>	
<b>1</b>	<ul style="list-style-type: none"> <li>▪ Installation of injection circuit in the case of a termination.</li> <li>▪ Inject artificial pulses in accessory with the following characteristics:               <ul style="list-style-type: none"> <li>- Rise time <math>\leq 1</math> ns</li> <li>- Pulse width <math>&gt; 500</math> ns (rectangular pulses)</li> <li>- PWHM <math>&gt; 20</math> ns (double exponential pulses)</li> <li>- Time between consecutive pulses <math>&gt;</math> duration of RF signal. (Usually less than 100 kHz).</li> </ul> </li> </ul>
<b>2</b>	<ul style="list-style-type: none"> <li>▪ Measure RF signal at receiving sensor.</li> <li>▪ Identify frequencies of high signal-to-noise ratio.</li> <li>▪ If signal is detected with good signal-to-noise ratio in at least one frequency the performance check is successful for the specific accessory.</li> </ul>

*Table 5.3: Steps for the on-site performance check of the RF PD measuring system in power cable accessories.*

## 5.3 Laboratory Test

The laboratory test performed at a specific cable setup as it is described in Table 5.1, has the following specific goals:

- i) To determine the sensitivity of the RF PD measuring system to possible defects.
- ii) To determine the minimum possible sensitivity in comparison to [pC] discharge levels of the RF PD measuring system.

In the following paragraphs two laboratory tests will be described. Each experiment focuses on one of the two goals correspondingly.

### 5.3.1 Experiment I

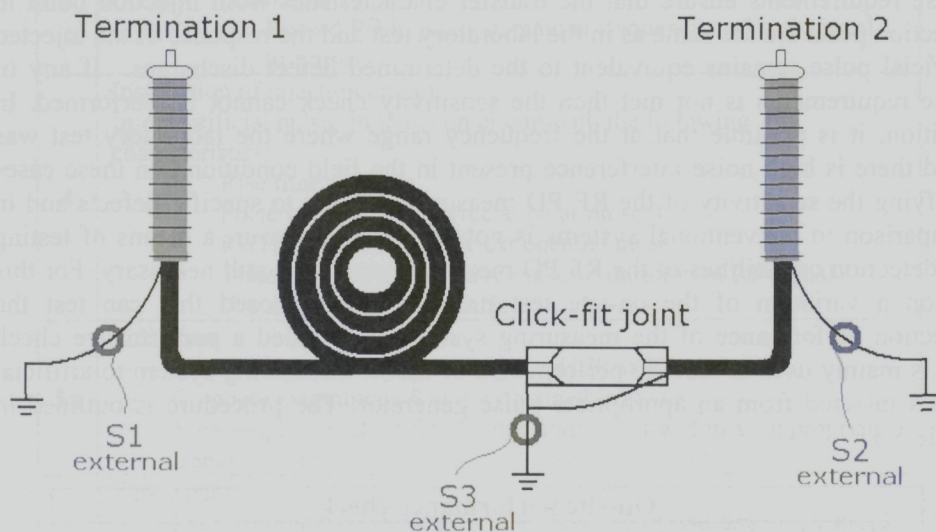


Figure 5.1: The 150kV XLPE cable set-up. Internal and external inductive RF sensors have been used close to each termination and joint.

The cable set-up indicated in Figure 5.1 was built in order determine the sensitivity of the RF PD measuring system to various defects appearing at the termination and joint of the setup. The set-up consisted of a 150kV HV XLPE cable of 100m of length, two terminations and a click-fit type joint. The type of cable and accessories is indicated in Table 5.4. Internal inductive RF sensors had been constructed close to each termination and joint. In the following paragraphs the laboratory test will be described for the case of three different defects.

	Termination	Joint	Cable
type	OTC - 170	CFJX - 170	XLPE EYLKrvlwd 87/150 kV 1x1200

Table 5.4: Type of cable and accessories used in the set-up of figure 5.1

Based on the procedure described in Table 5.1 the following steps were taken to apply the procedure on cable terminations:

➤ **Step 1:**

Two defect models were built and tested at different times. These defects are presented in Table 5.5.

➤ **Step 2:**

A conventional system was then attached on Termination 1 (see Figure 5.2) composed of the following:

- a) A 200kV test transformer with max. output 86kV RMS (limited by cable capacitance)
- b) Detector type: TE571
- c) Coupling capacitor (1056pF ) with coupling unit type: AKV 572 Haefely Trench (see Figure 5.3 (b))
- d) Voltage regulator

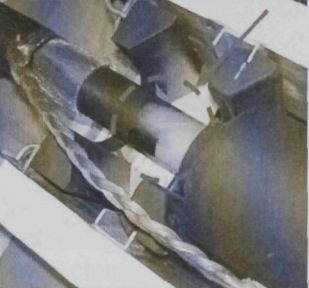
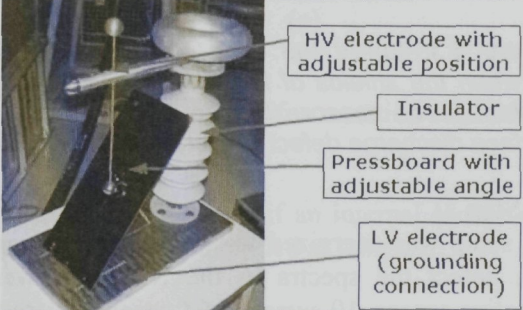
Defect:	Description:
<p><b>Missing insulation screen</b> at the cable/joint transition. PD due to incorrect distribution of electrical field inside joint /termination.</p>	
<p><b>Surface discharges</b> on termination. The discharges occur in the defect model which is connected to the termination.</p>	

Table 5.5: Artificial discharging defect models at the termination and joint.

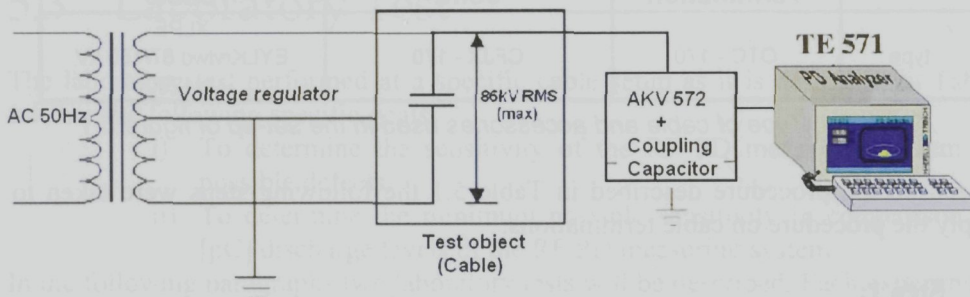


Figure 5.2: Schematic diagram of The 50Hz AC supply and the conventional PD measuring system (according to the IEC 60270 recommendations).

The RF PD detection system was applied by placing external inductive sensors at:

1. The grounding cable of the termination
2. Grounding cable at the joint that was formed as is demonstrated in Figure 5.3 (a).

The output of the RF detection system is measured by a spectrum analyzer.

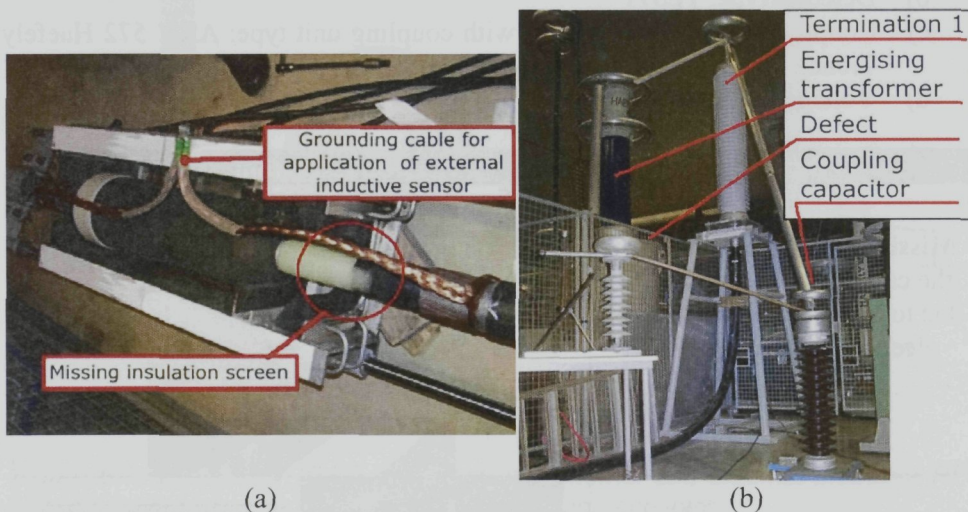


Figure 5.3: (a) At the click-fit joint it was necessary to create a connection between the shields of the two cable parts across the joint in order to mount a current probe sensor. (b) The connectivity of the conventional system and the surface discharge defect model are achieved with aluminium tubes.

### ➤ Step 3:

The setup was energized with 50 Hz of alternating current (AC). For the case of each defect the spectra in the RF range were measured at the corresponding inductive sensor. 10 sweeps of 5 seconds were taken along the RF range up to 600 MHz using the spectrum analyzer. The maximum amplitudes in each frequency

from the 10 sweeps were considered as the spectra of the RF signal 'magnitude  $A$ '. The maximum spectra of each defect and their corresponding [pC] level are displayed in Figure 5.4.

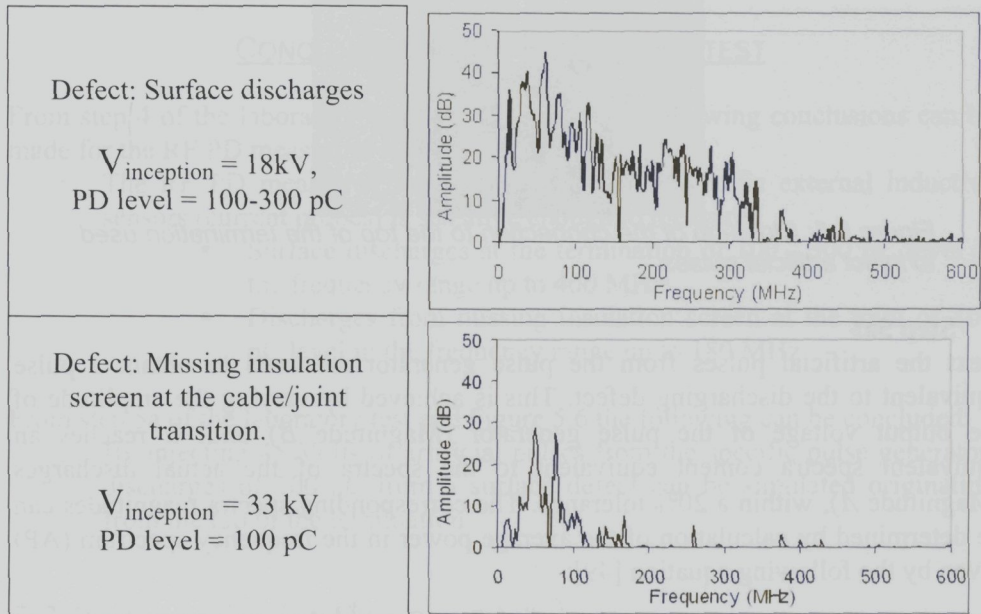


Figure 5.4: The measured spectra of each defect and their corresponding [pC] level.

➤ **Step 4:**

An artificial voltage pulse is then injected using a pulse generator which generates pulses with amplitudes up to 45 V, rise time of 400 ps and pulse width of 10 ns.

For the case of the terminations a split connector was used to connect the pulse generator to:

- i) The top of the termination via a wire clamped to the conductor of the termination (see Figure 5.5).
- ii) The grounding cable via a short 50 Ohm BNC wire clamped below the RF sensor.

This arrangement forms an injection circuit, which allows for injection of artificial voltage pulses at the top of the termination.

For the joint it is possible to inject artificial pulses only if an internal sensor was available. The injection circuit arrangement cannot be applied at joints.



Figure 5.5: Close-up of the connection to the top of the termination used to inject artificial pulses.

➤ **Step 5a:**

Next the artificial pulses from the pulse generator are used to obtain a pulse equivalent to the discharging defect. This is achieved by varying the amplitude of the output voltage of the pulse generator (Magnitude  $B$ ) until it reaches an equivalent spectra content equivalent to the spectra of the actual discharges (Magnitude  $A$ ), within a 20% tolerance. The corresponding spectra magnitudes can be determined by calculation of the average power in the frequency spectrum (AP) given by the following equation [49]:

$$AP = 10 \cdot \log \left( \sum_{i=1}^N \left( \frac{S_i + S_{i+1}}{2} \right)^2 \cdot \frac{1}{N} \right) \quad (5.1)$$

The equivalent spectra does not have to be determined for the full RF spectrum, but instead in a range of frequencies where this is possible, as is demonstrated in Figure 5.6 for the case of the surface discharges. In the figure the equivalent spectrum is determined for frequencies up to 200 MHz for a voltage output level of the pulse generator of 45 V.

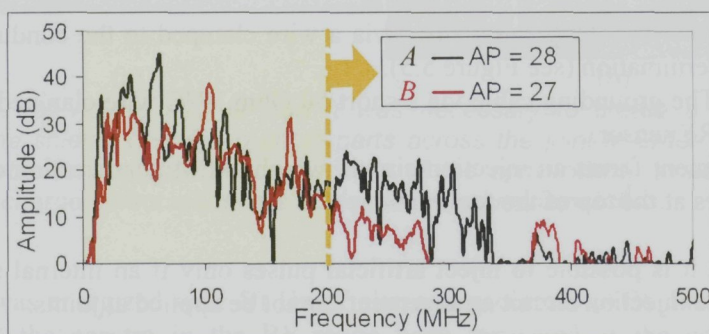


Figure 5.6: Comparison of frequency spectra measured by the RF PD measuring system resulting from A) the surface discharges defect, and B) The injected artificial pulses from a pulse generator.

➤ **Step 5b:**

This step was not performed in this laboratory test and will instead be demonstrated in the next experiment.

CONCLUSIONS FROM LABORATORY TEST

From step 4 of the laboratory test and Figure 5.4 the following conclusions can be made for the RF PD measuring system:

- The RF PD measuring system employing the specific external inductive sensors (current probes) is sensitive enough to measure:
  - Surface discharges at the termination of 100 - 300 pC level in the frequency range up to 400 MHz
  - Discharges from missing insulation screen at the joint of 100 pC level in the frequency range up to 180 MHz.

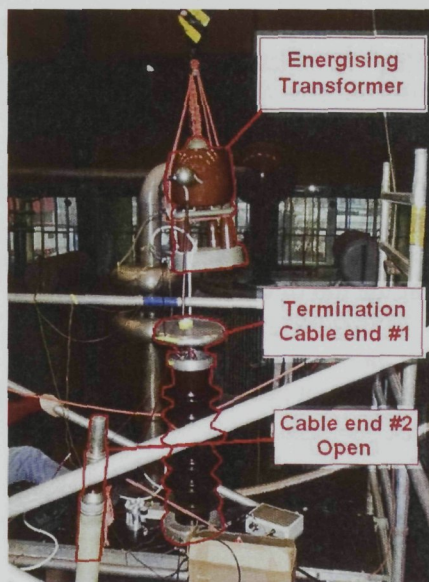
From step 5a of the laboratory test and Figure 5.6 the following can be concluded:

- By injecting 45 Volts of artificial pulses from the specific pulse generator, discharges of 300 pC from a surface defect can be simulated originating from the top of the termination.

### 5.3.2 Experiment II



(a)



(b)

Figure 5.7: Cable setup used for sensitivity check of the RF PD measuring system. (a) Cable part 12 m. (b) Cable endings with only one termination used.

The laboratory setup of a medium-voltage (MV) cable shown in Figure 5.7 will be used in this laboratory test to determine the minimum [pC] level that can be detected by the RF PD measuring system. Based on the procedure described in Table 5.1 the following steps were taken to apply the procedure on cable terminations:

➤ **Step 1:**

At the termination an artificial corona defect was built by attaching a copper wire with a sharp tip at the top-end of its conductor.

➤ **Step 2:**

A conventional system was used composed of a coupling capacitor, a coupling device and a TE 571 PD detector. It was connected on the termination of the cable (see Figure 5.7 (b)). The RF PD detection system was applied by placing an external inductive sensor at the grounding of the termination shield. The output of the RF detection system is measured by a spectrum analyzer.

➤ **Step 3:**

The setup was then energized and the corona defect was activated at inception voltage and resulted in a PD level up to 400 pC. In this experiment only the zero span measurements will be used for the demonstration of the later steps of the procedure. By using the spectrum analyzer as a tunable filter it is possible to measure the signal at a specific center (or midband) frequency and at a bandwidth of 3 MHz. The measurements are then synchronized to the supplying voltage (50 Hz) and a phase-resolved pattern of the discharges is obtained. This is demonstrated in Figure 5.8, where a zero span measurement of the corona at 80 MHz is displayed.

➤ **Step 4:**

An artificial voltage pulse is then injected using a pulse generator which generates pulses with rise time of 400 ps and pulse width of 10 ns. The pulse generator is connected as it was described in Experiment I in order to inject artificial voltage pulses at the top of the termination.

➤ **Step 5a:**

This step was not performed during this laboratory test and will be skipped.



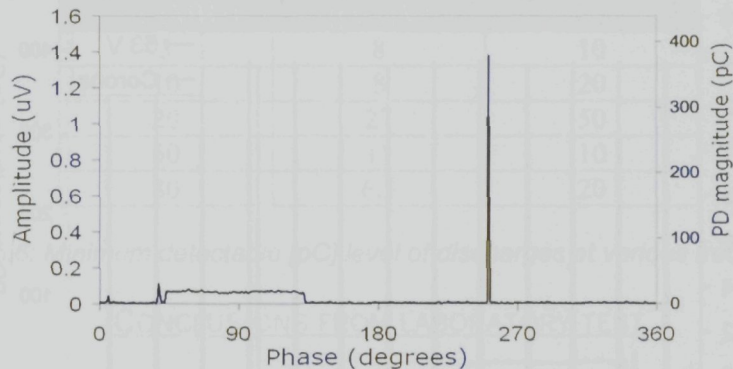


Figure 5.8: Using the SA as a tunable filter at 370 MHz the corona defect is measured in narrowband. The filtered signal was synchronized to the period of the supplying voltage

➤ **Step 5b:**

By comparing in phase domain the amplitude in [V] of the artificial pulses and the [pC] level of the actual PD signals, it is possible to obtain a [pC]/[V] ratio at all frequencies where the discharge is detected. The goal is to use the determined ratios during the on-site test in order to determine the minimum [pC] level that can be detected under field conditions where noise levels are higher.

Therefore, at the center frequency of 80 MHz that was demonstrated in a previous step, the magnitude of the corona pulses and the artificial injected pulses are compared. By increasing or decreasing the amplitude of the artificial pulses from the pulse generator it is possible to match the amplitude of the actual PD pulses and obtain a [pC]/[V] for each specific frequency.

In Figure 5.9 by increasing the voltage of the artificial pulses to 53 V a corona pulse of 400 pC is matched giving a ratio of  $[pC]/[V] = 7.5$ . In Figure 5.10 by decreasing the voltage of the artificial pulses to 3.6 V a corona pulse of 20 pC is matched giving a ratio of  $[pC]/[V] = 5.6$ . An average ratio of  $[pC]/[V] = 6.5$  can then be assumed for the frequency of 80 MHz.

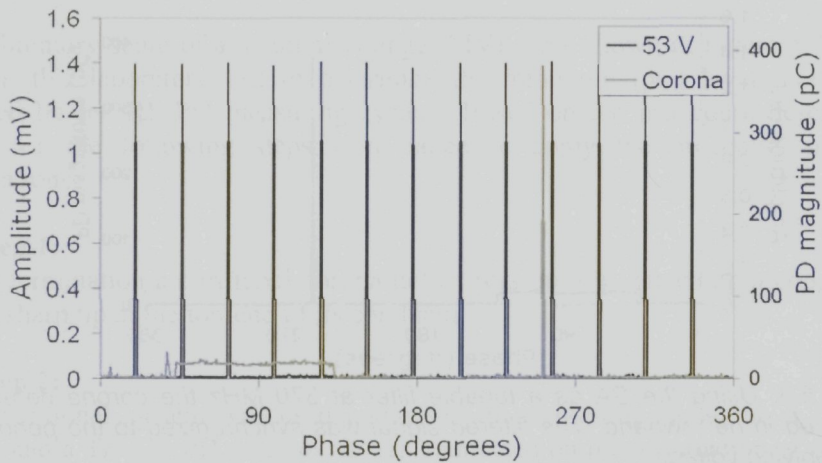


Figure 5.9: Comparing the periodic pulses from the pulse generator (53 Volts) with the pC amplitude of a corona defect in phase domain. The centre frequency is 80 MHz.

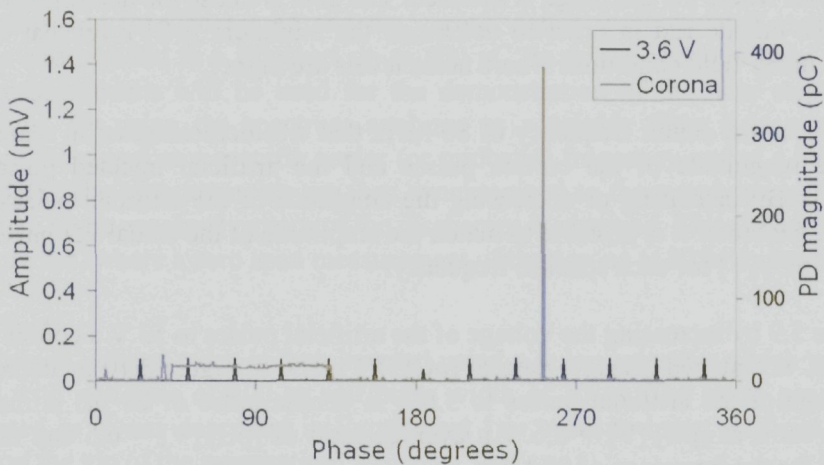


Figure 5.10: Comparing the periodic pulses from the pulse generator (3.6 Volts) with the pC amplitude of a corona defect.

Similarly, this procedure can be repeated for other center frequencies where the corona discharges are detected. At each center frequency a  $[pC]/[V]$  is determined by comparison of the artificial pulses with the actual corona pulses. Then the output voltage of the artificial pulses is varied to the minimum detectable level and the  $[pC]$  level is determined from the  $[pC]/[V]$  ratio. Finally a table is constructed that outlines the minimum  $[pC]$  level of discharges that can be detected in each center frequency, as is demonstrated in Table 5.6.

Freq. (MHz)	[pC]/[V]	Min (pC)
3	8	10
10	8	20
20	27	50
50	11	10
80	6.5	20

Table 5.6: Minimum detectable [pC] level of discharges at various frequencies.

### CONCLUSIONS FROM LABORATORY TEST

From step 4 of the laboratory test and Figure 5.8 the following conclusions can be made for the RF PD measuring system:

- The RF PD measuring system employing the specific external inductive sensors (current probes) is sensitive enough to measure:
  - A corona in air defect of the termination of 20 - 400 pC level in the frequency range up to 180 MHz.

From step 5b of the laboratory test and Figures 5.9 and 5.10 the following can be concluded when measuring in phase domain at 80 MHz:

- The RF PD measuring system was proven sensitive enough to measure discharges of 20 pC occurring at the top of the termination.
- All discharges of 20 pC appearing between the top of the termination and the RF sensor will be detected. This is because the corona discharges were generated at the farthest location from the PD sensor.
- By injecting 3.6 Volts of artificial pulses from the specific pulse generator, corona discharges of 20 pC can be simulated originating from the top of the termination.
- Similarly, using the average ratio of  $[pC]/[V] = 6.5$  pulses of different [pC] levels can be simulated at the frequency of 80 MHz.

## 5.4 On-site test

The on-site test is performed in order to evaluate the sensitivity of the RF PD measuring system for the noise levels present in the field. Noise levels outside the laboratory conditions are higher due to interferences that appear from multiple electrical sources that can be found in a substation or industrial area (an example is demonstrated in Figure 5.11). The field noise interference may reduce the signal-to-noise ratio of various frequency ranges where PD could be detected for specific defects, as it was defined in the laboratory test. For this reason the sensitivity of the RF PD measuring system to the various defects and [pC] levels has to be re-evaluated under the noisy conditions of the field.

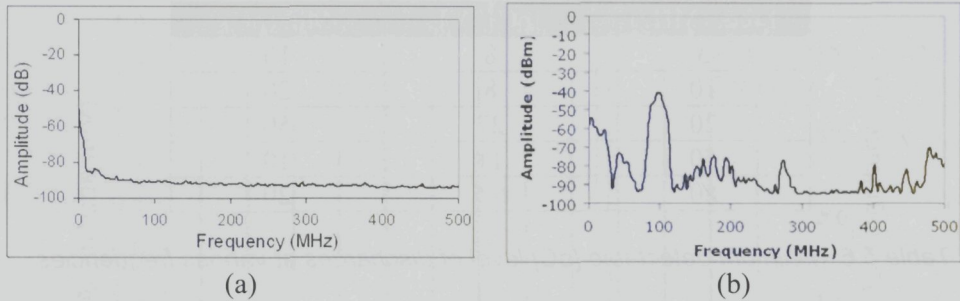


Figure 5.11: Noise levels in the RF range under (a) laboratory conditions, and (b) on-site field conditions.

However, in order to apply the results from the laboratory test to the on-site test the type of termination and power cable should be the same. In addition it has to be performed with the same RF sensor, grounding cable and pulse generator. Otherwise the transfer characteristics of the propagation path from the injection point to the measuring system is different. In this case the determined analogy between injected pulse and artificial PD pulse is not anymore the same as it was determined in the laboratory test.

Consider the cable setup that was described in Experiment I laboratory test. A sensitivity check has to be performed before actual PD measurements to determine the sensitivity of the system under the field noise conditions in terms of:

- i) Ability to detect the PD from the determined defects in the laboratory test
- ii) Frequencies where the specific defects can be detected with optimum sensitivity.

Then the on-site test is as follows:

➤ **Step 1:**

Using the same pulse generator from the laboratory test Experiment I, step 5a, artificial pulses are injected at the termination. The output voltage of the artificial pulses was determined in the laboratory test, step 5a, in order to simulate the surface discharges up to 200 MHz.

➤ **Step 2a:**

The measured signal-to-noise ratio under the new noise conditions (see Figure 5.11 (b)) is displayed in Figure 5.12. It can be concluded that surface discharges of 300 pC at the termination can be detected with sufficient sensitivity in the frequency range of 40 – 200 MHz.

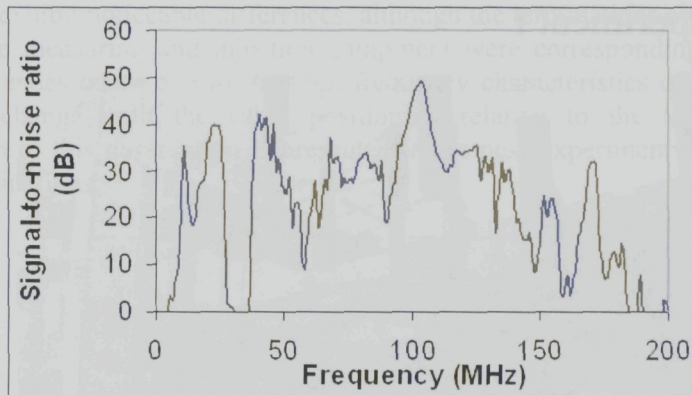


Figure 5.12: Signal-to-noise ratio obtained from injection of 45 V artificial pulses at the top of the termination. This way the surface discharges measured in the laboratory test can be simulated.

➤ **Step 2b:**

Cannot be performed since no Zero Span measurements were performed during the laboratory test. This step will be demonstrated in the following experiment.

CONCLUSIONS FROM ON-SITE SENSITIVITY CHECK

- The sensitivity of the RF PD measuring system can be confirmed under the field noise levels to the defects and [pC] levels determined in the laboratory test.
- The RF PD measuring system is sensitive enough to measure a corona defect of 20 pC on-site.
- All discharges of 20 pC appearing between the top of the termination and the RF sensor will be detected. This is because the artificial pulses were injected at the farthest location from the PD sensor.

## 5.5 On-site performance check

In the case where no laboratory test has been performed for a specific cable accessory, a performance check can be performed that provides an indication of the system's sensitivity under field conditions. The steps for the performance check are outlined in Table 5.3. In the following paragraphs two performance checks performed on-site will be presented. The first experiment presents the procedure of a simple performance check. The second experiment presents the results from injection measurements at 12 terminations of the same type and design.

### 5.5.1 Experiment I

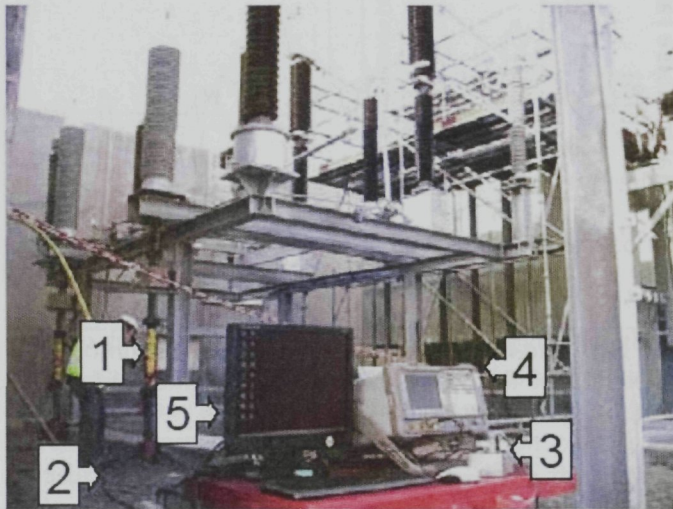


Figure 5.13: On-site testing of two 2-phase 150 kV cable systems with integrated inductive PD sensors. The RF PD detection system consists of (1) internal inductive sensor, (2) a coaxial cable, (3) an RF pre-amplifier, (4) spectrum analyser and (5) PC.

The experiment presented in the next paragraph is a performance check performed before the actual PD measurements and voltage withstand tests performed after laying of two 2-phase cable systems of 150 kV. Figure 5.13 shows the terminations of both circuits at the side of the transformer. In this case integrated inductive sensors were applied. No laboratory tests were performed for this type of terminations and thus a performance check was performed as follows:

#### ➤ Step 1:

Using the pulse generator artificial pulses of unknown equivalent pC level are injected at the top of each termination. The pulse generator is connected to the top of the termination via a 50 Ohm BNC wire clamped to the conductor of the termination. The artificial pulses had the following characteristics:

- Rise-time = 400 ps
- Pulse width = 10 ns (rectangular)
- 100 Hz repetition rate

#### ➤ Step 2:

The internal sensor then detected the injected pulses at several frequencies. The signal-to-noise ratios in the RF range are displayed for the case of each termination in Figure 5.14. The noise level during these measurements was shown previously in Figure 5.11 (b). A broad noise peak around 100 MHz makes these frequencies unusable for pulse detection. From Figure 5.14 it can be seen that the two signal-to-

noise ratios exhibit noticeable differences, although the terminations are of the same type and the measuring and injection equipment were correspondingly identical. These differences occur due to the high frequency characteristics of the injection cable that change with the cable positioning relative to the termination. A confirmation of this observation is presented in the next experiment in the case of several terminations.

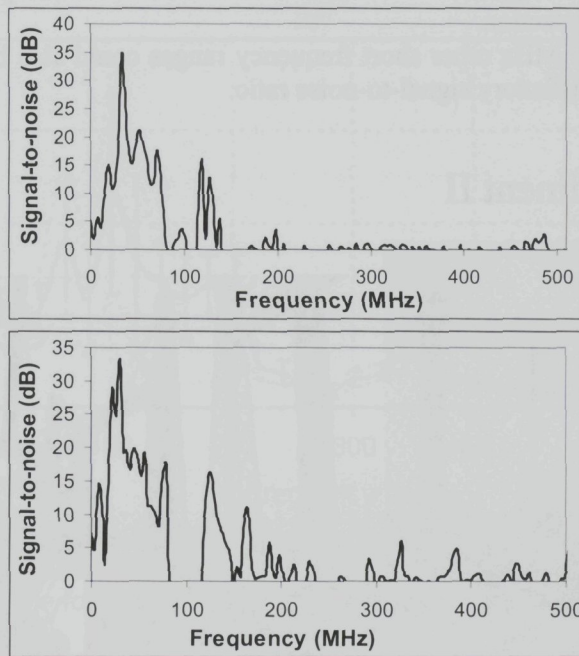


Figure 5.14: Signal-to-noise ratios as determined at each internal sensor of the terminations from injection of artificial pulses.

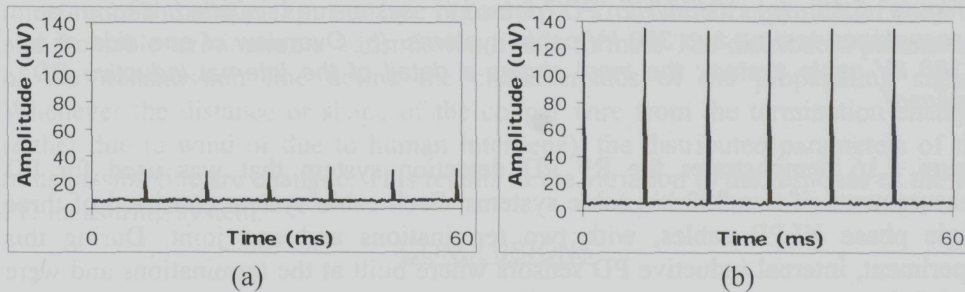


Figure 5.15: The injected pulses as detected by the SA at (a) 200 MHz, where  $S/N = 30/5 = 6$ , and (b) 50 MHz where  $S/N = 140/5 = 28$ .

### CONCLUSIONS FOR ON-SITE PERFORMANCE CHECK

From the results of the performance check presented in Figure 5.14 the following conclusions are made:

- The RF PD measuring system is able to detect possible PD pulses.
- The best measuring frequencies are below 200 MHz but not around 100 MHz due to high noise interference that makes these frequencies unusable for pulse detection.
- Above 100 MHz other short frequency ranges could also be identified that exhibit satisfactory signal-to-noise ratio.

#### 5.5.2 Experiment II

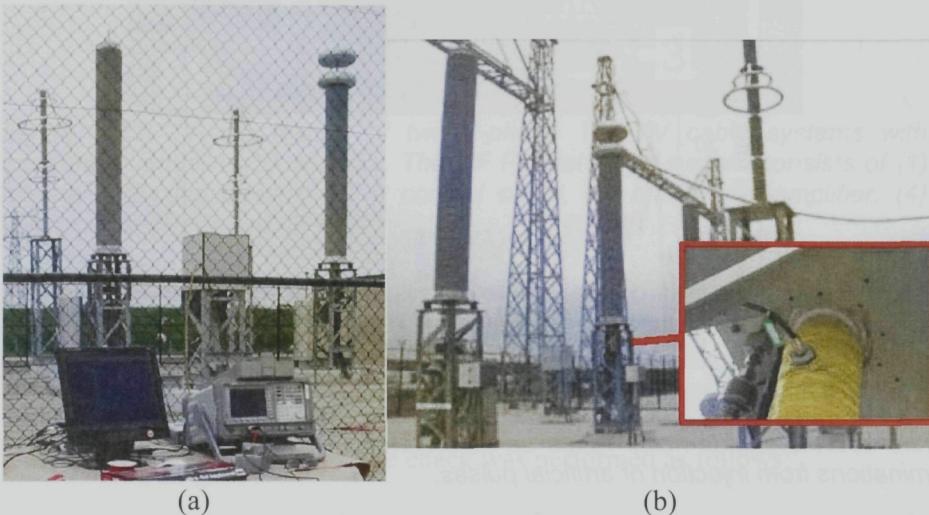


Figure 5.16: (a) VHF/UHF PD detection system as applied during an acceptance test on two 380 kV cable systems. (b) Overview of one side of a 380 kV cable system; the inset shows a detail of the internal inductive PD sensor.

Figure 5.16 demonstrates the RF PD detection system that was used for PD measurements of two 380 kV cable systems. Each cable system consisted of three single phase XLPE cables, with two terminations and one joint. During this experiment, internal inductive PD sensors were built at the terminations and were used. Prior to any measurements, a performance check was performed to determine the performance of each sensor in terms of the signal-to-noise ratio at various frequencies of the RF spectrum.

Therefore the same pulse generator as in the previous experiments was used to inject pulses in all 12 terminations of the cable systems that were of the same



model. Using the same equipment for all terminations the injection measurements were performed by tuning the RF measuring system at different center frequencies in steps of 3 MHz up to 500 MHz. The response in  $[\mu\text{V}]$  was measured in each frequency step and finally the average amplitude and its variance in  $[\mu\text{V}]$  was determined from the response in all terminations. The final result is shown in Figure 5.17.

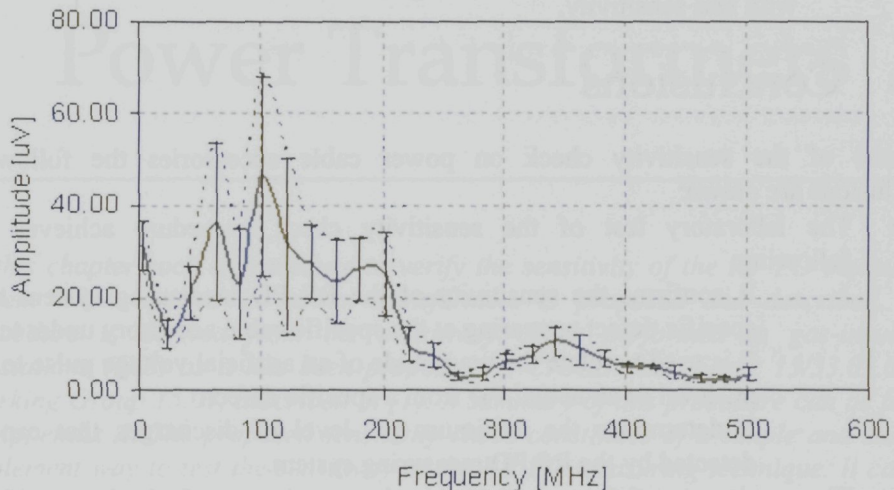


Figure 5.17: Average amplitude in  $[\mu\text{V}]$  and its spread (min to max measured value) in each measuring frequency. Results are obtained from injection measurements performed on 12 cable terminations of the same model.

From Figure 5.17 it can be seen that there is big variance in the response of the RF PD measuring system to the injections of the artificial pulse for frequencies up to 200 MHz. The variance that is noticed is mainly attributed to the wire used for injection of the artificial pulses (see Figure 5.5). From the arrangement of the wire and the cable termination a transmission line is formed. The distributed parameters of the transmission line define the characteristics of the propagating signal. Whenever the distance or shape of the copper wire from the termination changes (either due to wind or due to human intervene), the distributed parameters of the transmission line are changed. This results in the variation to the response of the RF PD measuring system.

### CONCLUSIONS

From Figure 5.17 the following conclusions can be made:

- The response of the RF PD measuring system to the injection of artificial pulses is defined by the transfer characteristics of the measuring equipment but also defined by the transfer characteristics of the injection circuit as well.

- Variance to the response of the RF PD measuring system is introduced from repositioning if the injecting wire.
- Despite the generated variance two frequency ranges of good sensitivity can be determined:
  - The general sensitivity remains strong in the frequency range up to 200 MHz.
  - In the frequency range 300 - 500 MHz detection is also possible but with less sensitivity.

## 5.6 Conclusions

In case of the sensitivity check on power cable accessories the following conclusions are drawn:

- The laboratory test of the sensitivity check procedure achieves the following:
  - It confirms the sensitivity of the RF PD measuring system to a specific defect appearing at the specific cable accessory under test
  - It is used to relate the magnitude of an artificial voltage pulse to the pC level of an actual PD from a specific defect.
  - It determines the minimum pC level of discharges that can be detected by the RF PD measuring system.
- The on-site test of the sensitivity check procedure confirms the sensitivity of the RF PD measuring system in the field where the noise levels are higher than in the laboratory.
- The sensitivity check procedure, in the laboratory and on-site, can only be performed for the same type of termination and power cable. In addition the same RF sensor and pulse generator should be used. Otherwise the transfer characteristics will be different from the laboratory to the on-site tests and the equivalent pC level of the pulse generator is no longer valid.
- If no laboratory test has been performed for a cable accessory a performance check can be done instead of a sensitivity check. The performance check gives a general impression of the system's sensitivity to a "hypothetical" PD under field noise conditions. The "hypothetical" PD can be simulated by artificial voltage pulses of appropriate frequency content emitted by a pulse generator.
- The injection circuit as was applied in this research generates a variance to the characteristics of the injected pulses.

---

# Sensitivity Check for Power Transformers

---

*In this chapter such a procedure to verify the sensitivity of the RF PD measuring system when applied in power transformers is proposed and described. The procedure is derived from the sensitivity check performed in gas-insulated substations (GIS) as it has been proposed by CIGRE Task Force 15/33.03.05 of Working Group 15.03, described in [1]. A summary of this procedure can be found in Appendix A. The proposed sensitivity check constitutes of a simple and easy to implement way to test the sensitivity of the RF PD measuring technique. It can be used instead of a numerical technique [38, 43, 73-75] because it is a quicker procedure that takes into account the real construction of the transformer and the current noise conditions.*

## 6.1 Introduction

In the previous chapters of the thesis it has been shown that a PD will generate electromagnetic waves that can propagate within the high-voltage equipment. The emitted signals can be detected in the radio frequency (RF) range of the spectrum with the use of proper antennas. However, there are cases where the sensitivity of the RF measuring system in transformers is hindered:

- ◆ The windings provide a major obstacle for electromagnetic waves travelling from one side of the tank to the other (see Chapter 3).
- ◆ There can also be other obstacles that obstruct the view of an RF sensor placed in their vicinity, such as the tap-changer.
- ◆ In addition, when an antenna is used through an oil-valve of the transformer, it is used outside of its operating bandwidth. In this case the antenna is less efficient and its transfer is different in each measuring frequency.

Therefore, a means of verifying the sensitivity of the RF PD measuring system is needed. In this chapter such a procedure to verify the sensitivity of the RF PD measuring system in power transformers is described. During the years of this research this procedure has been applied in the laboratory and field by other researchers in TUDelft. In a recent CIGRE publication [86] the procedure is also presented for the purposes of the sensitivity check of the PD measuring techniques in the UHF range.

## 6.2 Sensitivity check procedure

The transformer is a metallic cage with a complex interior structure that interferes with the propagation of the emitted signals within the tank. The complex interior structure results in complex propagation paths of the signals in contrast to the case of the GIS where the electromagnetic signals travel along its coaxial structure. Therefore a sensitivity check in transformers has to verify the sensitivity of the RF sensors at various possible PD defects and locations inside the tank. Based on the sensitivity check procedure for GIS, as is presented by [1] (see Appendix A), the proposed procedure adopted for transformers is similarly divided in the laboratory and on-site tests, which are described in Tables 6.1 and 6.2.

In the case of the on-site test the number of sensors used and their relative locations define the effectiveness of the sensitivity check. This is because the sensitivity of each sensor can be tested for possible PD locations in the area of the injecting sensor. If there is no sensor mounted on one side of the tank the sensitivity of the other sensors to a PD located in that side cannot be determined, since no injection is possible at that side.

There are cases where results from the laboratory test cannot be applied in the field. This happens when:

- ◆ There is high noise interference in the field at the frequency range where the laboratory test was valid, or
- ◆ The sensor that is used to inject artificial pulses is different to the sensor that was used in the laboratory tests, or
- ◆ There is only one RF sensor available on the tank.

In these cases verifying the sensitivity of the RF PD measuring system in comparison to conventional systems is not possible. However, a means of testing the detection capabilities of the RF PD measuring system is still necessary. For this reason a variation of the on-site test procedure is proposed that can test the detection performance of the measuring system. It is called a performance check and the procedure for a minimum of two sensors is outlined in Table 6.3.

<b>Laboratory Test</b>	
<b>1</b>	Installation of an artificial PD defect either within the transformer or at an opening on the tank.
<b>2</b>	<ul style="list-style-type: none"> <li>▪ Installation of a pair of RF sensors: 1) close to the defect setup (S1), and 2) on the same side of the transformer (S2).</li> <li>▪ Connection of a PD detection circuit (IEC 60270).</li> </ul>
<b>3</b>	<ul style="list-style-type: none"> <li>▪ Energizing of the defect and PD detection using both systems:</li> <li>▪ IEC 60270 conventional system in order to determine the discharge level in pC.</li> <li>▪ RF PD detection system in order to record the RF magnitude <math>A</math> at sensor S2 .</li> </ul>
<b>4</b>	Inject artificial pulses in sensor (S1) with the following characteristics: <ul style="list-style-type: none"> <li>- Rise time <math>\leq 1</math> ns</li> <li>- Pulse width <math>&gt; 500</math> ns (rectangular pulses)</li> <li>- PWHM <math>&gt; 20</math> ns (double exponential pulses)</li> <li>- Time between consecutive pulses <math>&gt;</math> duration of RF signal. (Usually less than 100 kHz).</li> </ul>
<b>5</b>	Acquire RF signal magnitude $B$ at sensor (S2). Compare magnitudes $B$ and $A$ obtained in step 3. Vary amplitude of artificial pulse until $B = A$ with an accepted tolerance of $\pm 20\%$ .

Table 6.1: Steps for the laboratory test for the sensitivity check of the RF PD measuring system in power transformers.

<b>On-site Test</b>	
<b>1</b>	Injection of the artificial voltage pulses as were obtained in step 5 of the laboratory step. The same type of equipment (pulse generator, cable and RF sensor) has to be used as for the laboratory test.
<b>2</b>	Measure RF signal at other coupler(s) mounted on the transformer. If signal is detected the sensitivity verification is successful for a PD located in the area of the injecting sensor.
<b>3</b>	If more than two sensors are employed, a sensitivity matrix can be built to compare the sensitivity of each sensor to the different areas of the transformer.

Table 6.2: Steps for the on-site test for the sensitivity check of the RF PD measuring system in power transformers.

<b>Performance Check</b>	
<b>1</b>	Inject artificial pulses in RF sensor with the following characteristics: Rise time $\leq 1$ ns Pulse width $> 500$ ns (rectangular pulses) PWHM $> 20$ ns (double exponential pulses) Time between consecutive pulses $>$ duration of RF signal. (Usually less than 100 kHz).
<b>2</b>	Measure RF signal at other sensor(s) mounted on transformer. If signal is detected the detection capabilities of that detecting sensor(s) to a PD located in the area of the injecting sensor are verified.
<b>3</b>	If more than two sensors are employed, a performance matrix can be built to compare the sensitivity of each sensor to the different areas of the transformer.
<b>4</b>	The average signal-to-noise ratio is determined for each sensor. Identify frequencies of high signal-to-noise ratio in the case of each sensor.

*Table 6.3: Steps for the performance on-site test of the RF PD measuring system in power transformers.*

In the case where only one sensor is available then injection of artificial pulses is not possible. The following can be performed instead:

- i) Injection of artificial pulses at the bushing of a transformer, or
- ii) Detection of pulses from the tap-changer if the tap-changer is located within the same tank.

In addition, in a laboratory setup, artificial discharging defects can be introduced at different areas of the tank in order to test the sensitivity of the single RF sensor in a specific transformer.

In this chapter experiments of laboratory test, field test and performance check for a minimum of two sensors will be presented. The steps described in Tables 6.1 to 6.3 will provide the main guidelines for applying each procedure.

## 6.3 Laboratory test

In the laboratory test the magnitude of an artificial voltage pulse is related to an actual PD of a desired pC level. The main difficulty for the laboratory test in transformers is the generation of an actual discharging defect. Actual destruction of the windings circuit is irreversible and is inappropriate for such expensive equipment. Therefore artificially built models of defects can only be used. Due to the closed tank, however, there are two ways to introduce discharges inside the tank:

- i) Through an opening of the tank, such as an oil or pressure valve.

- ii) Insertion of an artificial defect model inside the transformer by demounting the tank. The tank and oil are then replaced once the defect is placed.

In the following paragraphs, experiments for both cases of introducing a defect are presented.

### 6.3.1 Experiment I

In this experiment for the laboratory test procedure it will be presented how a defect can be introduced through a pressure valve at the top of the tank without the need to demount the transformer. The procedure was applied to a 14MVA-50kV transformer. A photograph of the transformer can be seen in Appendix D, Figure D.1 (a). Based on the steps for the laboratory test indicated in Table 6.1 the procedure was as follows:

➤ **Step 1:**

In this case a spark plug was used as a discharge source to create electromagnetic radiation inside the transformer. It was inserted from a pressure valve at the top of the tank.

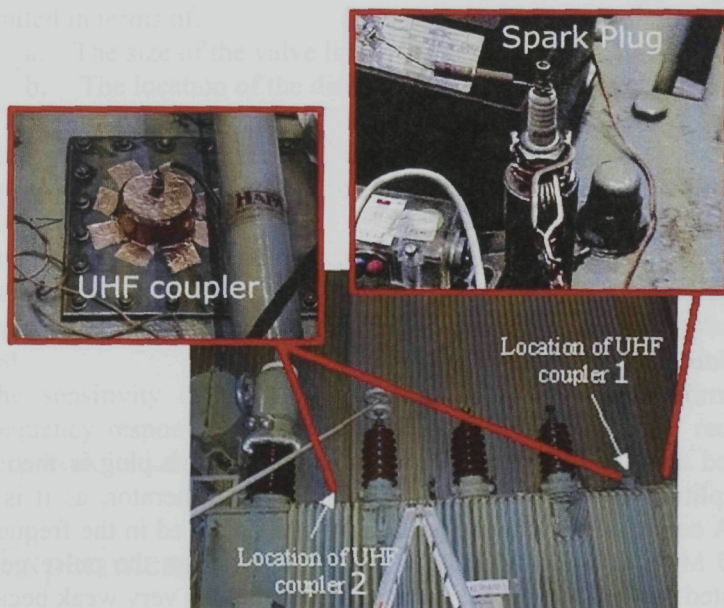


Figure 6.1: Laboratory setup used to perform a sensitivity check for RF PD Detection on power transformers. The location of the RF couplers and the spark plug are indicated.

➤ **Step 2:**

The transformer had two dielectric windows at the top where RF sensors could be attached (see Figure 6.1). RF coupler #1 was close to the spark plug as is demonstrated in the figure.

➤ **Step 3:**

The spark plug was energized in order to create discharges in the transformer. The corresponding discharge magnitude in pC is measured by the IEC method to be 30 pC. Then the RF signal is recorded at RF coupler #2 using a spectrum analyzer (SA).

➤ **Step 4:**

A pulse generator was used which generates pulses with amplitudes up to 45 V, rise time of 400 ps and pulse width of 10 ns. The frequency spectrum generated from the pulses of the pulse generator is displayed in Figure 6.2. The artificial pulses were injected at RF coupler #1. The corresponding RF signal is measured in RF coupler #2 using the SA.

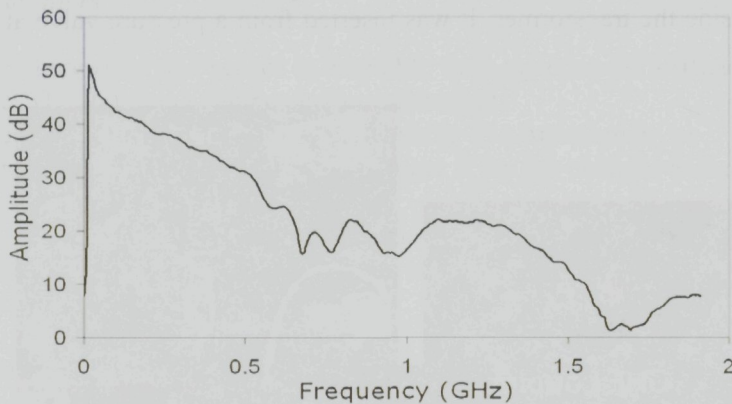


Figure 6.2: Frequency response of the pulse generator when measured by the SA via a 25dB attenuator.

➤ **Step 5:**

The measured amplitude of the discharges from the spark plug is then compared with the amplitude of the discharges from the pulse generator, as it is shown in Figure 6.3. A comparable frequency spectrum was achieved in the frequency range between 250 MHz and 600 MHz at a 14.2V output from the pulse generator. It should be noted that below 250 MHz the injected signal is very weak because of the low response in this frequency range of the RF sensors used for injection and detection. In addition, since the frequency content of the spark plug discharges reaches up to 600 MHz a comparison with the artificial pulses of the pulse generator beyond this frequency was not possible.



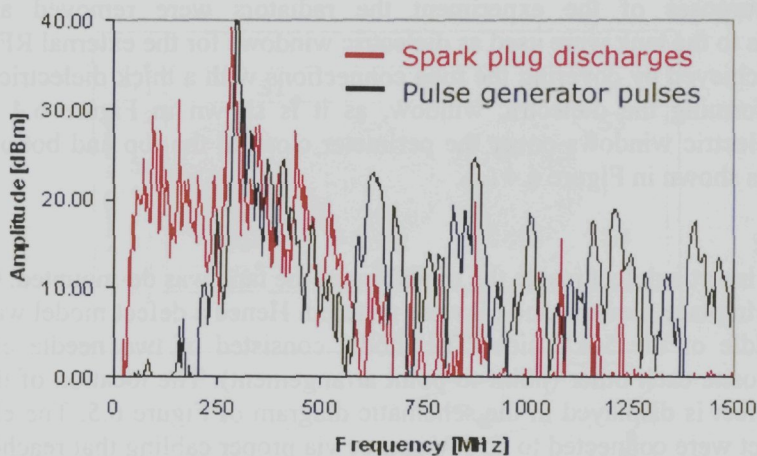


Figure 6.3: Signal-to-noise ratio of the frequency spectra obtained on RF sensor #2 for the case of: i) discharges from the spark plug (red) and ii) injected pulses with an amplitude of 14.2V (black).

### CONCLUSIONS FROM LABORATORY TEST

- Introducing a discharging defect via a valve on the transformer tank is limited in terms of:
  - a. The size of the valve limits the defect setup that can be used.
  - b. The location of the discharging defect is limited to the periphery of the tank.
- The artificial pulses injected using the specific pulse generator have an equivalent frequency content to a “defect” of 30 pC in the frequency range 300-600 MHz.
- The specific pulse generator can then be used to inject pulses in any other transformer to simulate the discharge of 30 pC. The RF measuring cables and sensor used for the injection should be the same as in the laboratory test.
- The sensitivity check below 300 MHz cannot be performed because frequency response of the antenna (used for injection and reception) was very weak in that frequency range.

## 6.3.2 Experiment II

In this experiment a laboratory test will be described where the discharging defects were placed inside the transformer after demounting of the tank. This way allows for the introduction of a defect setup that is more representative of actual transformer defects than the spark plug and at various locations inside the tank. The experiment was performed on the 14 MVA transformer, shown in Figure 6.4 (a).

For the purposes of the experiment the radiators were removed and their connections to the tank were used as dielectric windows for the external RF sensors. This was achieved by covering the tube connections with a thick dielectric sheet of Plexiglas forming the dielectric window, as it is shown in Figure 6.4 (b). The formed dielectric windows cover the perimeter close to the top and bottom of the tank, as it is shown in Figure 6.4 (c).

➤ **Step 1:**

In order to insert a defect inside the transformer, the tank was de-mounted. Once the defect was in place the tank and oil were restored. Hence a defect model was placed in the middle of the 50kV side. The model consisted of two needle electrodes placed opposite each other (point-to-point arrangement). The location of the point-to-point defect is displayed in the schematic diagram of Figure 6.5. The electrodes of the defect were connected to an HV source via proper cabling that reached out of the transformer through openings where the bushings used to be.

➤ **Step 2:**

For the purposes of the laboratory test sensor S5 was placed close to the defect. The rest of the sensors were placed sparsely around the transformer tank, so as to cover as much area of the tank as possible. The final arrangement of the sensors is displayed in Figure 6.5.

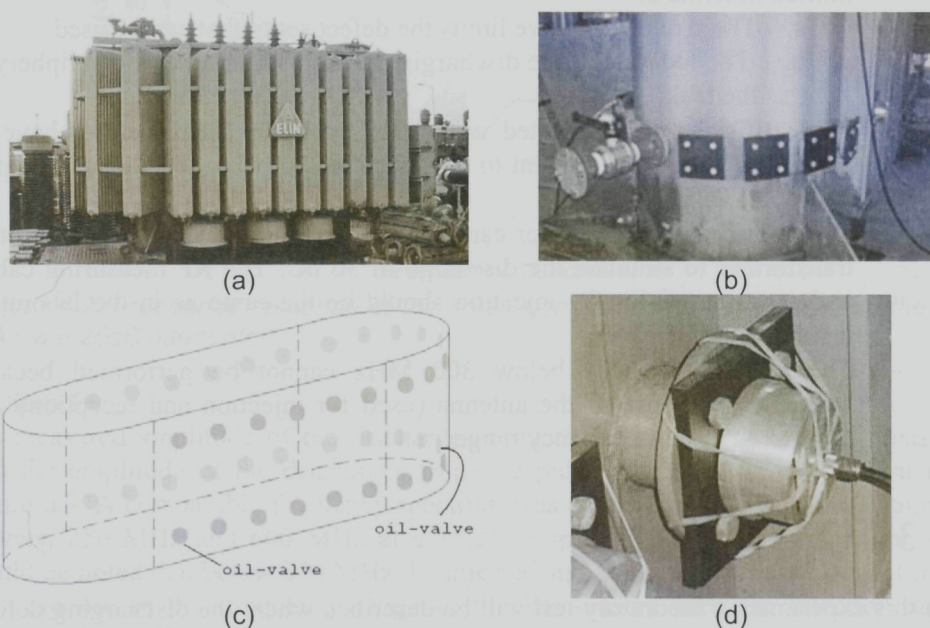


Figure 6.4: (a) The 14 MVA transformer with the radiators. (b) The radiators are removed and dielectric plates are mounted on the connections to the tank. (c) Available windows for RF sensor placement. (d) Extruded window with dielectric plate and RF sensor mounted.

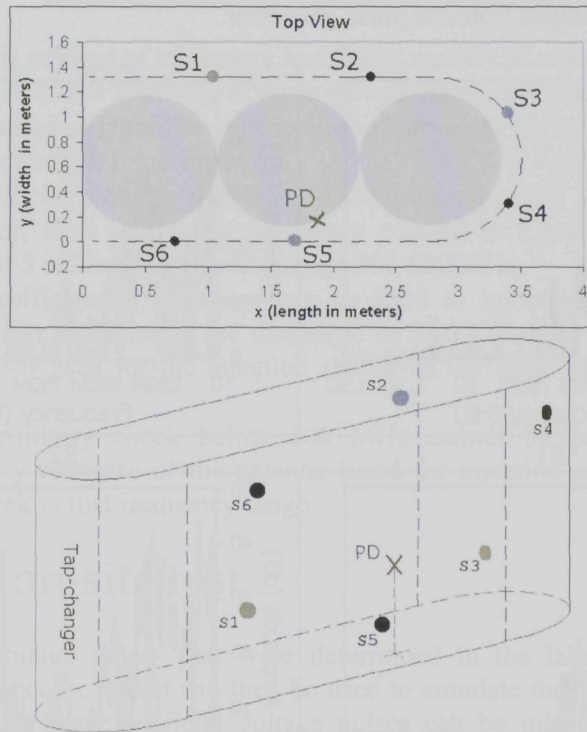


Figure 6.5: Schematic diagrams indicating the locations of the PD source and the RF sensors on the transformer tank. The indicated windings are sketched only, since the actual dimensions were unknown.

➤ **Step 3:**

When the PD source was activated the generated discharges were measured with an IEC 60270 system. The discharge level was generally unstable and varied between 600pC and 5nC. It was detected by all sensors and was recorded using a spectrum analyzer (SA).

➤ **Step 4:**

A pulse generator was used which generates pulses with amplitudes up to 45 V, rise time of 400 ps and pulse width of 10 ns. Artificial pulses were then injected in sensor S5. The frequency spectra were then recorded at the other sensors using the SA.

➤ **Step 5:**

The measured spectra of the discharges from the defect model were then compared with the spectra of the discharges from the pulse generator at different voltage output levels of the pulse generator. As it can be seen from Figure 6.6 a comparable

frequency spectrum was achieved in the frequency range between 300 MHz and 600 MHz at 45V output from the pulse generator.

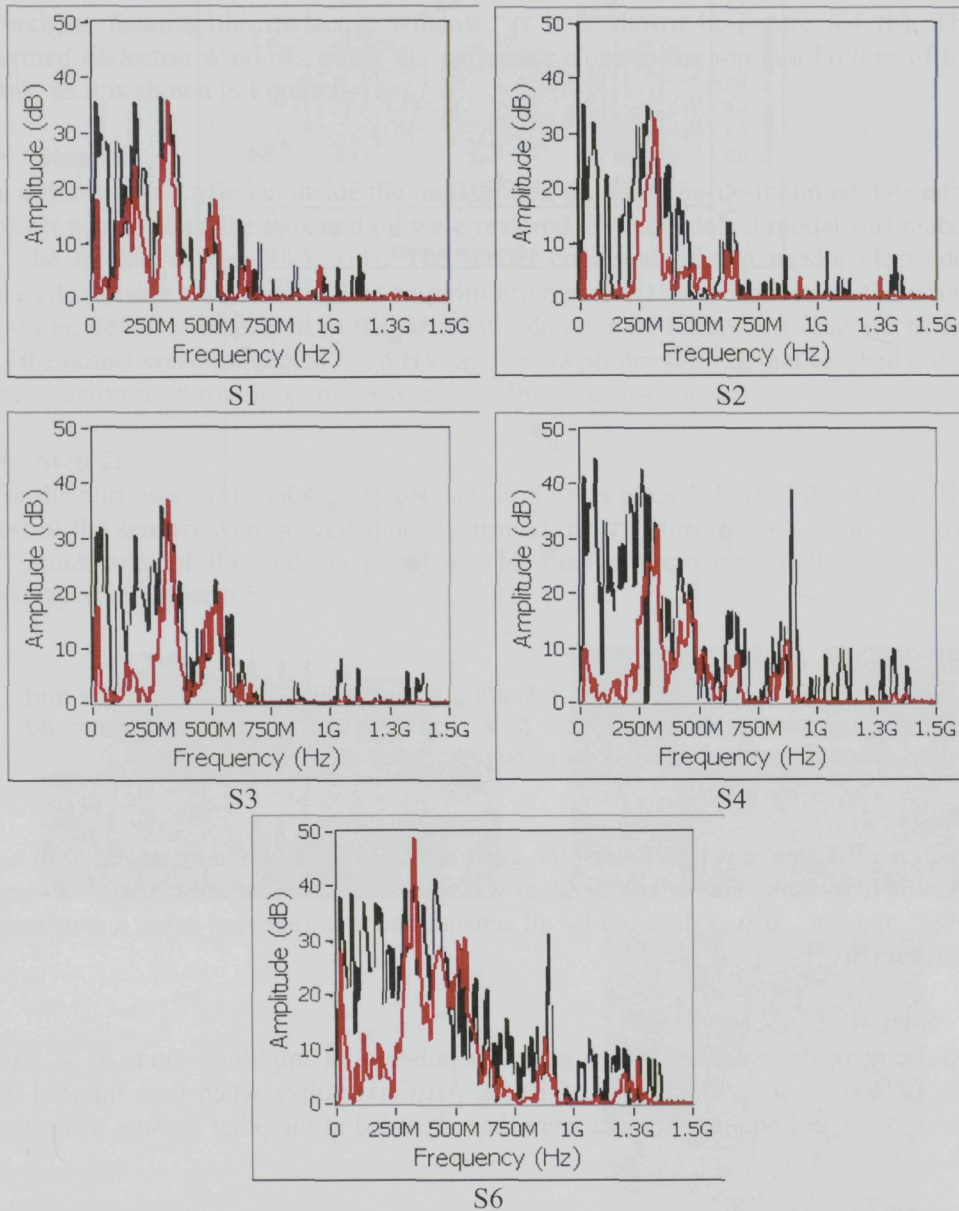


Figure 6.6: Signal-to-noise ratios of the frequency spectra obtained in the case of: i) discharges from the point-to-point defect (black) and ii) injected pulses with an amplitude of 45V (red).

### CONCLUSIONS FROM LABORATORY TEST

- With this method of laboratory test defect models of any size and geometry can be used. The locations of these defects can be anywhere inside the tank.
- This method of laboratory test is more appropriate for transformers than the one described in Experiment I.
- The artificial voltage pulses of 45V, injected using the specific pulse generator, have equivalent frequency content to a point-to-point corona defect of 5 nC in the frequency range 300-600 MHz.
- The specific pulse generator can be used to inject pulses in any other transformer to simulate the discharge of 5 nC. The RF measuring cables and sensor used for the injection should be the same as in the laboratory test.
- The sensitivity check below 300 MHz cannot be performed because frequency response of the antenna (used for injection and reception) was very weak in that frequency range.

## 6.4 The on-site test

The artificial voltage pulses that were determined in the laboratory test to be equivalent to a specific defect can then be used to simulate that defect in the field. In the on-site test these artificial voltage pulses can be injected inside the HV equipment via an RF sensor and the detection sensitivity of the successive sensors is verified following the steps described in Table 6.2. If the sensitivity check is successful, it is then assumed that all defects can be detected that:

- Have the equivalent pC level (or higher), and
- Are located at the vicinity of the tank where the injecting sensor resides.

In the following paragraphs, three on-site tests will be presented. In all experiments the sensitivity of the RF PD measuring system will be tested for the 30pC defect presented in the first experiment of the laboratory test (paragraph 6.2.1).

### 6.4.1 Experiment I

In this experiment the on-site test procedure will be performed on a 75 MVar and 52.5 kV reactor, shown in Figure 6.7 (b). The tank of the reactor was originally equipped with four dielectric windows mounted on each side of the tank. Four identical external RF sensors were mounted on the dielectric windows of the same type as the ones used in the laboratory tests. An oil-valve was also available that allowed for the insertion of an internal sensor. The locations of the dielectric windows and the oil-valve are shown in Figure 6.7 (a).

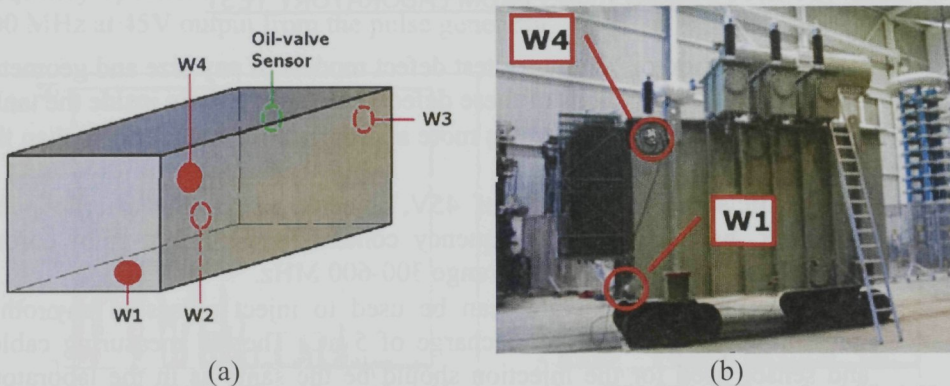


Figure 6.7: (a) Schematic diagram of the positions of RF sensors' positions. (b) Picture with sensors W1 and W4 visible.

The on-site test procedure described in Table 6.2 takes place as follows:

➤ **Step 1:**

Using the pulse generator from step 5 of the laboratory test (Figure 6.2) artificial pulses equivalent to 30 pC were injected in one of the RF sensors.

➤ **Step 2:**

The sensitivity of the other sensors was then confirmed for a 30 pC defect in the frequency range of 300-600 MHz. In Appendix F the detected frequency spectra from the injection measurements can be found. This procedure was then repeated by injecting with the same pulse generator at the rest of the sensors and detecting at the others.

➤ **Step 3:**

An effective way to present the sensitivity of all the RF sensors, as it was obtained during the pulse injection procedure, is in a matrix format as follows:

- The corresponding spectra magnitudes can be determined by calculation of the average power in the frequency spectrum (AP) given by equation (5.1) that is reproduced here [49]:

$$AP = 10 \cdot \log \left( \sum_{i=1}^N \left( \frac{S_i + S_{i+1}}{2} \right)^2 \cdot \frac{1}{N} \right) \quad (6.1)$$

where  $AP$  is the average power of the signal at the sensor,  $S_i$  and  $S_{i+1}$  are the amplitudes of the signal-to-noise ratio of two successive data points, and  $i$  is the index of the data point.

- All signal  $APs$  are then normalized to the highest average power ( $AP_{max}$ ) and displayed as a percentage in a *sensitivity matrix*, as shown in Figure 6.8.

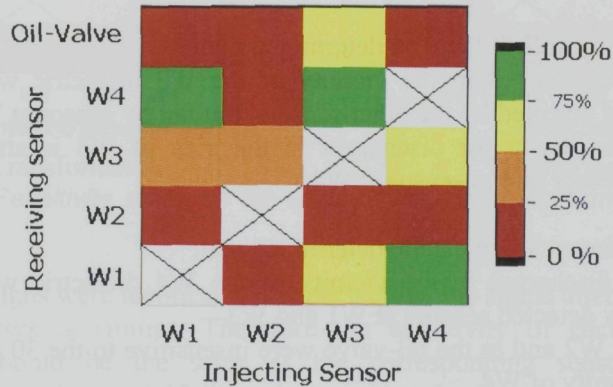


Figure 6.8: Sensitivity matrix obtained from injecting a pulse in one sensor and measuring at the others in the frequency range of 300-600 MHz.

The percentage ranges indicated in the sensitivity matrix of Figure 6.8 are translated as follows:

- From 50% to 100%: signals are clearly detectable;
- 25% to 50%: Received signals are highly attenuated but still detectable;
- Lower than 25%: The measured spectra of the received signals are negligible and hence the signal is barely detected or not at all.

It should be noted that no conclusions on the sensitivity of the RF PD measuring system to the 30pC defect can be drawn from pulse injection at the internal sensor (oil-valve). This is because the frequency response of the internal sensor is different to the frequency response of the RF sensor used in the laboratory test to inject the pulses. Therefore, the frequency response of the injected artificial pulses is not equivalent to the actual defect used in the laboratory test.

### CONCLUSIONS OF FIELD TEST

From the obtained sensitivity matrix in Figure 6.8, the following can be concluded for the sensitivity of the RF PD measuring system in the frequency range of 300-600 MHz to a defect that generates 30 pC of discharges:

From pulse injection at W1 it can be determined that:

- Possible discharges in the vicinity of the W1 dielectric window can be detected efficiently only by sensor at W4.
- Sensor at W3 can also be used for detection of discharges at the area of W1 but with limited sensitivity. Sensor at W4 should be preferred.

From pulse injection at W2 it can be determined that:

- Only the sensor at W3 can be used to detect discharges originating from the location of W2.

From pulse injection at W3 it can be determined that:

- Possible discharges in the vicinity of the W3 dielectric window can be efficiently detected by the other sensors, but not by sensor at W2.
- Higher sensitivity for discharges in the area of W3 is attributed to the internal sensor and to sensor at W4.

From pulse injection at W4 it can be determined that:

- Possible discharges in the vicinity of the W4 dielectric window can be efficiently detected sensors at W1 and W3
- Sensor at W2 and in the oil-valve were insensitive to the 30 pC PD located at the vicinity of W4.
- Higher sensitivity for discharges in the area of W4 was attributed to sensor at W1 and.

## 6.4.2 Experiment II

Similarly to the previous experiment the on-site test was performed on two 90 MVA - 150 kV transformers of the same design, shown in Figure 6.9 (a). Both transformers were each equipped with four RF sensors placed at the corresponding positions indicated in the schematic diagram of Figure 6.9 (b). The results from the on-site test performed on each transformer are displayed in the sensitivity matrix format in Figure 6.10.

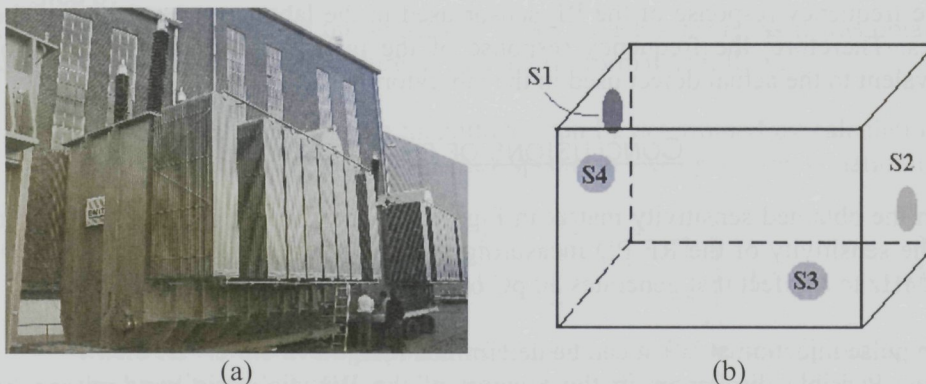


Figure 6.9: (a) Two 90 MVA, 150 kV power transformers of the same built. (b) Schematic diagram indicating the locations of the four RF sensors on the transformer tank of the transformers.



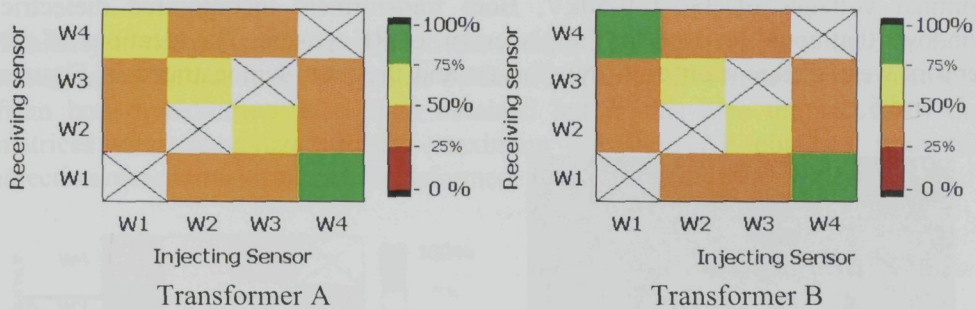


Figure 6.10: Sensitivity matrices for each of the two transformers of the same model.

Since both designs were identical it is expected that the signal attenuation within the two transformers is similar. Therefore the sensitivity of each sensor in one transformer should be the same at the corresponding sensor on the other transformer. From Figure 6.10 it can be seen that the sensitivity is the same for all corresponding sensors of the two transformers except in the case of sensor at W1, which is less in the case of transformer A. This difference occurs due to changes observed in the noise level during the injection measurements of sensor at W1 of transformer A.

### CONCLUSIONS OF FIELD TEST

By comparing the sensitivity matrices of the two 'twin' transformers the following can be concluded:

- o In terms of the sensitivity of the RF PD measuring system: all sensors should be capable to detect a PD source equivalent to 30 pC in the frequency range of 300-600 MHz.
- o Transformers of the same design, which also incorporate sensors at the same corresponding locations, have the same sensitivity in term so the sensor locations. The sensitivity of the sensors of the RF PD measuring system can be established for all transformers by performing the sensitivity check on one of them.
- o It is necessary to perform a sensitivity check prior to actual PD measurements in order to establish the sensitivity of the RF PD measuring system as is defined by the current noise levels.

### 6.4.3 Experiment III

In this experiment another case of two transformers of the same design will be examined. In this case, however, the transformers incorporate RF sensors at different locations on the tank. The transformers' specifications were: 500 MVA at

nominal voltages of 380-150-50kV. Both transformers incorporated dielectric windows that could be used for the placement of RF sensors. The locations of the sensors were different on each transformer and they are demonstrated in Figures 6.11 and 6.12.

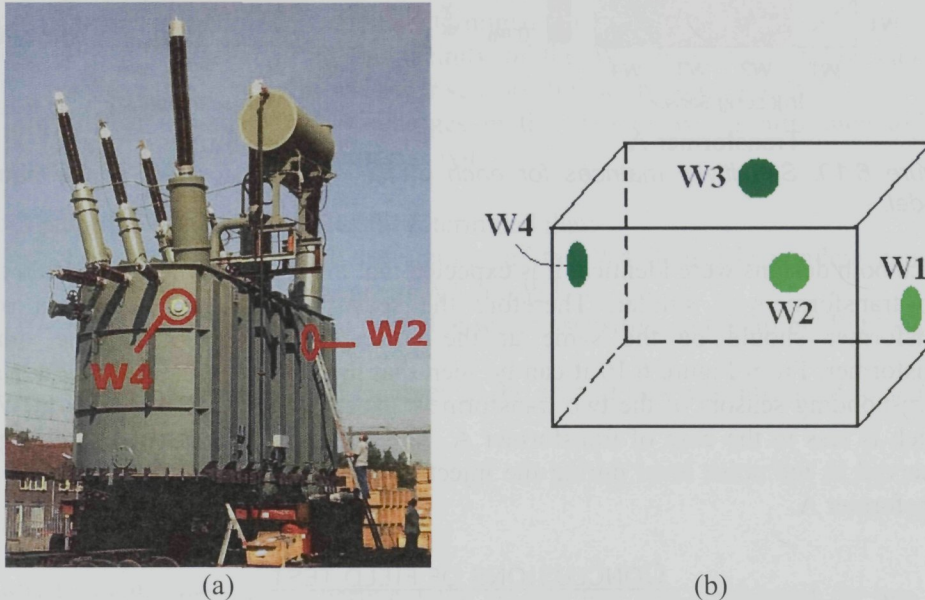


Figure 6.11: Transformer A: (a) 500 MVA, nominal voltages of 380-150-50kV. (b) Schematic diagram indicating the locations of the four RF sensors on the transformer tank.

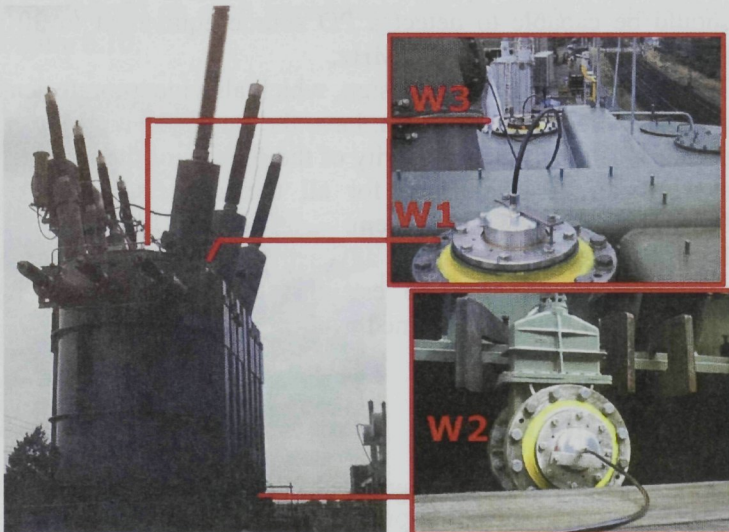


Figure 6.12: Transformer B: 500 MVA, 380-150-50kV nominal voltages. The locations of the three RF sensors are also demonstrated.

Similarly to the previous experiments the sensitivity check was performed on both transformers following the procedure outlined in Table 6.2. The sensitivity matrices from both transformers were then obtained but in this case the values of the matrices were normalized to the maximum measured AP obtained from the injection measurements of both transformers. Results are displayed in Figure 6.13.

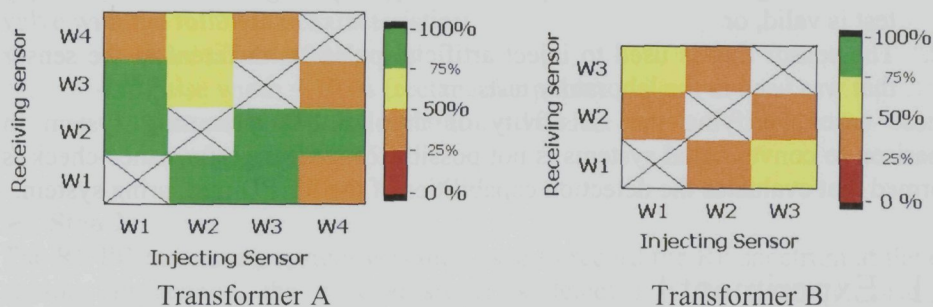


Figure 6.13: Sensitivity matrices for each of the two 500 MVA transformers. The values of the matrices were normalised to the maximum measured AP obtained from the injection measurements of both transformers.

The two sensitivity matrices cannot be compared directly since the sensor locations are different in each case. For the case of transformer A very good overall sensitivity is observed. From this sensitivity matrix no conclusions can be made for the sensitivity of the sensors to PD sources located at the top or bottom area of the tank. Obstacles such as the bushing housings or connections to the windings could block the propagation path of PD signals originating at that area. The sensitivity check in transformer B can then be used to complement the results of the sensitivity check of transformer A. In the case of transformer B the sensitivity of sensors across the bottom and top of the transformer is confirmed. Therefore it can be said that the electromagnetic PD signals can travel from the top to the bottom of the tank without any major attenuation. This indicates that a sensor located at the sides of the tank can detect PD sources from the top area of the transformer.

### CONCLUSIONS OF FIELD TEST

The following can be concluded from this field test:

- o The sensor arrangement used in the case of transformer A provides sufficient sensitivity for all locations of PD that correspond to areas of injecting sensors from transformer A and B.
- o The sensitivity check can be used with different sensor arrangements in transformers of the same design to make general conclusions on the sensitivity of various possible PD locations.

## 6.5 Performance Test

There are cases where results from the laboratory test cannot be applied in the field. This happens when:

1. There is high noise interference at the frequency range where the laboratory test is valid, or
2. The sensor that is used to inject artificial pulses is different to the sensor that was used in the laboratory tests

In these cases verifying the sensitivity of the RF PD measuring system in comparison to conventional systems is not possible. Instead a performance check is performed that evaluates the detection capabilities of the RF PD measuring system.

### 6.5.1 Experiment I

In the case of the 75 MVA and 52.5 kV reactor, shown in Figure 6.7 (b), the sensitivity check could not be completed for the case of the internal sensor through the oil-valve. The frequency response of the internal sensor is different to the frequency response of the dielectric window type of sensor that was used during the laboratory test. This difference results in a different artificial pulse to be injected via the internal sensor instead of the one that was determined by the laboratory test to correspond to the 30pC defect. This can be seen if the spectra obtained at the dielectric window sensors are averaged and compared for two cases of pulse injection:

1. Pulse injecting in the internal sensor
2. Pulse injection in a dielectric window sensor.

The averaged spectra are displayed in Figure 6.14. It can be seen that the spectra from each injection are different depending on the transfer of each sensor that attenuates different frequencies of the injected pulse.

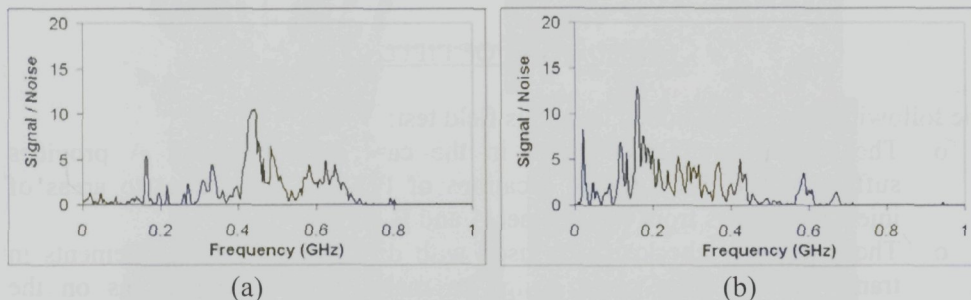


Figure 6.14: Signal-to-noise ratios obtained from averaging the spectra of received signals at sensors at W1, W2 and W4 when injecting in (a) sensor at W3, and (b) internal sensor at oil-valve.

Therefore, for the internal sensor a performance check should be applied to verify its detection capabilities in the whole RF range. Therefore, following the steps of Table 6.3 a performance check was performed:

➤ **Step 1:**

A pulse generator was used to inject artificial pulses at the internal sensor in the oil-valve with the following characteristics:

- Rise time = 400 ps
- Pulse width = 10 ns (rectangular pulse)
- Frequency of pulse repetition = 100 Hz
- Voltage output = 45 V

➤ **Step 2:**

The RF PD measuring system was then used to record the RF spectrum at the other sensors. In general, the injected signal is detected if the signal-to-noise ratio measured at the receiving sensors is increased.

➤ **Step 3:**

From injection measurements at each sensor a performance matrix is built and is displayed in Figure 6.15.

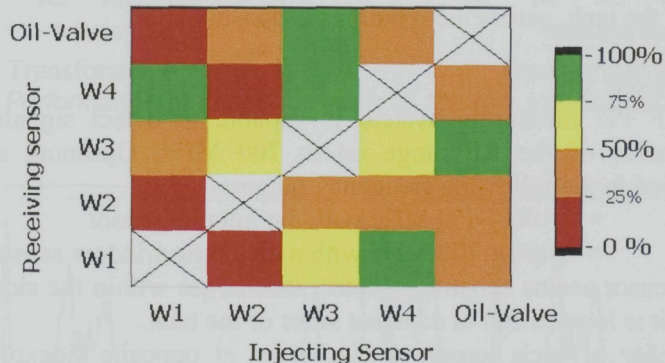


Figure 6.15: Performance matrix obtained from injection measurements in the RF range.

Similar to the sensitivity matrix the percentage ranges are translated as follows:

- From 50% to 100%: signals are clearly detectable;
- 25% to 50%: Received signals are highly attenuated but still detectable;
- Lower than 25%: The measured spectra of the received signals are negligible and hence the signal is barely detected or not at all.

By comparing the sensitivity matrix of Figure 6.8 and the performance matrix of Figure 6.15, it can be seen that the sensitivity in the case of some sensors has

changed. This occurs because in this case the signal-to-noise ratio of the signals is compared for the whole RF range and not only between 300-600 MHz. Therefore, signals of higher or lower frequency content, that were ignored in the sensitivity check before, are considered in the performance check and the AP values of the signal-to-noise ratios increase.

➤ **Step 4:**

The average spectra for the internal and the dielectric windows sensors were displayed in Figure 6.14. From these figures the frequencies where signals are detected with optimum signal-to-noise ratio at all or individual sensors are identified. In this case the internal sensor (Figure 6.14 (b)) seems to have a preference in the frequency range 100 - 450 MHz, while the dielectric windows sensors (Figure 6.14 (a)) have a better response in the frequency range 300 - 600 MHz.

### CONCLUSIONS FROM PERFORMANCE CHECK

For the case of the oil-valve sensor the following can be concluded:

- Its optimum sensitivity is in the frequency range 100-450 MHz
- From injecting signals at sensors at W2, W3 and W4: its sensitivity to PD sources at adjacent sides of the transformer is acceptable.
- From injecting at sensor at W1: its sensitivity to PD sources in the opposite side of the tank, across the windings is questionable.

General conclusions are:

- The RF PD measuring system is capable to detect signals in various frequencies of the RF range up to 700 MHz. Optimum sensitivity is identified in the following frequency ranges:
  - 100 – 450 MHz with the internal sensor
  - 400 – 700 MHz with a dielectric window sensor
- Each sensor seems capable to detect discharges within the side of the tank where it is located and in adjacent sides of the tank.
- Sensitivity of each sensor to discharges at opposite side of the tank is hindered across the transformer's length. Especially in sensors at W1-W2 and Internal-W1.
- One sensor at each side of the tank provides sufficient sensitivity to discharges in the periphery of the tank.

## 6.5.2 Experiment II

The case of the two 90 MVA - 150 kV transformers of the same design, shown in Figure 6.9 (a), is revisited in this paragraph. A performance check is performed in both transformers and performance matrices are obtained and displayed in Figure

6.16. The averaged signal-to-noise ratios from all injection measurements (see step 4 in Table 6.3) were also determined and are displayed in Figure 6.17.

From Figure 6.10 it can be seen that the determined sensitivity is different between the two transformers. These differences occur due to changes observed in the noise level during the various injection measurements. As it can be seen from Figure 6.18 the noise spectra for sensors at W1 of both transformers have differences in the RF range, especially below 400 MHz. This explains the lower sensitivity of the sensors in transformer B, which can also be seen in the average signal-to-noise ratio displayed in Figure 6.17. at the frequencies below 400 MHz the signal-to-noise ratio is lower than in the case of transformer A. For other frequencies the differences could be due to noise fluctuations that were not recorded, but they could also be due to small differences in the construction of the transformers occurred during their manufacturing.

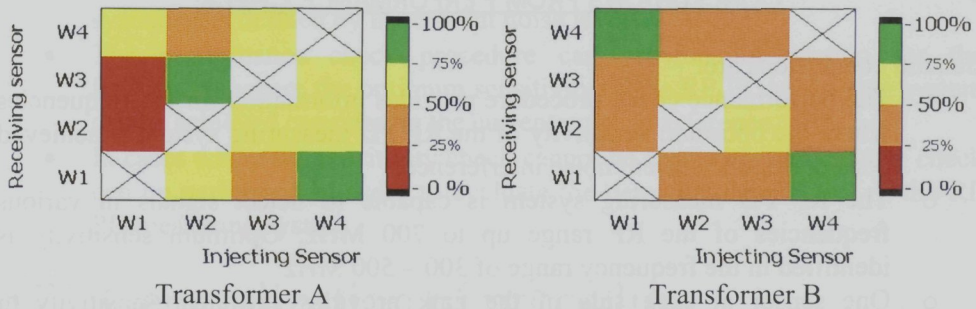


Figure 6.16: Performance matrices for each of the two transformers of the same model.

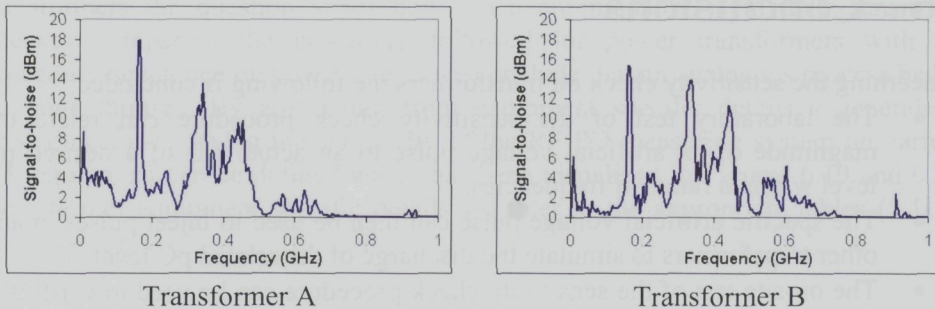


Figure 6.17: Signal-to-noise ratios obtained from averaging the spectra of received signals at all sensors, which were obtained from injection of artificial pulses.

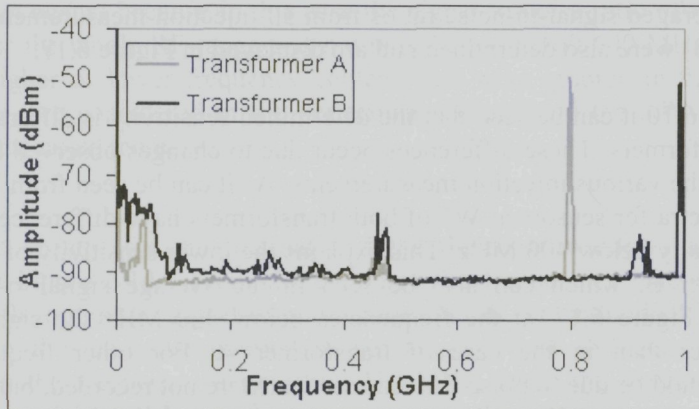


Figure 6.18: Noise spectra measured at sensor at W1.

### CONCLUSIONS FROM PERFORMANCE CHECK

General conclusions are:

- The performance check procedure provides information for the frequencies where the optimum sensitivity of the RF PD measuring system is achieved considering the current noise interference.
- The RF PD measuring system is capable to detect signals in various frequencies of the RF range up to 700 MHz. Optimum sensitivity is identified in the frequency range of 300 – 500 MHz
- One sensor at each side of the tank provides sufficient sensitivity to discharges in the periphery of the tank.

## 6.6 Conclusions

Concerning the sensitivity check on transformers the following is concluded:

- The laboratory test of the sensitivity check procedure can relate the magnitude of an artificial voltage pulse to an actual PD of a desired pC level within a range of frequencies.
- The specific artificial voltage pulse can then be used to inject pulses in any other transformers to simulate the discharge of the related pC level.
- The on-site test of the sensitivity check procedure can be used to verify the sensitivity of the RF PD measuring system to various defects and [pC] levels in the transformer under test. This way it offers a sensitivity check comparable to conventional systems.
- In this chapter the sensitivity of the RF PD measuring system to a corona defect of 30 pC was confirmed for the following HV equipment:
  - Reactor of 75 MVA<sub>r</sub>, 52.5 kV.
  - Transformer of 90 MVA - 150 kV



- Transformer of 500 MVA, 380-150-50kV
- At least one sensor at each side of a transformer is required for sufficient sensitivity at all areas of the complete structure.
- In this case a sensitivity matrix can provide important information for the sensitivity of each sensor to different areas of the transformer.
- The sensitivity check can be used with different sensor arrangements in transformers of the same design to make general conclusions on the sensitivity of various possible PD locations.
- Transformers of the same design, which also incorporate sensors at the same corresponding locations, have the same sensitivity in terms of their sensor locations. Therefore, the sensitivity of the sensors of the RF PD measuring system can be established for all transformers by performing the sensitivity check on one of them.
- It is necessary to perform a performance check prior to actual PD measurements in order to establish the sensitivity of the RF PD measuring system as is defined by the current noise levels.
- The performance check procedure can provide information for the frequencies where the optimum sensitivity of the RF PD measuring system can be achieved considering the current noise interference.
- In cases where the sensitivity check cannot be applied a performance check can be performed in order to evaluate the detection capabilities of the RF PD measuring system.

## 6.7 Generalization of procedure

Having learned from the foregoing application in GIS< power cables and transformers the question arises how much commonality is in their sensitivity checks. Comparing the procedure followed for power transformers with the procedure developed on power cables we conclude that an analogous process had to be gone through. By abstracting from equipment specific details a generalised procedure for verifying the sensitivity of the RF PD measuring system on various HV equipment can be defined which has been visualized in Figures 6.19 and 6.20. To interpret equipment specific details we refer to the appropriate tables (5.1-5.3 and 6.1-6.3)

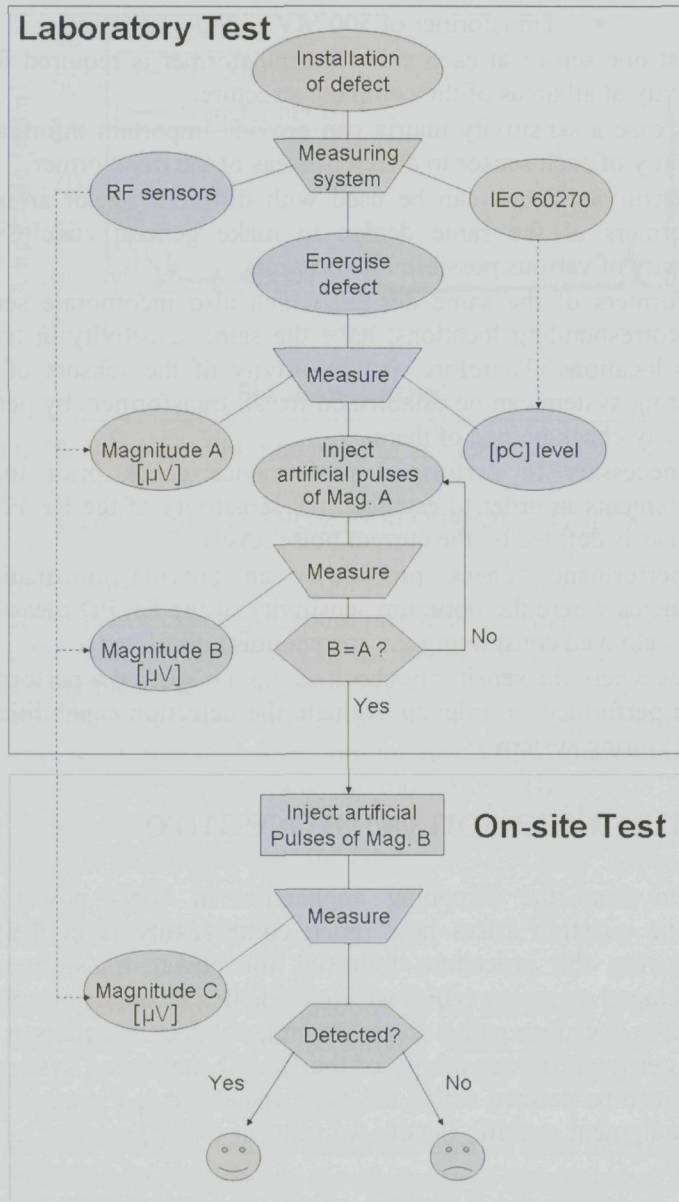


Figure 6.19: The generalised sensitivity check procedure.

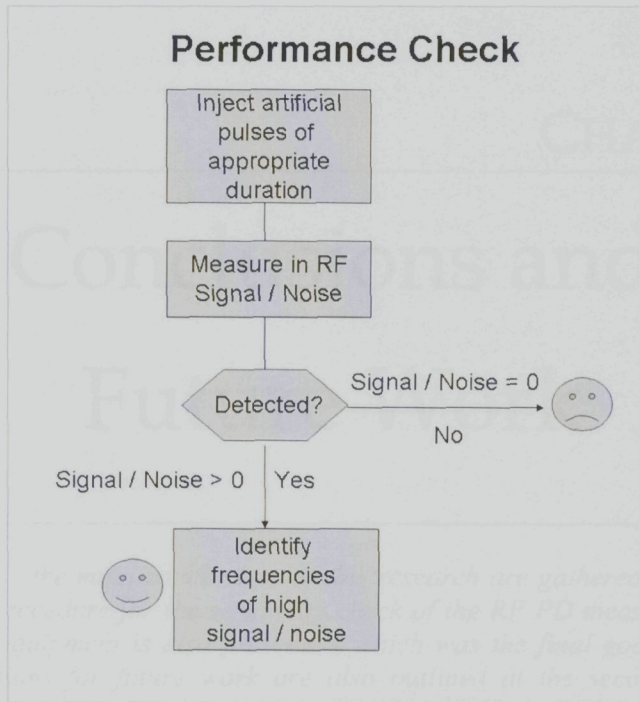
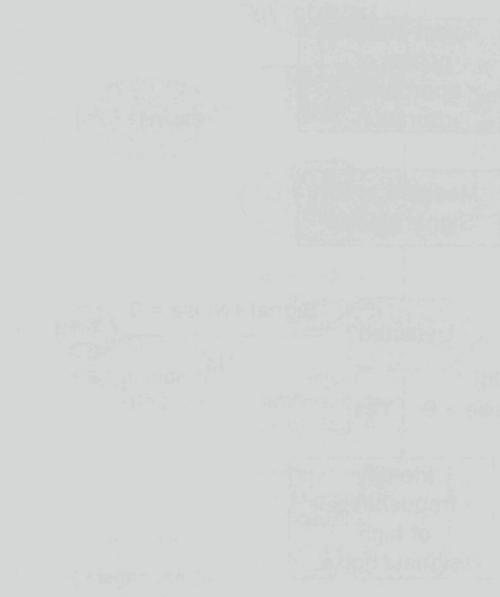


Figure 6.20: If a laboratory test is not performed then a performance check is performed on-site instead.

### Performance Check



The performance check is a laboratory test that is used to determine the effectiveness of a performance check. It is a laboratory test that is used to determine the effectiveness of a performance check.

---

## CHAPTER 7:

---

# Conclusions and Future Work

---

*In this chapter, the main conclusions of this research are gathered and presented. The general procedure for the sensitivity check of the RF PD measuring system in high voltage equipment is also presented, which was the final goal of this thesis. Recommendations for future work are also outlined at the second part of this chapter.*

## 7.1 Conclusions

With regard to non-standardized partial discharge (PD) measurements in the radio frequency range (RF), the research presented in this thesis resulted in a generalization of the method's applicability for high-voltage equipment, like GIS, power cables and power transformers. A generalized approach for a sensitivity check in HV equipment was obtained which was verified successfully for two study cases, i.e. power transformers and cable accessories. Major conclusions are as follows.

1. The sensitivity of the RF PD measuring technique differs from its application at different types of HV components.
2. Laboratory experiments on full size objects are a very important step in terms of:
  - a. Appropriate application of the technique for optimum sensitivity, and
  - b. Confirmation of the technique sensitivity to specific defects.
3. The sensitivity check procedure offers a means of verifying the sensitivity of the RF PD measuring technique with results comparable to the conventional and standardized systems measuring the PD in [pC]

## 7.1 Conclusions

---

4. General guidelines can be deduced for a sensitivity check procedure for all HV equipment.

Furthermore, concerning more specific issues on the RF PD measuring methodology we concluded the following:

- 1) Insulation discharging defects in power cables and transformers emit electromagnetic waves in frequency ranges high enough to be detected by a RF PD detection system.
- 2) The frequency spectra emitted by discharging insulation defects depend on the type of insulation, physical parameters of the defect and construction of the HV equipment.
- 3) Insulation defects in power cables and transformers emit electromagnetic waves in frequency ranges high enough to be detected by a RF PD detection system.
- 4) The propagating waves are affected by reflection and attenuation introduced by the HV component. In the case of power transformers, the complex inner structure obstructs the propagation. In the case of power cables the major attenuation originates from the semiconducting screens.
- 5) The VHF-range is most applicable in case of power cables, the UHF-range in case of power transformers.
- 6) The major influence on the detected signal's transfer is introduced by the RF sensors. As a result, to optimize the sensitivity, the sensors should be suited for the specific application.
- 7) The sensitivity check procedure offers a means of verifying the sensitivity of the RF PD measuring technique with comparable results to the conventional systems measuring the PD in [pC]
- 8) Sensitivity of the system to specific defects in HV equipment can be evaluated in the laboratory resulting in on one hand the minimum pC level of discharges that can be detected and on the other hand a artificial pulse for on-site sensitivity evaluation.

- 9) Identify the frequencies where the optimum sensitivity of the RF PD measuring system can be achieved considering the current noise interference.
- 10) A sensitivity check should always be performed prior to actual PD measurements in order to establish the sensitivity of the RF PD measuring system as is defined by the current noise levels.

Overall it can be concluded that the developed sensitivity check procedure is an easy to implement procedure that considers the actual structure of the high-voltage equipment and the current noise levels at the time of PD measurement. In addition it proves that the RF detection system has at least similar sensitivity as the conventional detection technique according to the IEC 60270 recommendation. The generalised procedure for verifying the sensitivity of the RF PD measuring system on various HV equipment was described in Figures 6.19 and 6.20.

## 7.2 Future Work

With regard to un-conventional PD detection on the accessories of HV power cables the following issues are of interest:

- The possibility of a different way to inject signals in terminations should be established. The variation from the current injection circuit is too broad and should be reduced. This way the repeatability of the procedure will be improved and a sensitivity check will be performed with better accuracy. A suggestion would be to induce pulses in the accessory using a current transformer placed around it.
- The possibility to inject in joints should also be examined. Either via internal sensors or via current transformers placed around the cable as it was suggested for the case of terminations.
- Additional discharging defect models have to be tested to further establish the sensitivity of the RF PD measuring system at defects of various types and at different accessories.
- As it was already shown, internal sensors have better sensitivity to current probes applied externally at the grounding of the sheath. Therefore further research should be performed to optimize the sensitivity of the externally applied sensors. This can be achieved by determining the appropriate type and dimensions of the grounding wire for optimum transmission of the transient PD current.

Referring to un-conventional PD detection on power transformers the following aspects should be investigated in the future:

- For the laboratory tests in transformers, further research is suggested in order to study how the [pC] measuring of the conventional system to the defect under test, is affected if the coupling capacitor is connected to the different bushings of the transformer. If the [pC] measuring greatly differs for the discharges of the same defect then a standard connection of the conventional system should be suggested for the comparison with the RF measuring system during the laboratory tests.
- Improvement of the internal sensor design to ameliorate its sensitivity in the RF range. In this thesis a spiral variation of the monopole was used in an effort to lengthen the conductive elements of the antenna and hence increase the detected current. A more detailed design of this antenna can be performed.
- The sensitivity to defects inside the windings has to be confirmed. This can be achieved in appropriate laboratory setups but also with extensive field measurements on older transformers. In combination with other diagnostic techniques that can detect discharges the detection of this type of defects can be found in aged transformer populations. Such a complementary diagnostic technique can be DGA, which can detect the occurrence of discharges from the released gases.
- Additional discharging defect models have to be tested to further establish the sensitivity of the RF PD measuring system at defects of various geometries and at different oil conditions. It should be established if the sensitivity of the RF PD measuring system is indeed defect-dependent as it was observed in the cavity model of Chapter 2. If yes then the risk involved with the defects that cannot be detected should be determined.
- The higher sensitivity of the sensors closer to the PD indicates possibilities for locating the PD source. It has been shown by several researchers that it is possible to locate using time-of-flight signal data. It should be examined if it is possible to determine the location of the PD source from the attenuation of the signals too.

In general, the major purpose of calibration procedures of conventional PD systems is to scale the reading of the systems in that way that the measuring results are comparable with the results in other conventional measuring systems. Now, for all HV components acceptance criteria for the PD inception voltage level (PDIV) and PD-magnitudes in [pC] or [nC] are indicated. So finally the challenging question



remains “Which PD parameters (the same or other) have to be used to define these criteria for non-conventional PD measurements?”

## REFERENCES

[1] J. Van den Broek, “VDE: ‘PD Detection Systems for GIS: Sensitivity and Accuracy of the ‘E’ Method and the Acoustic Method”, *Electra*, No.102, April 1992.

[2] IEC 60076-4:2002, “High Voltage Test Techniques for Power Transformers – Measurements”, International Electrotechnical Commission, Geneva, Switzerland, 3rd edition.

[3] IEC 60076-4:2002, “High Voltage Test Techniques for Power Transformers – Measurements”, International Electrotechnical Commission, Geneva, Switzerland, 3rd edition.

[4] IEC 60076-4:2002, “High Voltage Test Techniques for Power Transformers – Measurements”, International Electrotechnical Commission, Geneva, Switzerland, 3rd edition.

[5] IEC 60076-4:2002, “High Voltage Test Techniques for Power Transformers – Measurements”, International Electrotechnical Commission, Geneva, Switzerland, 3rd edition.

[6] IEC 60076-4:2002, “High Voltage Test Techniques for Power Transformers – Measurements”, International Electrotechnical Commission, Geneva, Switzerland, 3rd edition.

[7] IEC 60076-4:2002, “High Voltage Test Techniques for Power Transformers – Measurements”, International Electrotechnical Commission, Geneva, Switzerland, 3rd edition.

[8] IEC 60076-4:2002, “High Voltage Test Techniques for Power Transformers – Measurements”, International Electrotechnical Commission, Geneva, Switzerland, 3rd edition.

[9] IEC 60076-4:2002, “High Voltage Test Techniques for Power Transformers – Measurements”, International Electrotechnical Commission, Geneva, Switzerland, 3rd edition.

[10] E.F. Stenzen, S.M. Bredas, P.A. de Wit, T. Van der Weide, J. Van der Weide, M.M. van Riet, G.P.T. van der Weide, “Leistungsfähigkeit von GIS”, *Electra*, No.102, April 1992.

...with the [pC] measuring system. The [pC] measuring system is used to compare the results of the RF PD measuring system with the results of the [pC] measuring system. The results of the RF PD measuring system should be investigated in the future.

- o For the laboratory work in windings, further research is suggested in order to study how the [pC] measuring of the conventional system to the defect under test is affected if the coupling capacitor is connected to the different bushings of the transformer. If the [pC] measuring greatly differs for the discharges of the same defect than a standard connection of the conventional system should be suggested for the comparison with the RF measuring system during the laboratory tests.
- o Improvement of the internal sensor design to increase its sensitivity in the RF range. In this thesis a spiral variation of the monopole was used as an effort to lengthen the conductive elements of the antenna and hence increase the detected current. A more detailed design of this antenna can be performed.
- o The sensitivity to defects inside the windings has to be confirmed. This can be achieved in appropriate laboratory setups but also with extensive field measurements on older transformers. In combination with other diagnostic techniques that can detect discharges the detection of this type of defects can be found in aged transformer populations. Such a complementary diagnostic technique can be DGA, which can detect the occurrence of discharges from the released gases.
- o Additional discharging defect models have to be tested to further establish the sensitivity of the RF PD measuring system at defects of various geometries and at different oil conditions. It should be established if the sensitivity of the RF PD measuring system is indeed defect-dependent as it was observed in the cavity model of Chapter 2. If yes then the risk involved with the defects that cannot be detected should be determined.
- o The higher sensitivity of the sensors closer to the PD indicates possibilities for locating the PD source: it has been shown by several researchers that it is possible to locate using time-of-flight signal data. It should be examined if it is possible to determine the location of the PD source from the attenuation of the signals too.

In general, the major purpose of calibration procedures of conventional PD systems is to scale the reading of the systems in that way that the measuring results are comparable with the results in other conventional measuring systems. Now, for all HV components acceptance criteria for the PD inception voltage level (PDIV) and PD-magnitudes in [pC] or [nC] are indicated. So finally the challenging question

## REFERENCES

---

- [1] CIGRE TF 15/33.03.05, "PD Detection System for GIS: Sensitivity Verification for the UHF Method and the Acoustic Method", *Electra* No.183, April 1999
- [2] IEC 60270: "IEC International Standard 60270. "High Voltage Test Techniques - Partial Discharge Measurements". International Electrotechnical Commission (IEC), Geneva, Switzerland, 3rd edition, 2000.
- [3] IEC 60505: "Evaluation and qualification of electrical insulation systems", third edition, 2004
- [4] IEC 60840: "Power cables with extruded insulation and their accessories for rated voltages from 30 kV up to 150 kV", second edition, 1999
- [5] IEC 60267: "Tests for power cable systems: cables with extruded insulation and their accessories for rated voltages above 150 kV ( $U_m = 170$  kV) up to 500 kV ( $U_m = 525$  kV)", first edition, 2001
- [6] CIGRÉ Working Group D1.11: 'Service Aged Materials' (Task Force D1.11.01): "Service Aged Insulation: Guidelines on Managing the Ageing Process", June 2003, Brochure No. 228
- [7] CIGRÉ Task Force 15.01.04: "Partial Discharges in Transformer Insulation", Session 2000, No. 15-302
- [8] A.K. Lokhanin, G.Y. Shneider, V.V. Sokolov, V.M. Chornogotsky, T.I. Morozova: "Internal Insulation Failure Mechanisms Of HV Equipment Under Service Conditions", CIGRÉ Session 2002, No. 15-201
- [1] CIGRE TF 15/33.03.05, "PD Detection System for GIS: Sensitivity Verification for the UHF Method and the Acoustic Method", *Electra* No.183, April 1999
- [9] CIGRE WG 15.03, "Diagnostic Methods for GIS Insulating Systems", CIGRE Paper 15/23-01, Paris 1992.
- [10] E.F. Steennis, S.M. Berlijn, F.H. de Wild, F. van den Boogaard, C.G.N. de Jong, M.J.M. van Riet, G.P.T. van der Wijk: "Learning from high-voltage

- XLPE cable system testing and monitoring”, Ref. No: 21-203, Cigré, Paris, France, 2000.
- [11] E. Pultrum, E.F. Steennis, M.J.M. Van Riet et al.: “Test After Laying, Diagnostic Testing Using Partial Discharge Testing at site.”, paper 15/21/33-12, Cigré, Paris, France, 1996
- [12] E. Pultrum, S.A.M. Verhoeven: “Testing of extruded cables: Experience in type testing, PQ testing and test after installation. What do we learn from it?”, Session paper, Ref. No: B1-104, Cigré, 2004
- [13] Stefan Tenbohlen, Sacha M. Markalous, Stefan M. Hoek, Richard Huber, Thomas Strehl, T. Klein, D. Denissov, Uwe Riechert: “Electromagnetic (UHF) PD Diagnosis Of GIS, Cable Accessories And Oil-Paper Insulated Power Transformers For Improved PD Detection And Localization”, Ref. No: D1-104, Cigré, 2006
- [14] J.B.Kim, M.S.Kim, H.S.Kim, W.P.Song, H.S.Lee, J.R. Jung, Y.J. Choi: “Experience Of The On-Line Intelligent Partial Discharge Monitoring (Ipdm) System For GIS Using UHF Method”, Ref. No: D1-108, Cigré, 2006
- [15] E. Gulski ,S. Meijer, J.J. Smit, A. Bun, A. Jansen, H. Geene, R. Koning, L. Lamballais, T.J.W.H. Hermans, E.R.S. Groot, J. Slangen, M.J.M. Boone, J. Kanters, F. De Vries, R. Leich: “Condition Assessment And AM Decision Support For Transmission Network Components”, Ref. No: D1-110, Cigré, 2006
- [16] CIGRE WG 21.05, 2002: “*Experience with AC Tests After Installation on the main insulation of polymeric (E)HV cable systems*”, Electra, No. 205, December 2002
- [17] CIGRE WG 21.09, 1997: “*After Laying Tests on High Voltage Extruded Insulation Cable Systems*”, Electra, No. 173, August 1997
- [18] M. Muhr, T. Strehl, E. Gulski, K. Feser, E. Gockenbach, W. Hauschild: “Sensors And Sensing Used For Non-Conventional PD Detection”, Ref. No: D1-102, Cigré, 2006
- [19] J. S. Pearson, O. Farish, B. F. Hampton, M. D. Judd, D. Templeton, B. M. Pryor and I. M. Welch, "Partial discharge diagnostics for gas insulated substations", IEEE Trans. Dielectrics and Electrical Insulation, Vol. 2, No. 5, pp. 893-905, October 1995

- [20] S. A. Boggs, "Partial Discharge – Part III: Cavity-Induced PD in Solid Dielectrics", IEEE Electrical Insulation Magazine, Nov./Dec. 1996, Vol. 6, No. 6, pp. 11-20.
- [21] G.C. Stone and S.A. Boggs. Propagation of Partial Discharge pulses in shielded power cable. Annual report Conference on Electrical Insulation and Dielectric Phenomena, National Academy of Sciences, Washington, DC. pp 275-280, 1982.
- [22] G. Mugala. High Frequency Characteristics of Medium Voltage XLPE Power Cables. Doctoral Thesis, Stockholm, Sweden, 2005, ISBN 91-7178-215-X.
- [23] A.R Blythe and D. Bloor. Electrical Properties of Polymers. 2nd edition, Cambridge University Press, 2005, ISBN 0521552192.
- [24] G. Mugala, R. Eriksson, U. Gäfvert, and P. Pettersson. Measurement Technique for High Frequency Characterization of Semi-conducting Materials in Extruded Cables. IEEE Transactions on Dielectrics and Electrical Insulation Vol. 11, No. 3, page 471 to 480, 2004.
- [25] Boggs S. and Densley J., "Fundamentals of Partial Discharge in the Context of Field Cable Testing", IEEE Electrical Insulation Magazine, Vol. 16, No. 5, pp. 13-18, (2000).
- [26] S.A. Boggs, A. Pathak, and P. Walker, "Partial Discharge XXII: High Frequency Atenuation in Shielded Solid Dielectric Power Cable and Implications Thereof for PD Location", IEEE Electrical Insulation Magazine, Vol. 12, Jan/Feb 1996, pp. 9-16
- [27] Stewart B.G., Judd M.D., Reid A.J., Fouracre R.A.: "Suggestions to augment the IEC60270 partial discharge standard in relation to radiated electromagnetic energy", Electrical Insulation Conference and Electrical Manufacturing Expo, 2007, 22-24 Oct., pp: 175-178.
- [28] A. Convery, M D Judd: "Measurement of propagation characteristics for UHF signals in transformer insulation materials", Proc. 13th Int. Symp. on High Voltage Engineering (Delft), August 2003
- [29] E. Gulski, J. J. Smit, F. Wester: "PD Knowledge Rules for Insulation Condition Assessment of Distribution Power Cables", IEEE Transactions on Dielectrics and Electrical Insulation Vol. 12, No. 2; April 2005, pp: 223-239.

- [30] E.Gulski, J.J.Smit, and R.Brooks: "Partial Discharge Databases For Diagnosis Support Of HV Components" IEEE International Symposium on Electrical Insulation, Arlington, Virginia, USA, (1998), pp. 424-427
- [31] Gulski, E. Burger, H.P. Vaillancourt, G.H. Brooks, R.: "PD pattern analysis during induced test of large power transformers", IEEE Transactions on Dielectrics and Electrical Insulation, Feb 2000, Volume: 7, Issue: 1, page(s): 95-101.
- [32] Gulski, E. Cichecki, P. Wester, F. Smit, J. Bodega, R. Hermans, T. Seitz, P. Quak, B. Vries, F.: "On-site testing and PD diagnosis of high voltage power cables", IEEE Transactions on Dielectrics and Electrical Insulation, December 2008, Volume: 15, Issue: 6, page(s): 1691-1700
- [33] E.Gulski, J.J.Smit, R. Schomper J. Slangen, P. Schikarski: "Condition Assessment Model for Power Transformers", Proc.14th International Symposium on HV Engineering (ISH), Beijing 2005
- [34] B. R. Hamerling, F. J. Wester, E. Gulski, J. J. Smit, and E. R. S. Groot, "Fundamental aspects of on-line PD measurements on distribution power cables", Proceedings of the 7 th IEEE International Conference on Solid Dielectrics (ICSD), pp. 408-411, Eindhoven, the Netherlands, June 2001.
- [35] B.F. Hampton and R. J. Meats, "Diagnostic measurements at UHF in gas insulated substations", IEE Proceedings, Vol. 135, Pt. C, No. 2, 1988, pp. 137-144.
- [36] C. G. Henningsen, K. Polster, B. A. Fruth and D. W. Crass, "Experience with an on-line monitoring System for 400 kV XLPE cables", IEEE Transmission and Distribution Conf., Los Angeles, 1996, pp. 515-520
- [37] M.D.Judd, O.Farish, J.S.Pearson and B.F.Hampton: "Dielectric Windows for UHF Partial Discharge Detection", IEEE Transactions on Dielectrics and Electrical Insulation, Vol. 8, No. 6, pp. 953-958 (2001)
- [38] M.D.Judd, L.Yang, I.B.B.Hunter: "Partial Discharge Monitoring for Power Transformers Using UHF Sensors Part 1: Sensors and Signal Interpretation", IEEE Electrical Insulation Magazine, Vol. 21, No. 2, (2005)
- [39] M. D. Judd, L. Yang, I. B. B. Hunter: "Partial discharge monitoring for power transformers using UHF sensors Part 2: Field Experience", IEEE Insulation Magazine Vol. 1, No. 3, pp. 5-13, May/June 2005

- [40] M. D. Judd, G. P. Cleary and C. J. Bennoch, "Applying UHF Partial Discharge Detection to Power Transformers", IEEE Power Engineering Review, August 2002, p.57.
- [41] M. D. Judd, O. Farish, J. S. Pearson, T. Breckenridge and B. M. Pryor: "Power Transformer Monitoring Using UHF Sensors: Installation and Testing", IEEE International Symposium on Electrical Insulation, Anaheim, CA, USA, April 2-5, 2000, page(s) 373-376.
- [42] M D Judd, O Farish and B F Hampton, "Broadband couplers for UHF detection of partial discharge in gas insulated substations", IEE Proc., Science, Measurement and Technology, Vol. 142, No. 3, pp. 237-243, May 1995
- [43] M.D. Judd, L. Yang and I. J. Craddock: "Locating Partial Discharges using UHF Measurements: A Study of Signal Propagation using the Finite-Difference Time-Domain Method", 14th International Symposium on High Voltage Engineering, August 25-29,2005 Tsinghua University, Beijing, China
- [44] M. Kawada, K. Isaka: "Visualization of Electromagnetic Waves Emitted from Partial Discharge using the Constrained Interpolation Profile (CIP) Method", IEEE Transactions On Electrical And Electronic Engineering, 2007, vol.1, page(s): 97-99
- [45] F. Massingue, S. Meijer, P.D. Agoris, J.J. Smit, J. Lopez-Roldan: "*Partial Discharge Pattern Analysis of Modeled Insulation Defects in Transformer Insulation*", Conference Record of the 2006 IEEE International Symposium on Electrical Insulation, Toronto, Ont., 11-14 June 2006, page(s): 542-545
- [46] Y. Lu, X. Tan and X. Hu: "PD detection and localisation by acoustic measurements in an oil-filled transformer", IEE Proc.-Sci. Meas. Technol., Vol. 147, No. 2, (2000).
- [47] L. E. Lundgaard, "Partial Discharge - Part XIII: Acoustic Partial Discharge Detection-Fundamental Considerations", IEEE Electrical Insulation Magazine July/August 1992, Vol.8, No.4, pp25-31
- [48] L.E. Lundgaard, "Partial Discharge - Part XIV: Acoustic Partial Discharge Detection - Practical Application", 5 IEEE Electrical Insulation Magazine, September/October 1992, Vol.8, No.5, pp.34-43

- [49] S. Meijer: "Partial Discharge Diagnosis of High-Voltage Gas-Insulated Systems", PhD thesis, Technical University of Delft, 2001, The Netherlands, ISBN: 90-77017-23-2.
- [50] S. Meijer, P. D. Agoris, E. Gulski, P. P. Seitz, T. Hermans and L. Lamballais: "Advanced Partial Discharge Measuring System for Simultaneous Testing of Cable Accessories", 8th International Conference on Properties and applications of Dielectric Materials, Bali, June 2006, page(s): 687-690
- [51] S. Meijer, P. D. Agoris, E. Gulski, P. P. Seitz, T. Hermans and L. Lamballais: "Condition Assessment of Power Cable Accessories using Advanced VHF/UHF PD detection", ISEI conference proceedings, Toronto, Canada, 2006
- [52] S. Meijer, P.D. Agoris, E. Gulski, P.P. Seitz, T. Hermans, L. Lamballais, "Simultaneous Condition Assessment of Accessories of Power Cables using a Wireless VHF/UHF PD Detection System", Conference Proceedings CMD, Changwon, Korea, 2006.
- [53] S. Meijer, E. Gulski, J.J. Smit, H.F. Reijnders, "Sensitivity check for UHF PD detection on power transformers", Conference Proceedings ISEI, Indianapolis, USA, 2004.
- [54] S. Meijer, P.D. Agoris, J.J. Smit, M.D. Judd, L. Yang: "Application of UHF Diagnostics to Detect PD During Power Transformer Acceptance Tests", Conference Record of the 2006 IEEE International Symposium on Electrical Insulation, Toronto, Ont., 11-14 June 2006, page(s): 416-419
- [55] S. Meijer, P.D. Agoris, J.J. Smit: "UHF PD Sensitivity Check on Power Transformers", 14th International Symposium on High Voltage Engineering, Beijing, China, 2005
- [56] S. Meijer, P.D. Agoris, J.J. Smit: "Location of Insulation Defects in Power Transformers Based on Energy Attenuation Analysis", Conf. Proc. ISEIM, Japan 2005
- [57] S. Meijer, P. Cichecki, P.D. Agoris, J.J. Smit, H.F. Reijnders: "UHF Sensors for Partial Discharge Diagnostics of Power Transformers", Proceedings of the International Conference on Electrical Engineering and Informatics Institut Teknologi Bandung, Indonesia June 17-19, 2007



- [58] NEN 3630: "Cables with insulation of cross-linked polyethylene and their accessories for voltages of 50 kV up to and including 150 kV", ICS code 29.060.20, Commission number 364020, 2004.
- [59] W.P.Song, J.B.Kim, M.S.Kim, J.R.Jung, "UHF Narrow Band Type Partial Discharge Method for the Internal Insulation Performance Verification of the Gas Insulated Switchgear", Trans. KIEE, vol. 54C, no. 9, pp. 414-420, 2005.
- [60] A. Wilson: "Condition and Life Assessment: Failure Analysis in Power Transformers", The Life of A Transformer Seminar, Rome, Italy, 27-29 Oct. 2003
- [61] "High Voltage Engineering and Testing", edited by Hugh M. Ryan, IEE Power and energy series 32, 2<sup>nd</sup> edition, 2001, The institution of Electrical Engineers, ISBN 0-852967756
- [62] "Electrical Power Cable Engineering", edited by William A. Thue, 1999 published by Marcel Dekker, Inc., ISBN: 0-8247-9976-3
- [63] "Advances in High Voltage Engineering", edited by A. Haddad and D. Warne, IEE Power & Energy series 40, 1<sup>st</sup> edition, 2004, The institution of Electrical Engineers, ISBN 0-852961588
- [64] Constantine A. Balanis, Antenna Theory: Analysis and Design, 3rd Edition, John Wiley & Sons, USA, 2005, ISBN 0-471-66782-X
- [65] John D. Kraus, Electromagnetics, 4th Edition, McGraw-Hill International, 1991, ISBN, 0-07-035621-1
- [66] John D. Dyson, "The Equiangular Spiral Antenna", IRE Transactions on Antennas and Propagation, April 1959, Vol. AP-7, pp. 181-187.
- [67] G. Wanninger, "Apparent charge measurement in GIS by modern diagnostic methods," Eur. Trans. Elect. Power, vol. 7, pt. 4, pp. 251-255, Jul/Aug 1997.
- [68] F.H. Kreuger, Industrial High Voltage, Vol. 1 & 2, Delft University Press, 1991.
- [69] P.H.F. Morshuis, Partial discharge mechanism. Ph.D. Thesis Delft University Press, Delft University of Technology, The Netherlands (1993) ISBN 90-6275-931-9.

- [70] Pompili, M. Mazzetti, C. Bartnikas, R. : "PD pulse burst characteristics of transformer oils", IEEE Transactions on Power Delivery, April 2006, Volume: 21, Issue: 2, page(s): 689- 698.
- [71] CIGRÉ Working Group A2.18, "Guide for Life Management Techniques For Power Transformers", CIGRÉ Broschure 227, 20 January 2003, CIGRÉ: Paris, France.
- [72] S. M. Markalous, Detection and Location of Partial Discharges in Power Transformers using acoustic and electromagnetic signal, PhD Thesis, University of Stuttgart, 2006
- [73] Judd, M.D.: "Using finite difference time domain techniques to model electrical discharge phenomena", Annual Report Conference on Electrical Insulation and Dielectric Phenomena, 2000, Volume: 2, On page(s): 518-521.
- [74] Yang, L. Judd, M.D. Costa, G.: "Simulating propagation of UHF signals for PD monitoring in transformers using the finite difference time domain technique", Annual Report Conference on Electrical Insulation and Dielectric Phenomena (CEIDP), 2004, 17-20 Oct.,page(s): 410 - 413
- [75] Xiao, S. Moore, P.J. Judd, M.D. Portugues, I.E. : "High frequency finite element analysis of electromagnetic radiation due to partial discharges in high voltage equipment", IEEE Power and Energy Society General Meeting - Conversion and Delivery of Electrical Energy in the 21st Century, 2008, 20-24 July, page(s): 1 - 7.
- [76] Agoris, P.; Meijer, S.; Smit, J.J.: "Sensitivity Check of an Internal VHF/UHF Sensor for Transformer Partial Discharge Measurements", IEEE Lausanne Power Tech, 2007, 1-5 July, page(s):2065 - 2069
- [77] Agoris, P.; Cichecki, P.; Meijer, S.; Smit, J.J.: "Building a Transformer Defects Database for UHF Partial Discharge Diagnostics", 2007 IEEE Lausanne Power Tech, 1-5 July, page(s):2070 - 2075
- [78] Agoris, P.D.; Meijer, S.; Smit, J.J.; Lopez-Roldan, J.: "Sensitivity Check of Internal Sensor for Power Transformer Partial Discharge Measurements", 8th International Conference on Properties and applications of Dielectric Materials, 2006, June 2006, page(s):230 - 233
- [79] Agoris, P.D.; Meijer, S.; Gulski, E.; Smit, J.J.; Hermans, T.J.W.; Lamballais, L.: "Sensitivity check for on-line VHF/UHF PD detection on

Transmission cables”, 8th International Conference on Properties and applications of Dielectric Materials, 2006, June 2006, page(s):204 - 207

- [80] Agoris, P.D.; Meijer, S.; Gulski, E.; Smit, J.J.: “Threshold selection for wavelet denoising of partial discharge data”, Conference Record of the 2004 IEEE International Symposium on Electrical Insulation, 2004, 19-22 Sept., page(s):62 – 65
- [81] Harry van Breen, Condition assessment of stator insulation using partial discharge diagnostics, PhD Thesis, Technical University of Delft, 2005.
- [82] K. Lonngren, S. Savov: Fundamentals of Electromagnetics with MATLAB, 1<sup>st</sup> edition, published by SciTech Publishing, March 21, 2005, ISBN-13: 978-1891121388.
- [83] A. J. Reid, M. D. Judd, B. G. Stewart, R. A. Fouracre: “Partial discharge current pulses in SF<sub>6</sub> and the effect of superposition of their radiometric measurement”, Journal Of Physics D: Applied Physics, Institute Of Physics Publishing, 15 September 2006, vol. 39, pp: 4167–4177.
- [84] S. W. Wentworth, Applied Electromagnetics – Early Transmission Lines Approach, published by John Wiley & Sons, 2007, ISBN-10: 0-470-04257-5.
- [85] P.A. Rizzi. Microwave Engineering - Passive Circuits. Prentice Hall, 1987, ISBN 0135867029.
- [86] CIGRÉ Working Group D1.33: “Guidelines for Unconventional Partial Discharge Measurements”, 2009.

[76] Agost, P.D., Mejer, S., Guzik, E., Sant, J.J. "Transient detection of partial discharge in power transformer" IEEE Transactions on Dielectrical and Electrical Insulation, 2006, 13, no. 2, pages 123-130.

[77] Agost, P.D., Mejer, S., Guzik, E., Sant, J.J. "Building a Transformer Discharge Detector for UHF Partial Discharge Diagnosis" 2007 IEEE Lausanne Power Tech, 4-5 July, 2007, pages 2167-2172.

[78] Agost, P.D., Mejer, S., Guzik, E., Sant, J.J., Lapin-Kotkova, S. "A novel method for internal sensor for power transformer partial discharge measurements" 10th International Conference on Properties and applications of Dielectric Materials, 2006, June 2006, pages 19-23.

[79] Agost, P.D., Mejer, S., Guzik, E., Sant, J.J., Heikkilä, J., W. J. Lambert, L. "Sensitivity analysis of UHF PD detection in power transformer" IEEE Transactions on Dielectrical and Electrical Insulation, 2006, 13, no. 2, pages 131-138.

[80] Agost, P.D., Mejer, S., Guzik, E., Sant, J.J. "Guidelines for Unconventional Partial Discharge Detection in Power Transformer" IEEE Transactions on Dielectrical and Electrical Insulation, 2006, 13, no. 2, pages 139-146.

[81] Agost, P.D., Mejer, S., Guzik, E., Sant, J.J. "Partial Discharge Detection in Power Transformer" IEEE Transactions on Dielectrical and Electrical Insulation, 2006, 13, no. 2, pages 147-154.

[82] Agost, P.D., Mejer, S., Guzik, E., Sant, J.J. "Partial Discharge Detection in Power Transformer" IEEE Transactions on Dielectrical and Electrical Insulation, 2006, 13, no. 2, pages 155-162.

[83] Agost, P.D., Mejer, S., Guzik, E., Sant, J.J. "Partial Discharge Detection in Power Transformer" IEEE Transactions on Dielectrical and Electrical Insulation, 2006, 13, no. 2, pages 163-170.

[84] Agost, P.D., Mejer, S., Guzik, E., Sant, J.J. "Partial Discharge Detection in Power Transformer" IEEE Transactions on Dielectrical and Electrical Insulation, 2006, 13, no. 2, pages 171-178.

[85] Agost, P.D., Mejer, S., Guzik, E., Sant, J.J. "Partial Discharge Detection in Power Transformer" IEEE Transactions on Dielectrical and Electrical Insulation, 2006, 13, no. 2, pages 179-186.

[86] Agost, P.D., Mejer, S., Guzik, E., Sant, J.J. "Partial Discharge Detection in Power Transformer" IEEE Transactions on Dielectrical and Electrical Insulation, 2006, 13, no. 2, pages 187-194.

[87] Agost, P.D., Mejer, S., Guzik, E., Sant, J.J. "Partial Discharge Detection in Power Transformer" IEEE Transactions on Dielectrical and Electrical Insulation, 2006, 13, no. 2, pages 195-202.

[88] Agost, P.D., Mejer, S., Guzik, E., Sant, J.J. "Partial Discharge Detection in Power Transformer" IEEE Transactions on Dielectrical and Electrical Insulation, 2006, 13, no. 2, pages 203-210.

[89] Agost, P.D., Mejer, S., Guzik, E., Sant, J.J. "Partial Discharge Detection in Power Transformer" IEEE Transactions on Dielectrical and Electrical Insulation, 2006, 13, no. 2, pages 211-218.

[90] Agost, P.D., Mejer, S., Guzik, E., Sant, J.J. "Partial Discharge Detection in Power Transformer" IEEE Transactions on Dielectrical and Electrical Insulation, 2006, 13, no. 2, pages 219-226.

[91] Agost, P.D., Mejer, S., Guzik, E., Sant, J.J. "Partial Discharge Detection in Power Transformer" IEEE Transactions on Dielectrical and Electrical Insulation, 2006, 13, no. 2, pages 227-234.

[92] Agost, P.D., Mejer, S., Guzik, E., Sant, J.J. "Partial Discharge Detection in Power Transformer" IEEE Transactions on Dielectrical and Electrical Insulation, 2006, 13, no. 2, pages 235-242.

[93] Agost, P.D., Mejer, S., Guzik, E., Sant, J.J. "Partial Discharge Detection in Power Transformer" IEEE Transactions on Dielectrical and Electrical Insulation, 2006, 13, no. 2, pages 243-250.

[94] Agost, P.D., Mejer, S., Guzik, E., Sant, J.J. "Partial Discharge Detection in Power Transformer" IEEE Transactions on Dielectrical and Electrical Insulation, 2006, 13, no. 2, pages 251-258.

[95] Agost, P.D., Mejer, S., Guzik, E., Sant, J.J. "Partial Discharge Detection in Power Transformer" IEEE Transactions on Dielectrical and Electrical Insulation, 2006, 13, no. 2, pages 259-266.

[96] Agost, P.D., Mejer, S., Guzik, E., Sant, J.J. "Partial Discharge Detection in Power Transformer" IEEE Transactions on Dielectrical and Electrical Insulation, 2006, 13, no. 2, pages 267-274.

[97] Agost, P.D., Mejer, S., Guzik, E., Sant, J.J. "Partial Discharge Detection in Power Transformer" IEEE Transactions on Dielectrical and Electrical Insulation, 2006, 13, no. 2, pages 275-282.

[98] Agost, P.D., Mejer, S., Guzik, E., Sant, J.J. "Partial Discharge Detection in Power Transformer" IEEE Transactions on Dielectrical and Electrical Insulation, 2006, 13, no. 2, pages 283-290.

[99] Agost, P.D., Mejer, S., Guzik, E., Sant, J.J. "Partial Discharge Detection in Power Transformer" IEEE Transactions on Dielectrical and Electrical Insulation, 2006, 13, no. 2, pages 291-298.

[100] Agost, P.D., Mejer, S., Guzik, E., Sant, J.J. "Partial Discharge Detection in Power Transformer" IEEE Transactions on Dielectrical and Electrical Insulation, 2006, 13, no. 2, pages 299-306.

# Sensitivity Check Procedure in GIS

---

In GIS, due to the high pressures of the SF<sub>6</sub> gas, the discharge currents at the defects can be less than one hundred picoseconds [15/33]. Therefore the generated electromagnetic transients can have a frequency content that can exceed 2 GHz. The electromagnetic waves then propagate within the coaxial busbars of the GIS by many different modes (TEM and TE or TM higher modes). The various reflections of the signals at the discontinuities create standing waves, which result in complex resonance patterns of the electromagnetic waves within the GIS compartments.

These reflections, however, result in reduction of the transmitted signals along the GIS. For this reason, many RF sensors have to be installed in a complete GIS in order to be able to detect PD along the whole structure. Apart from the signal attenuation along the GIS, it was also observed that “*the magnitude of the detected signals strongly depends on the location and to a minor degree on the orientation of the defect and the sensor*” [1]

It eventually became necessary to be able to verify the sensitivity between successive sensors mounted on a GIS. Therefore, a sensitivity check procedure was proposed by CIGRE Task Force 15/33.03.05 of Working Group 15.03 in 1999. The procedure is described in [1] and it ensures that defects generating an apparent charge of 5 pC (or more) can be detected by the RF measuring equipment.

The procedure consists of two main parts [15/33]:

- C. Laboratory Test: An artificial pulse is determined which emits a signal similar to that of an actual defect and is equivalent to an apparent charge of 5 pC.
- D. On-site Test: This artificial pulse is then injected in the GIS and the RF sensors are used to detect the pulse at different positions on the GIS.

Each part is performed in several steps that are described in Tables A.1 and A.2.

<b>Laboratory Test</b>	
<b>1</b>	Installation of an artificial PD defect of 5 pC PD level in a compartment of a laboratory GIS set-up
<b>2</b>	<ul style="list-style-type: none"> <li>▪ Installation of a pair of RF sensors: 1) on the same compartment close to the defect setup (C1), and 2) on an adjacent compartment (C2).</li> <li>▪ Connection of a PD detection circuit (IEC 60270).</li> </ul>
<b>3</b>	Energizing of the defect and PD detection using both systems: <ul style="list-style-type: none"> <li>▪ IEC 60270 conventional system in order to determine the discharge level in pC.</li> <li>▪ RF PD detection system in order to record the RF magnitude <math>A</math> at sensor on (C2).</li> </ul>
<b>4</b>	Inject artificial pulses in sensor on (C1) with the following characteristics: <ul style="list-style-type: none"> <li>▪ Rise time <math>\leq 1</math> ns</li> <li>▪ Pulse width <math>&gt; 500</math> ns (rectangular pulses)</li> <li>▪ PWHM <math>&gt; 20</math> ns (double exponential pulses)</li> <li>▪ Time between consecutive pulses <math>&gt;</math> duration of RF signal. (usually less than 100 kHz).</li> </ul>
<b>5</b>	Acquire RF signal magnitude $B$ at sensor on (C2). Compare magnitudes $B$ and $A$ obtained in step (3). Vary amplitude of artificial pulse until $B = A$ with an accepted tolerance of $\pm 20\%$ .

Table A.1: Steps for the laboratory test for the sensitivity check of the RF PD measuring system in GIS.

<b>Field Test</b>	
<b>1</b>	Injection of the artificial voltage pulses as were obtained in step (5) of the laboratory step. The same type of equipment (pulse generator, cable and RF sensor) has to be used as for the laboratory test.
<b>2</b>	Measure RF signal at second coupler mounted on another compartment. If signal is detected the sensitivity verification is successful for the GIS section between these couplers (i.e. for all compartments in between).

Table A.2: Steps for the on-site test for the sensitivity check of the RF PD measuring system in GIS.

In the laboratory test the magnitude of an artificial voltage pulse is related to an actual PD of a desired pC level. The actual discharges were generated by a free moving particle. According to [1], in a GIS configuration of 420 kV components with a bare enclosure, at a voltage of 385 kV a bouncing metallic particle with a

length of 3 mm caused an apparent charge of 5 pC. This type of defect was chosen because it is the most frequent and critical defect in GIS [1]. Artificial pulses were then emitted inside the GIS using a pulse generator connected to an RF sensor. The injecting RF sensor was mounted at the same compartment where the particle defect was introduced. By varying the amplitude of the artificial pulses it was then possible to achieve an equivalent frequency response on the receiving sensors to the previous frequency response of the particle defect.

The determined artificial pulses could then be used to simulate a bouncing particle defect. The pulse generator can be easily applied in an on-site situation instead of an actual defect that is difficult to build and test in the field. In the on-site test the pulse generator is then used to inject pulses within the GIS via an RF sensor and the detection sensitivity of the successive sensors is verified following the steps described in Table A.2. According to [1] if the sensitivity check is successful, it is then assumed that *all* defects that cause at least 5 pC and are located between the injecting and receiving RF sensors can be detected. An important benefit that this procedure offers is that the sensitivity check is comparable to the conventional systems based on the IEC 60270.

length of 3 mm caused an apparent increase in the number of defects. This type of defect was observed because it is the most frequent type of defect observed in the experiments. The defects were then mounted inside the GDS using a special procedure described in the text. The defect was mounted inside the GDS using a special procedure described in the text. The defect was mounted inside the GDS using a special procedure described in the text.

The defect was mounted inside the GDS using a special procedure described in the text. The defect was mounted inside the GDS using a special procedure described in the text. The defect was mounted inside the GDS using a special procedure described in the text. The defect was mounted inside the GDS using a special procedure described in the text. The defect was mounted inside the GDS using a special procedure described in the text.

The defect was mounted inside the GDS using a special procedure described in the text. The defect was mounted inside the GDS using a special procedure described in the text. The defect was mounted inside the GDS using a special procedure described in the text. The defect was mounted inside the GDS using a special procedure described in the text. The defect was mounted inside the GDS using a special procedure described in the text.

The defect was mounted inside the GDS using a special procedure described in the text. The defect was mounted inside the GDS using a special procedure described in the text. The defect was mounted inside the GDS using a special procedure described in the text. The defect was mounted inside the GDS using a special procedure described in the text. The defect was mounted inside the GDS using a special procedure described in the text.

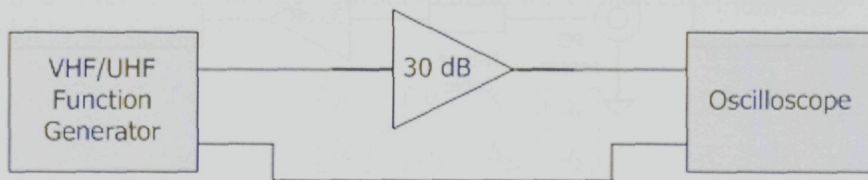


# Frequency Response Measurements

## POWER AMPLIFIER FREQUENCY RESPONSE:

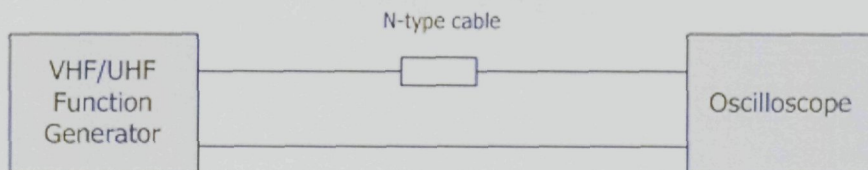
This setup consists of two different function generators that cover the range 0 > 500 MHz together. The gain of the VHF/UHF 30 dB amplifier is determined over the frequency range 0 > 500 MHz. Just measure the voltages at the scope's input and calculate the gain:

$$Gain = 20 \log \left( \frac{U_{30dB}}{U_{direct}} \right) \quad (B.1)$$



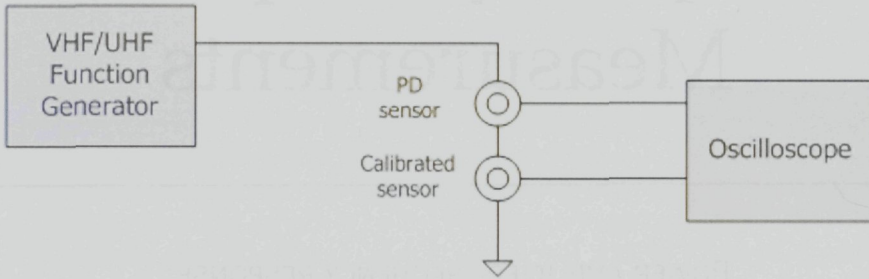
## COAXIAL CABLE (N-TYPE) FREQUENCY RESPONSE:

The same principle as in setup 1 can be applied. Determine the attenuation of the N-type cable by comparing the two inputs over the spectrum 0 > 500 MHz. Vary the cable length and the positioning of the cable.



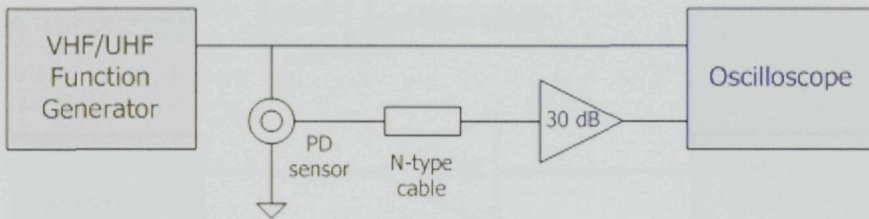
### CURRENT PROBE'S FREQUENCY RESPONSE :

Now the behaviour of the HF PD sensors is determined. The frequency is again varied from 0 > 500 MHz. As a reference, I use a calibrated current sensor of which the transfer impedance is known. So at every frequency, I know what is the actual current. In this way, I can determine the transfer impedance of our PD sensors.



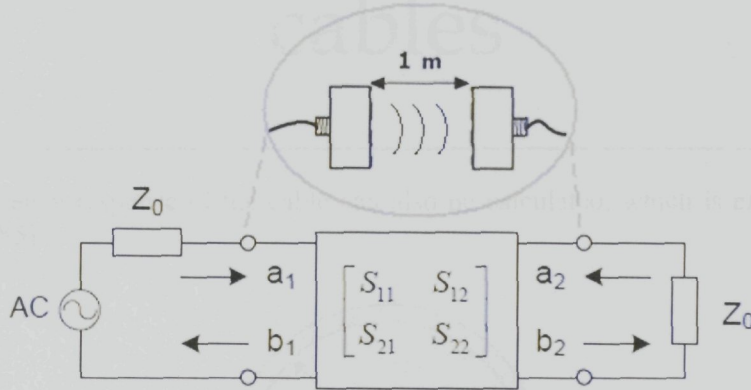
### RF MEASURING SYSTEM'S FREQUENCY RESPONSE :

Check if the combined frequency responses of the different components are validated.



## RF ANTENNA'S FREQUENCY RESPONSE

The frequency response of the antennas was measured using a network analyzer as follows. Two sensors were placed on wooden stands in such a way that they are opposite and facing each other at a distance of 1m. Then using the network analyzer it was possible to measure the response of each antenna by treating them as a two-port network as is shown in the figure below.



The two-port network in the figure shows the normalized incident waves ( $a_1$ ,  $a_2$ ) and reflected waves ( $b_1$ ,  $b_2$ ) used in S-parameter definitions. The measurement system source and load impedances are  $Z_0$ . The S-parameters relate the waves scattered or reflected from the network to those waves incident upon the network as defined by the S-matrix:

$$\begin{bmatrix} b_1 \\ b_2 \end{bmatrix} = \begin{bmatrix} S_{11} & S_{12} \\ S_{21} & S_{22} \end{bmatrix} \begin{bmatrix} a_1 \\ a_2 \end{bmatrix} \quad (\text{B.2})$$

The S-matrix represents the relationships between the independent variables ( $a_1$ ,  $a_2$ ) and the dependent variables ( $b_1$ ,  $b_2$ ), which are normalized incident and reflected voltage waves respectively. Note that the elements from the S-matrix may have a complex value. After an S-parameter measurement, the transfer of a two-port network can be calculated by filling in  $S_{21}$  into the following equation:

$$Gain_{dB} = 20 \log |S_{21}| \quad (\text{B.3})$$

## ANTENNA'S FREQUENCY RESPONSE

### RF ANTENNA'S FREQUENCY RESPONSE

The antenna's frequency response is determined by the antenna's input impedance, which is a function of the antenna's geometry and the frequency of the incident wave. The antenna's input impedance is a complex quantity, and it is possible to measure the response of each antenna by means of a two-port network as is shown in the figure below.



Check if the combined antenna response and the different components are validated.

The two-port network in the figure shows the normalized incident waves (a1, a2) and reflected waves (b1, b2) used in 2-parameter definition. The independent system source and load impedances are  $Z_{in}$ . The 2-parameters  $S_{11}$  and  $S_{21}$  are defined by the S-matrix:

$$\begin{bmatrix} b_1 \\ b_2 \end{bmatrix} = \begin{bmatrix} S_{11} & S_{12} \\ S_{21} & S_{22} \end{bmatrix} \begin{bmatrix} a_1 \\ a_2 \end{bmatrix} \quad (8.3)$$

The S-matrix represents the relationships between the independent variables (a1, a2) and the dependent variables (b1, b2), which are normalized incident and reflected voltage waves respectively. Note that the elements from the S-matrix may have a complex value. After an S-parameter measurement, the transfer of a two-port network can be calculated by fitting in S21 into the following equation:

$$\text{Gain}_{dB} = 20 \log |S_{21}| \quad (8.3)$$

# Attenuation in coaxial cables

The frequency response of the cable can also be calculated, which is explained as follows [85].

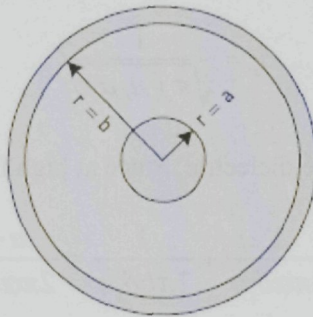


Figure C.1: Cross-section of coaxial cable indicating the conductor radii  $a$  and  $b$

The inductance and capacitance of a coaxial line may be written on a per unit length basis by:

$$L' = \frac{\mu_0 \mu_r}{2\pi} \ln \frac{b}{a} \quad \text{and} \quad C' = \frac{2\pi \epsilon_0 \epsilon_r}{\ln(b/a)} \quad (\text{C.1})$$

respectively, where the conductor radii  $a$  and  $b$  are defined in figure C.1.  $\mu_0$  is the permeability of free space and has the value  $4\pi \times 10^{-7}$  H/m,  $\mu_r$  is the relative permeability,  $\epsilon_0$  is the permittivity of free space and has the value  $8.85 \times 10^{-12}$  F/m and  $\epsilon_r$  is the relative permittivity.

By using

$$Z_0 \approx \sqrt{\frac{L'}{C'}} \quad (\text{C.2})$$

and equations C.1, the characteristic impedance of a coaxial line can be written as:

$$Z_0 = 60 \sqrt{\frac{\mu_r}{\epsilon_r}} \ln \frac{b}{a} = 138 \sqrt{\frac{\mu_r}{\epsilon_r}} \log \frac{b}{a} \quad (\text{C.3})$$

in Ohms. As we can see,  $Z_0$  is a function of the cross-sectional dimensions of the coaxial line as well as the electrical properties of the insulating material between the conductors. The shunt conductance per unit length may be obtained from:

$$G' = \omega \frac{2\pi\epsilon_0\epsilon_r}{\ln(b/a)} \tan \delta \quad (\text{C.4})$$

$\tan \delta$  being the dielectric loss tangent of the insulator. The series resistance per unit length is the sum of the resistances due to the inner and outer conductors. Skin depth is a measure of the degree to which an electromagnetic field penetrates a conducting material, and is a function of frequency: the depth of the penetration decreasing with increasing frequency. The skin depth can be calculated with:

$$\delta_s = \frac{1}{\sqrt{\pi f \mu_r \mu_0 \sigma}} \quad (\text{C.5})$$

$\sigma$  being the conductivity of the dielectric. Since at high frequencies  $\delta_s \ll a$ ,

$$R' \approx \frac{1}{2\pi a \delta_s \sigma} + \frac{1}{2\pi b \delta_s \sigma} = \frac{a+b}{2\pi a b \delta_s \sigma} \quad (\text{C.6})$$

$\delta_s$  being the skin depth in the metal conductors. By combining equations C.3, C.4 and C.6, the attenuation per unit length,  $\alpha$ , for a low-loss line can be written as:

$$\alpha \approx \frac{R'}{2Z_0} + \frac{G'Z_0}{2} = \alpha_c + \alpha_d \quad (\text{C.7})$$

where  $\alpha_c$  and  $\alpha_d$  represent the portions due to the imperfect conductors and insulator, respectively. The following expressions for  $\alpha_c$  and  $\alpha_d$  can be derived:

$$\alpha_c = 13.6 \frac{\delta_s \sqrt{\epsilon_r} \{1 + (b/a)\}}{\lambda_0 b \ln(b/a)} \quad \text{and} \quad \alpha_d = 27.3 \frac{\sqrt{\epsilon_r}}{\lambda_0} \tan \delta \quad (\text{C.8})$$

in dB/length, with the speed of light  $c$  ( $3.0 \times 10^8$  m/s),  $\lambda_0 = c/f$  being the wavelength in free space. With the help of expressions C.8 and the parameters of the concerning cable, expression C.7 can be encapsulated in:

$$\alpha \approx K_1 \cdot \sqrt{f_{\text{MHz}}} + K_2 \cdot \sqrt{f_{\text{MHz}}} \quad (\text{C.9})$$

in dB/m, with  $K_1 = \alpha_c / \sqrt{f_{\text{MHz}}}$  and  $K_2 = \alpha_d / f_{\text{MHz}}$ .  $K_1$  and  $K_2$  are constants which are different for every type of coaxial cable and reduces the preceding formulae to a minimum. For the RG-213 cable,  $K_1$  and  $K_2$  are  $6.26 \times 10^{-3}$  and  $41.3 \times 10^{-6}$  respectively. These values can be calculated or looked up in tables given in cable catalogs, which is easier. Note that the frequency has to be filled in MHz units.

It is necessary to insert a sensor at a sufficient depth within the transformer tank for optimum detection. This is confirmed in the following laboratory experiment. The sensor that was used is demonstrated in Figure D.1. The transformer, shown in Figure D.1(a), incorporates an oil-valve that will be used to insert a sensor employing the monopole antenna type<sup>17</sup>, as is shown in Figure D.2 (b). Diagonal windows at the top of the transformer allow for the mounting of another RF probe that will be used for injecting signals in the transformer from a pulse generator (PG). While injecting, the signals at the monopole sensor were measured at the following cases:

1. The sensor is not fully inserted, and the oil-valve is shut.
2. The oil valve is fully opened and the sensor is inserted until it reaches the inner surface of the tank (0 cm insertion depth).
3. The monopole sensor is further inserted by 4 cm.

For the first three cases the signals were measured in time domain (wideband up to 4 GHz). Results are shown in Figure D.3. From Figure D.3 (a), it can be seen that a small signal of relatively low frequency content is detected, which may be considered via the transformer tank. Once the oil-valve is opened and the sensor is inserted up to the inside the valve, there is a stronger signal detected by the sensor with an added DC component of -50 mV. The signal of Figure D.3 (a) is negligible. When the sensor is further inserted by 4 cm the signal becomes stronger by more than double. It is also observed that the DC component of the measured signal decreases, which was caused by the tank influencing the reactive field of the monopole.

Results in the frequency domain are also displayed in Figure D.3. It can be seen that spectra with a 100 MHz resolution shows impulses significantly. The graphs are not shown in this paper.

<sup>17</sup>The monopole antenna was designed by the author as the 1st element of a linear UWB antenna for the detection of signals in a transformer tank.

and constant  $C_1$ , the characteristic impedance  $Z_0$  can be written in the form

$$Z_0 = \frac{1}{2\pi} \sqrt{\frac{\epsilon_0}{\epsilon}} \ln \frac{2a}{r} \quad (2.3)$$

where  $\epsilon$  is the permittivity of the dielectric material between the conductors and  $\epsilon_0$  is the permittivity of free space. With the help of equations (2.2) and (2.3) the characteristic impedance  $Z_0$  can be written as

$$Z_0 = \frac{1}{2\pi} \sqrt{\frac{\epsilon_0}{\epsilon}} \ln \frac{2a}{r} \quad (2.4)$$

where  $\epsilon$  is the dielectric constant of the dielectric material between the conductors and  $\epsilon_0$  is the permittivity of free space. With the help of equations (2.2) and (2.3) the characteristic impedance  $Z_0$  can be written as

$$\delta = \frac{1}{\sqrt{\pi f \mu_0 \sigma}} \quad (2.5)$$

where  $\sigma$  being the conductivity of the dielectric. Since at high frequencies  $\delta \ll a$ ,

$$R = \frac{1}{2\pi a \sigma} + \frac{1}{2\pi b \sigma} + \frac{1}{2\pi r \sigma} \quad (2.6)$$

where  $\delta$  being the skin depth of the metal conductors. By combining equations (2.3), (2.4) and (2.6), the characteristic impedance  $Z_0$  can be written as

$$Z_0 = \frac{1}{2\pi} \sqrt{\frac{\epsilon_0}{\epsilon}} \ln \frac{2a}{r} \left( \frac{1}{2\pi a \sigma} + \frac{1}{2\pi b \sigma} + \frac{1}{2\pi r \sigma} \right) \quad (2.7)$$

where  $\sigma_1$  and  $\sigma_2$  represent the surface conductivities of the inner conductor and insulation respectively. The characteristic impedance  $Z_0$  can be derived as

$$Z_0 = \frac{1}{2\pi} \sqrt{\frac{\epsilon_0}{\epsilon}} \ln \frac{2a}{r} \left( \frac{1}{2\pi a \sigma_1} + \frac{1}{2\pi b \sigma_2} + \frac{1}{2\pi r \sigma} \right) \quad (2.8)$$



# Insertion depth in oil-valve sensors

---

It is necessary to insert a sensor at a sufficient depth within the transformer tank for optimum detection. This is confirmed in the following laboratory experiment. The setup that was used is demonstrated in Figure D.1. The transformer, shown in Figure D.1(a), incorporates an oil-valve that will be used to insert a sensor employing the monopole antenna type<sup>11</sup>, as is shown in Figure D.1 (b). Dielectric windows at the top of the transformer allow for the mounting of another RF sensor that will be used for injecting signals in the transformer from a pulse generator (PG). While injecting, the signals at the monopole sensor were measured at the following cases:

1. The sensor is not fully inserted, and the oil-valve is shut.
2. The oil valve is fully opened and the sensor is inserted until it reaches the inner surface of the tank (0 cm insertion depth).
3. The monopole sensor is further inserted by 4 cm.

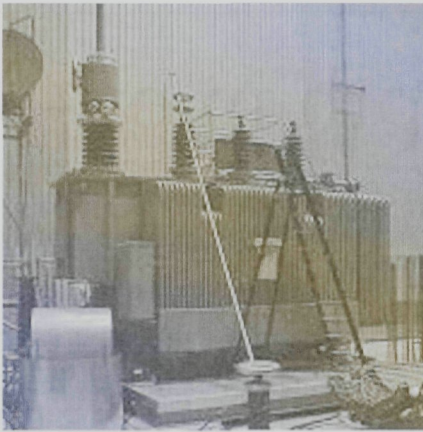
For the first three cases the signals were measured in time domain (wideband up to 3GHz). Results are shown in Figure D.3. From Figure D.3 (a), it can be seen that a small signal of relatively low frequency content is detected, which may be transmitted via the transformer tank. Once the oil-valve is opened and the sensor is moved deeper inside the valve there is a stronger signal detected by the sensor with an added DC component of -50 mV. The signal of Figure D.3 (a) is negligible. When the sensor is farther inserted by 4 cm the signal becomes stronger by more than double. It is also observed that the DC component of the measured signal disappears, which was caused by the tank influencing the reactive field of the antenna.

Results in the frequency domain are also displayed in Figure D.2. It can be seen that sensitivity in certain frequency ranges improves significantly. The graphs are not,

---

<sup>11</sup> The monopole sensor was designed by and built in the Universität Stuttgart, ETI Institut für Energieübertragung und Hochspannungstechnik.

however, representative of the frequency response of the monopole sensor since the transfer of the injecting antenna amplifies and attenuates different frequency ranges.

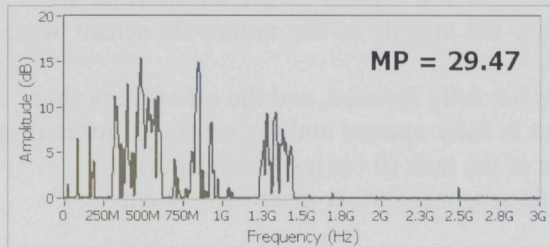


(a)

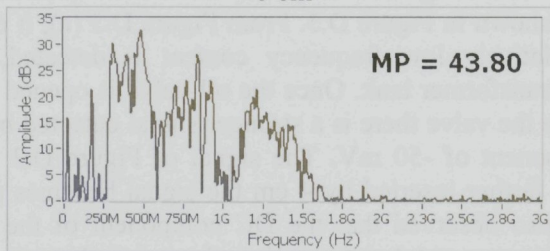


(b)

Figure D.1: (a) 14 MVA transformer in the laboratory. (b) Photo of a monopole sensor mounted at the oil-valve.

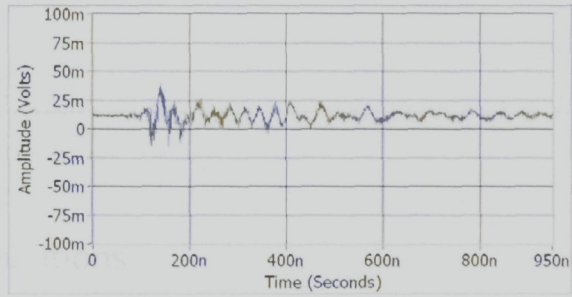


0 cm

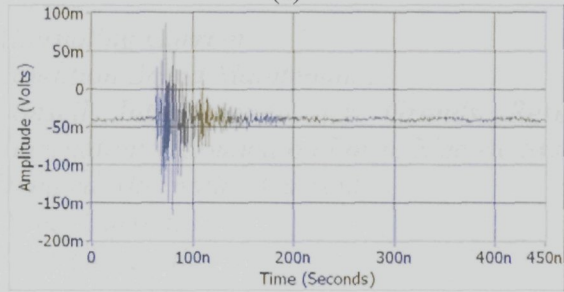


4 cm

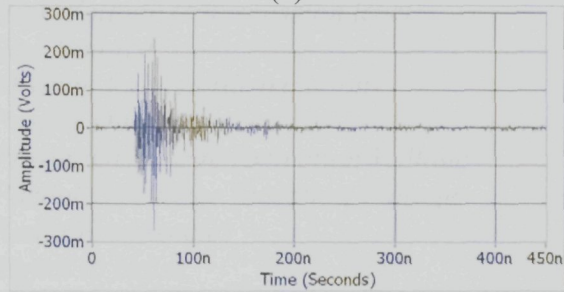
Figure D.2: By moving the sensor 4 cm deeper than the tank's inner surface the sensitivity of the sensor considerably improves.



(a)



(b)



(c)

Figure D.3: Time domain measurements with the internal sensor (conical spiral antenna), when injecting at sensor S2. (a) Oil-valve is shut, (b) oil-valve is opened, and (c) sensor is inserted at 0 cm insertion depth.

however, representative of the frequency response of the monopole sensor since the transfer of the injecting antenna amplifier and attenuator is flat in different frequency ranges.



Figure 2: (a) Photograph of a monopole sensor mounted at the oil valve. (b) Photograph of a monopole sensor mounted at the oil valve.



Figure 3: Time domain measurements with the internal sensor (conical spiral antenna) when injecting at valve 25. (a) Oil valve is shut. (b) Oil valve is opened. and (c) sensor is fixed at C (conical spiral antenna).

Figure 4: Comparison of the frequency response of the internal sensor (conical spiral antenna) and the external sensor (monopole antenna) at valve 25.

## List of abbreviations

---

<i>AC</i>	<i>Alternating Current</i>
<i>CBM</i>	<i>Condition Based Maintenance</i>
<i>CIGRÉ</i>	<i>Conseil International des Grands Reseaux Électriques (International Council on Large Electric Systems)</i>
<i>DAC</i>	<i>Damped Alternating Current</i>
<i>DC</i>	<i>Direct Current</i>
<i>EM</i>	<i>Electromagnetic</i>
<i>HF</i>	<i>High Frequency</i>
<i>HV</i>	<i>High Voltage (transmission level)</i>
<i>LV</i>	<i>Low Voltage</i>
<i>MV</i>	<i>Medium Voltage (distribution)</i>
<i>PD</i>	<i>Partial Discharge</i>
<i>PDEV</i>	<i>Partial Discharge Extinction Voltage</i>
<i>PDIV</i>	<i>Partial Discharge Inception Voltage</i>
<i>RF</i>	<i>Radio Frequencies</i>
<i>S/N</i>	<i>Signal to Noise</i>
<i>SA</i>	<i>Spectrum Analyser</i>
<i>TEM</i>	<i>Transverse Electromagnetic</i>
<i>TF</i>	<i>Task Force</i>
<i>UHF</i>	<i>Ultra High Frequency</i>
<i>VHF</i>	<i>Very High Frequency</i>
<i>VLf</i>	<i>Very Low Frequency</i>
<i>WG</i>	<i>Working Group</i>
<i>XLPE</i>	<i>Group Cross-Linked Polyethylene</i>

## List of units

$Q, q$	Electric Charge	C	(Coulomb)
$t$	time	s	(second)
$V$	Voltage	V	(Volt)
$I$	Current	A	(Ampere)
$R$	Resistance	$\Omega$	(Ohm)
$C$	capacitance	F	(Farad)
$L$	inductance	H	(Henry)
$J$	current density	$A \cdot m^{-2}$	(Ampere / square meter)
$\sigma$	conductivity	$S \cdot m^{-1}$	(Siemens / meter)
$E$	Electric Field	$V \cdot m^{-1}$	(voltage / meter)
$\epsilon$	permittivity ( $=\epsilon_0 \cdot \epsilon_r$ )	$F \cdot m^{-1}$	(Farad / meter)
$\epsilon_0$	vacuum permittivity ( $\approx 8.854 \times 10^{-12} F \cdot m^{-1}$ )	$F \cdot m^{-1}$	(Farad / meter)
$\epsilon_r$	relative permittivity	-	
$c_0$	speed of light in vacuum ( $\approx 299792458 m \cdot s^{-1}$ )	$m \cdot s^{-1}$	
$\mu$	permeability ( $=\mu_0 \cdot \mu_r$ )	$H \cdot m^{-1}$	(Henry / meter)
$\mu_0$	vacuum permeability ( $= 4\pi \times 10^{-7} H \cdot m^{-1}$ )	$H \cdot m^{-1}$	(Henry / meter)
$\mu_r$	relative permeability	-	
$\lambda$	wavelength	m	(meter)
$f$	frequency	Hz	(Hertz)
$T$	period	s	(seconds)
$\omega$	angular frequency	$rad \cdot s^{-1}$	(radians/second)
$\gamma$	propagation constant		
$\alpha$	attenuation constant	$Np \cdot m^{-1}$	(nepers/meter)
$\beta$	phase constant	rad/m	(rad/meter)
$\eta$	refractive index	-	
$S$	Poynting vector	$W \cdot m^{-2}$	

## ACKNOWLEDGEMENTS

---

Alas, a few words are not enough to express my gratitude to all who have helped in a direct or indirect way to make the completion of this thesis possible.

First of all, I would like to thank my promoter, professor Johan Smit, for trusting me with the work of this research project in the department of Electrical Sustainable Energy. Mainly I would like to thank him for providing me the opportunity to meet and collaborate with an array of exceptional people within and outside of this department. And I think this was the greatest personal gain I could achieve during the years of my research.

I would like to thank my daily supervisor, dr.ir. Sander Meijer, for guiding me all these years. Sander, you have helped me during this research with the greatest patience a supervisor could possess. It was real fun working with you, and your exceptional skills as a researcher and an engineer will be an inspiration to me in my next projects.

I would also like to thank dr.hab.ir. Edward Gulski for his invaluable support during the most difficult times of this work. His coaching managed to keep me going when I was most desperate and he helped me overcome the obstacles ahead.

None of the work in this book could have been done without the invaluable help of Paul van Nes, Aad van der Graaf and Bertus Naagen. Paul, I appreciate your advice and guidance in organizing all my research ideas. Aad, thank you for materializing all these ideas, and especially thank you for building all the RF sensors for assisting my measurements. They truly are pieces of engineering art! Bertus, thank you for all your practical help and for making even the longest of measurements enjoyable.

I would also like to thank TenneT, the Dutch grid company, for starting up this research project, for the financial support and for providing me with opportunities to monitor their transformers. Additional thanks to Smit Transformers, Pauwels Transformers, Alliander and the Greek public corporation of electricity ( $\Delta.E.H.$ ) for allowing me to monitor their transformers for PDs using the RF PD measuring system. Finally, thanks to Prysmian for providing me with opportunities to test the RF PD measuring system with their cable systems in their laboratory and in the field.

And then I would like to thank my friends from the department that provided the enjoyable working atmosphere. Which can be very crazy sometimes when crazy scientists work under noisy conditions (isn't that right Rogier? Is that video still on

youtube Dhiradj?). Rogier it was a real pleasure being your roommate, I can say I know at least a hundred jokes about blondes by now! Good old times are gone but now new better ones come. I wish you all the best with your new family and maybe you should consider giving your baby a Greek name!

Dhiradj, thanks to your assistance with all the bureaucracy of the doctorate and for the required translations to Dutch. You were kind of the man who's been dragged through all this s... first and guides his buddies through with safety. I've seen too many movies I guess. And yes, the glory day(s?) of the High Voltage Band (or was it Los Casas Bonitas, or the High Voltage Nodes?) have to be revived.

Piotr, special thanks to you for doing all my last minute work for the thesis and for your assistance in its completion. It has been great fun working with you even at the most difficult of conditions with no food and water under the hot sun. I prefer the polish vodka nights however! I hope to see you and your wife soon in Greece!

Ruben, it has been a long time. Thank you for your work in your master thesis which was essential for my research. The High Voltage Band will never find a better bass player.

Thomas I am looking forward to seeing you as the new bassist of the High Voltage Band (no hard feelings Ruben). Roma you would make an excellent drummer ...if you knew how to play the drums. Moe thanks for the stimulating discussions on technical and non-technical subjects and good luck with your work and family! Roy, keep on beating everyone at go-carts, especially Piotr. Tom, I hope next time we work on an "XboX" it will be to actually play a video game. Thank you for your assistance on that project. Barry, Qikai and Gautam I wish you all the best with your work at the university.

I would like to thank the former PhD students Ben, Tjerk, Robert, Harry and Ricardo for the insightful conversations and collaborations. In addition I am grateful to the M.Sc. students Feliciano and Charles for their assistance during this research.

I would also like to thank all the people I've collaborated with in Prysmian, Pauwels Transformers, Alliander and Smit Transformers. I hope we get a chance to work together again.

And then there are the people outside of the university, friends who became an inseparable part of my life during these years. No words can describe the moments we all had together so I can only name them here. And each name brings millions of memories. First my flatmates from Zusterlaan and my very first friends in Holland George, Anish and Pawel. Then the flatmates from Rotterdam Pablo, Garci, Antonis, Theodoros, Carlos, George, Claudia and Mateo. To my latest flatmates



Maria, Dimitris and Sadek thanks for hosting me at your amazing place, and especially thanks to Sadek for giving me one of his rooms to stay in. I also want to thank Marja for cutting all the stencils for my best and only artwork (so far) residing in that house. I could never finish it without your help. To the rest of my friends in Holland George and Joanna, Dodoros and Argyro, Marnix and Michela, David and Ruth, Nikos and Ana, Maria and Maria and so many others that let me crash at their place one night or more, and for the great times we had together. See you sooner than you think!

The last part is reserved for the most important people in my life, my family. First of all, I would like to thank my mother and sister for being home in my heart. Then I would also like to thank my uncles, aunts, cousins and my grandmother, who are always there for me whatever the circumstances.

Most importantly I would like to thank my father Demosthenes whose guidance helped me become who I am today. I cannot wish for things to be different so I dedicate this work to his loving memory. He will always be remembered.

Σας Ευχαριστώ!

I dedicate the following lyrics to all of you people and the future days to come:

*«Here comes another revelation  
A revolution for us all  
I never believed what you said  
I only believe what we've done  
We are the Energy»*

Song: Youth

by the *Love and Rockets*



## BIOGRAPHY

---



**Pantelis Agoris** was born on February 24, 1982, in Athens, Greece. He received his high school degree from Varvakio High School of Athens, in 1999. He then studied at the University of Cardiff until 2003 where he received his M.Eng. degree in Electrical Engineering. His individual thesis project in the 3<sup>rd</sup> year of his studies was “LEDs that emit in the blue region of the spectrum”. His final thesis project (4<sup>th</sup> year) was under the group research: “PWM excitation of induction machines”. His individual work focused on “Neural networks for the prediction of losses by PWM excitation in induction machines”. It handled the design and training of neural networks for the extrapolation of data concerning losses at the core of induction machines due to PWM excitation.

He started his Ph.D. research project in 2003 in the High Voltage Technology and Management group (in the department of Electrical Sustainable Energy) of the Delft University of Technology. In co-operation with Dutch TSO TenneT his research concentrated on the development of the radio frequency (RF) partial discharge (PD) detection technique in transformers. He developed the software for the detection and identification of PDs in the RF range, which he has applied several times in transformer PD measurements in the field. He has also programmed the software for Prysmian in order to use it for PD RF measurements in power cables. He has also participated in several PD measurements in the field assisting Prysmian with the monitoring of PDs in newly installed power cables in the Netherlands and abroad.

# BIOGRAPHY

Pantelis Agoris was born on February 24, 1982, in Athens, Greece. He received his high school degree from Varvakeio High School of Athens in 1999. He then studied at the University of Cardiff until 2003 where he received his MEng degree in Electrical Engineering. His industrial thesis project in the 3<sup>rd</sup> year of his studies was "FDx bus control in the brake region of the spectrum". His final thesis project in the 4<sup>th</sup> year was under the group research "TWO: Evaluation of induction machines". His industrial work focused on "New algorithms for the prediction of losses by induction machines" under the supervision of design and training of industrial engineers. He completed his master's thesis on "The impact of the electromagnetic losses of the core of induction machines on the PWM control" in 2005.



He received his PhD in 2007 from the Department of Electrical and Electronic Engineering of the University of Cardiff, Wales, UK. His PhD thesis was titled "The impact of the electromagnetic losses of the core of induction machines on the PWM control". He worked as a research fellow at the University of Cardiff from 2005 to 2007. He is currently an Assistant Professor in the Department of Electrical and Electronic Engineering of the University of Cardiff, Wales, UK. He is also a senior research fellow at the Cardiff Research Centre for Power Electronics and Drives. He is a member of the Institution of Electrical Engineers (IET) and the Institution of Mechanical Engineers (IMECH). He has published several papers in international journals and conferences. He is also a member of the editorial board of the *Journal of Power Electronics*.



Performing partial discharge measurements in the radio frequency range, on an on-line transformer, under rainy conditions.



## **Stellingen / Propositions**

behorende bij het proefschrift / accompanying the doctoral thesis

" Sensitivity Verification of Radio Frequency  
Partial Discharge Detection in High Voltage Equipment "

Pantelis D. Agoris

4 november 2009 / November 4<sup>th</sup>, 2009

1. Prior to actual radio-frequency (RF) partial discharge (PD) measurements, a sensitivity check should always be carried out in order to take into account the actual noise levels. [*this thesis*]

*Voorafgaand aan daadwerkelijke partiële ontladingsmetingen (PD-meting) in het radiofrequentiegebied (RF), moet een gevoeligheidstest worden uitgevoerd om met het actuele ruisniveau rekening te houden.*

2. The sensitivity of the RF PD measuring system is unique to the combination of the RF measuring equipment used, the specific discharging defect and the tested HV equipment. [*this thesis*]

*De gevoeligheid van het RF PD meetsysteem is uniek voor de combinatie van de gebruikte RF meetset, het specifieke ontladingsdefect en de geteste hoogspanningscomponent.*

3. Inside a power transformer the propagation paths of the signals originating from a PD are so complicated that calibration of conventional and un-conventional PD measurement systems is impossible. [*this thesis*]

*Binnen een vermogenstransformator zijn de propagatiepaden van de signalen afkomstig van een PD zo gecompliceerd dat calibratie van conventionele en de niet-conventionele PD meetsystemen onmogelijk is.*

4. The main reason for the RF PD measuring method to relate RF-spectral amplitudes to standardized discharge values, is to familiarize the industries with the technique. [*this thesis*]

*De voornaamste reden voor de RF PD meetmethode om spectrale amplitudes in het radiofrequente gebied te relateren aan gestandaardiseerde ontladingswaarden, is het laten wennen van de industrie aan het toepassen van deze techniek.*



5. Large central power stations degenerate to behemoths of the industrialization age, as individuals, businesses and communities fully apply small-scale generation and self-sustainable buildings.

*De grote energiecentrales degenereren tot mammoeten uit het tijdperk van de industrialisatie, als particulieren, bedrijven en gemeenschappen kleinschalige energie opwekking en "self-sustainable" gebouwen volledig toepassen.*

6. The current economic crisis will force industrial corporations to distinguish themselves by adopting more client-friendly and environment-friendly oriented strategies and products.

*De huidige economische crisis zal industriële bedrijven aanzetten om zich te onderscheiden door het toepassen van meer klantvriendelijke en milieuvriendelijke strategieën en producten.*

7. To deal with the yearly sudden increase of energy demand on the Cyclades islands during the summer tourist season, a more economic option is to apply renewable energy sources that are in accordance with the cultural aesthetics of the islands.

*Om aan de jaarlijkse plotselinge stijging van de energiebehoefte op de Cycladen te kunnen voldoen tijdens het toeristische zomerseizoen, zal het economisch gezien het voordeliger zijn om hernieuwbare energiebronnen te gebruiken waarbij rekening gehouden moet worden met de culturele esthetiek van de eilanden.*

"Μελέτη Ανάπτυξης Συστήματος Μεταφοράς 2008-2012", Administrator of Greek System of Transport of Electric Energy S.A., (Δ.Ε.Σ.Μ.Η.Ε), [www.desmic.gr](http://www.desmic.gr)

8. Expenditures on basic scientific research are highly profitable because the devices and techniques developed for the research turn out to have other use e.g. in modern factories or clinical medicine.

*De uitgaven voor fundamenteel wetenschappelijk onderzoek zijn zeer profijtelijk, omdat de apparaten en technieken die ontwikkeld zijn andere toepassingen blijken te hebben in bijv. de industrie en klinisch medisch onderzoek.*

“CERN technology transfers to industry and society”, European Organisation for Nuclear Research, (C.E.R.N.), [www.cern.ch](http://www.cern.ch)

9. In order for neuroscience to discover the neural correlates of consciousness it is necessary to explore also different forms of art, because art captures a layer of reality that science does not.

*Om ervoor te zorgen dat de neurologie de neurale connecties van het bewustzijn kan ontdekken, is het noodzakelijk dat ook verscheidene vormen van kunst worden onderzocht, omdat kunst een bepaald niveau van realiteit bevat, dat de wetenschap niet heeft.*

10. Groups should not aim for the homogeneity of each member, but instead they should preserve and encourage the idiosyncrasy of the individual.

*Een groep mensen zou niet moeten willen dat elk lid hetzelfde is, maar juist dat de idiosyncrasie van de individuele leden behouden en aangemoedigd wordt.*

Deze stellingen worden opponeerbaar en verdedigbaar geacht en als zodanig goedgekeurd door de promotor, prof.dr. J.J. Smit.

These propositions are considered opposable and defensible and as such have been approved by the supervisor, prof.dr. J.J. Smit.

